[redacted]

#1

AXISYMMETRIC MODES IN HYDROMAGNETIC WAVEGUIDE

GERALD B. KLIMAN

TECHNICAL REPORT 449

FEBRUARY 28, 1967

MASSACHUSETTS INSTITUTE OF TECHNOLOGY
RESEARCH LABORATORY OF ELECTRONICS
CAMBRIDGE, MASSACHUSETTS

The Research Laboratory of Electronics is an interdepartmental laboratory in which faculty members and graduate students from numerous academic departments conduct research.

The research reported in this document was made possible in part by support extended the Massachusetts Institute of Technology, Research Laboratory of Electronics, by the JOINT SERVICES ELECTRONICS PROGRAMS (U.S. Army, U.S. Navy, and U.S. Air Force) under Contract No. DA36-039-AMC-03200(E); additional support was received from the National Science Foundation (Grant GK-524).

MASSACHUSETTS INSTITUTE OF TECHNOLOGY

RESEARCH LABORATORY OF ELECTRONICS

Technical Report 449

February 28, 1967

AXISYMMETRIC MODES IN HYDROMAGNETIC WAVEGUIDE

Gerald B. Kliman

Submitted to the Department of Electrical Engineering, M. I. T., May 28, 1965, in partial fulfillment of the requirements for the degree of Doctor of Science.

(Manuscript received November 1, 1965)

Abstract

The axisymmetric, transverse magnetic field modes of a hydromagnetic or Alfvén waveguide are studied experimentally and theoretically. An experiment was performed to examine with precision measurements the steady-state half-wave resonances of a short section of hydromagnetic waveguide with a liquid metal (NaK) used as the fluid conductor. The response to a step of current was also examined. The theory of uniform hydromagnetic waveguides is reviewed and extended by reconsideration of the propagation constant and theories for the effects of transverse fields, viscosity, finite conductivity walls, and bulk motion. A theory predicting the effects of nonuniform density or magnetic field is developed and verified in the experiment.

TABLE OF CONTENTS

CONTENTS

GLOSSARY

Symbol	Definition
ρ	Density
$\vec{V}, \vec{v}$	Velocity
P, p	Pressure
$\vec{J}, \vec{j}$	Current density
$\vec{B}, \vec{b}$	Magnetic field
σ	Conductivity
$\vec{E}, \vec{e}$	Electric field
μ_o	Magnetic susceptibility of free space
ω	Radian frequency
K, k	Propagation constant
α	Bessel function root
C, c	Alfvén speed
a	Waveguide radius
b	Wall thickness
g	Exciter radius
i	$\sqrt{-1}$
f	Frequency
I	Circuit current
T	Mode factor
η	Magnetic diffusivity
γ	Mode factor
ℓ	Resonator length
J_n	Bessel function
d	Expansion parameter
x	Normalized radius
ν	Viscous diffusivity
μ	Absolute viscosity

GLOSSARY

Symbol	Definition
C_{HM}	Hydromagnetic capacitance
$\vec{\psi}$	Vector field
$\vec{A}$	Vector field
ϕ	Scalar potential

I. INTRODUCTION

1.1 ORIENTATION

When a fluid is allowed to have electrical conductivity and magnetic fields are applied, a wide range of new and varied phenomena arise.[1] Among the most important of these is the possibility of a magnetohydrodynamic wave in which stored energy is exchanged between the wave magnetic field and the kinetic energy of motion in the fluid. Such waves were predicted by Alfvén,[2] in 1942, but were not actually observed[3] until 1954. These waves, now known as Alfvén waves, are of importance in the entire range of magnetohydrodynamic phenomena from power generation and thermonuclear fusion through microwave devices to the operation of the solar system and the galaxy.

In view of the importance of Alfvén waves, it is not surprising that there have been many theoretical studies of this phenomenon and its role in other processes. Experimental studies, however, have been few and more in the nature of demonstrations showing that an Alfvén type wave existed, rather than in the nature of a precise verification of the wave properties.

This study was undertaken in an attempt to perform an experiment of sufficient precision and accuracy to prove unequivocally the theory of Alfvén waves in detail and justify the assumptions upon which it is based. Since such experiments must be performed in a laboratory, they become studies of the Alfvén or hydromagnetic waveguide. Liquid metal was chosen as the fluid conductor in order to eliminate the bothersome and poorly understood properties of suitable plasmas so that only the magnetohydrodynamic interaction would be of importance.

During the design of the experiment, it became evident that there were some gaps in the theory of hydromagnetic waveguides, such as lack of theoretical developments and incomplete or inconvenient interpretations of existing theory. Therefore, theoretical studies were also undertaken in an effort to understand more fully the properties of hydromagnetic waveguides.

1.2 PREVIOUS EXPERIMENTS

There had been eight experiments to observe Alfvén waves in the laboratory before the present study was undertaken. A comparison of these experiments is presented in Section II. The experiments will be described in chronological order.

The first attempt to observe an Alfvén wave was made in Alfvén's laboratory in Sweden by S. Lundquist,[4] in 1949. His experiment consisted of a circular cylinder, its interior insulated, placed with its axis vertical and parallel to the magnetic field in which it was immersed. The conducting fluid was mercury. A finned disk was placed at the bottom of the cylinder and excited in torsional vibrations by a shaft brought through the bottom of the cylinder. Waves transmitted to the free surface near the top of the cylinder were observed by the motion of a small mirror floating there. This experiment

did not succeed in demonstrating Alfvén waves. It was thought that turbulence caused by the fins on the exciting disk was responsible, but it is shown in Section II that no Alfvén wave could exist in mercury at the magnetic field strength used.

The second experiment was done by B. Lehnert,[3] in 1954, also in Alfvén's laboratory. This experiment was quite similar to Lundquist's except that heated sodium was used as the fluid conductor, an electric field probe was used at the free surface in place of the mirror, and excitation was by means of a copper disk suspended on a coaxial shaft (also insulated). Except for the copper disk that was used to eliminate the supposed turbulence problem, all changes were made in order to contain the highly reactive liquid sodium under an inert atmosphere. This experiment succeeded in demonstrating the existence of an Alfvén wave, but with considerable discrepancy between experimental results and theory.

In 1961, two experiments were conducted in England and in the United States, in both of which transient plasmas were used as the fluid conductor. In the experiments of Wilcox, da Silva, Cooper and Boley, at the Lawrence Radiation Laboratory,[5] a copper cylinder, insulated at both ends and filled with hydrogen gas, was immersed in a magnetic field parallel to its axis. A cylindrical copper plug electrode was set coaxially into one of the end insulators. A capacitor bank was discharged from the coaxial electrode to the walls, thereby initiating a shock that propagated to the other end of the cylinder and left a region of decaying ionized hydrogen behind it. When the shock reached the end of the cylinder, the capacitor bank was short-circuited, and a short time later another capacitor bank was discharged from the coaxial electrode to the wall through the ionized gas. The capacitor bank was allowed to ring at a frequency below the ion-cyclotron resonance. The transit time of the waves that were generated was then measured. This experiment succeeded in demonstrating more of the qualitative properties of Alfvén waves, but uncertainties in the effective plasma density and conductivity prevented precise conclusions.

The experiments of Jephcott, Stocker, and Woods,[6] at the Culham Laboratory, were similar. In this case, the magnetic field coils were excited by a third capacitor bank, the cylinder was made of quartz, except for a narrow conducting ring near the excitation electrode, and the plasma was generated by a longitudinal arc. Again, Alfvén waves were observed, but precise comparisons with the theory could not be made, because of uncertainties of the magnetic field and the effective density. In both experiments, transit-time measurements were made from oscilloscope photographs of a single transient.

A series of experiments was carried out, in 1961, by Nagao and Sato,[32] at Tohoku University. The general arrangement, magnetic field, ionization, and excitation were almost identical to those of Jephcott, Stocker, and Woods.[6] The precision of their results was much poorer, but they also investigated the reflection of hydromagnetic waves from an abrupt change of magnetic field.

In 1962, experiments aimed at an investigation of the "Luxembourg effect" (intermodulation of radio waves in the ionosphere caused by motion of the ions) was initiated

at the Air Force Cambridge Research Laboratories by DeCourcy and Bruce.[7] They hoped to observe this effect, in the laboratory, by the coupling of Alfvén waves to electromagnetic waves. Their experimental apparatus was built of two coaxial quartz tubes sealed at the ends. The inner walls of the annulus were lined with copper screen in order to support both Alfvén and electromagnetic TEM modes. The inner cylinder contained a powerful ultraviolet source to ionize cesium vapor in the annulus by radiation. No results have been reported at this time.

Another series of experiments was carried out at the Massachusetts Institute of Technology, in which sodium-potassium eutectic alloy (78% potassium, 22% sodium), known as NaK, was used as the fluid conductor. The first set of experiments was done by N. Gothard,[8] in 1962. His apparatus consisted of a cylindrical tank, closed at both ends, constructed entirely of stainless steel and filled with NaK. Excitation was by means of a copper disk, insulated except for the edge, mounted on a cantilever some distance from one end of the cylinder. Waves were detected by a magnetic pickup coil mounted on a cantilever that could be traversed in both radius and height. This experiment again demonstrated the existence of Alfvén waves, but no attempt at precision measurements was made. In fact, many of the results were later shown to be of doubtful value, because of a lack of axisymmetry in the excitation and various mechanical vibrations induced in the detector by the motion of the cantilevered exciter.[9] Additional experiments were run at a later data in the same apparatus by Jackson and Carson.[10] Drastic modifications of this apparatus were made by Wessler, Jackson, and Kliman[11] to utilize the TEM modes for an educational film on Magnetohydrodynamics.

A series of steady-state experiments was carried out by P. Jameson,[12] in 1963, at Cambridge University. The apparatus consisted of two coaxial cylinders sealed at either end to form a closed annulus constructed entirely of stainless steel. A toroidal coil was wound on this structure, threading the core, as if it were an inductor with a liquid-metal core. The fluid conductor was heated sodium. The coil was excited with a current, which caused current sheets to form at each end, propagate out, and reflect from the other end. A magnetic pickup coil was used to detect the waveforms of the magnetic fields. The results of this experiment demonstrated Alfvén waves more precisely than previous work, but again without the precision attainable in steady-state resonance measurements.

1.3 REVIEW OF THEORETICAL PAPERS

The number of papers on hydromagnetic waves is voluminous (see, for instance, Ramer[13] or Clauser[14]). Only a few of the more pertinent papers will be mentioned here. One of the many treatments of waves in a compressible medium with an applied uniform steady magnetic field is that of Baños.[15]

The first treatment of a hydromagnetic waveguide was performed by Lundquist[4] in connection with his experiment. Essentially, he developed the behavior of the lowest axisymmetric transverse magnetic (TM) mode in a cylindrical waveguide. This theory

was later considerably improved by Lehnert,[3] who extended consideration to the entire set of axisymmetric TM modes in a coaxial structure, and took into account the finite size of his experimental apparatus and the exciter. Blue[16] attempted to explain the discrepancies of Lehnert's experiment, by considering the effect of viscosity in an exact manner, and found that it did not significantly affect the results.

Newcomb,[17] in 1957, first noted the similarities between hydromagnetic and electromagnetic waveguides. In a limited way, he examined the TM, TE, and TEM modes in waveguides filled with perfectly conducting fluid. Finite conductivity, compressibility, and ion-cyclotron effects were included as perturbations. Perfectly conducting waveguides were put on a firmer basis by Gajewski,[18] in 1959. This study included compressibility and considered both rigid and flexible walls. Soon thereafter, Shmoys and Mishkin[19] examined the same area, but from a different point of view. They considered the hydromagnetic waveguide as if it were an electromagnetic waveguide characterized by a dielectric tensor. Gould[20] considered the various modes in a cylindrical waveguide, and included a discussion of how modes could be excited. In 1961, Woods[21] made the most thorough and inclusive analysis, thus far, of the cylindrical hydromagnetic waveguide, in connection with the Culham Laboratory experiments.[6] This analysis included anisotropic conductivity, pressure and viscosity, ion-cyclotron resonance and the presence of ions, neutrals, and electrons. Aspects of hydromagnetic waveguides were studied by Rook,[22] in connection with his work on surface waves, from a somewhat more general point of view for a simple medium.

Hydromagnetic resonators were considered, in 1960, by Gajewski and Mawardi.[23] In this study, the fluid was a perfect conductor and the terminations either perfect conductors or insulators. In 1962, Rink[24] extended the theory of hydromagnetic resonators by including finite fluid conductivity and lossy reactive terminations. What was more important, he found the electrical input impedance of the resonator for a practical excitation structure, thereby allowing consideration of lumped terminations.

Nonuniform density or magnetic field problems have been considered primarily in connection with cosmic or ionospheric studies.[1,2,13,14] There has been, however, only one study of nonuniform density in a laboratory situation.[25] On the other hand, there has been a great deal of interest in lossless nonuniform electromagnetic waveguides and resonators (see, for instance, Berk[26]).

In 1961, Gajewski and Winterberg[27,28] made a thorough study of Alfvén waves in axisymmetric nonuniform magnetic fields, and in an unbounded incompressible medium of infinite conductivity. They showed that an Alfvén wave is always possible, as are other types of waves which do not exist in a uniform field. Their interest was primarily in the reflection of Alfvén waves, such as those in a magnetic mirror.

Pneuman[25] has analyzed what is essentially a cylindrical hydromagnetic waveguide with insulating walls and radial variation of density. His analysis was based on the assumption of infinite conductivity, leading to a nonuniform phase front after the wave had been launched from one end of the guide. Finite conductivity

was then included as a perturbation on this solution. It is shown in the present study, however, that the addition of finite conductivity allows the propagation of a plane wave front that responds to average, rather than local, properties of the medium.

1.4 ORGANIZATION OF THE REPORT

Section II lays the theoretical foundations of the experiment that forms the base of this work. Prior theoretical and experimental work on unterminated hydromagnetic waveguides is reviewed. New interpretations are placed on the dimensionless groups appearing in the propagation constant, which lead to a simple and convenient way of depicting its behavior. New results on the effects of viscosity, finite-conductivity walls, and transverse-field components are obtained (see also Appendix A). The response of a hydromagnetic resonator to steady-state sinusoids and suddenly applied steps of current is described. An equivalent circuit for the resonator near resonance is developed (see also Appendix L). The effect of bulk motion of the fluid on the steady state and step response is also considered (see also Appendix K). The response is found to consist of a damped sinusoid, because of the multiply reflected Alfvén wave superimposed on a ramp, resulting from the "motoring" of the fluid acting as a capacitance. A theory for nonuniform media is developed. A radially nonuniform density is considered (see also Appendix A), as well as a nonuniform but axisymmetric magnetic field. It is shown that, if the magnetic field does not vary too strongly, this case may be reduced to that of variable density (see also Appendix C). A perturbation theory is developed to solve the resulting equations. The expansion for the propagation constant obtained by this method indicates that the nonuniform hydromagnetic waveguide responds as if it were a uniform waveguide having averaged properties (see also Appendix B).

In Section III the experimental apparatus, procedures, and results are described. The apparatus may be divided into three groups: the resonator, which was specially constructed to conform as closely as possible to the theorectical model and to be safely and conveniently used with NaK (see also Appendix F); the electronic systems for exciting the resonator and measuring both steady-state resonance and step response (see also Appendix G); and the magnetic field. Two field configurations were used, one uniform and the other conforming to the relatively simple variation on which the nonuniform field theory was based (see also Appendix H). The experimental procedures were primarily developed to achieve maximum field strength and precision in the operation of the magnet. Care was taken to eliminate extraneous signals and to achieve maximum precision in all measurements. The principal results of the experiments are summarized.

Section IV presents an analysis of the experimental data and compares the results with theory. The resonator behavior is shown to conform closely to the performance

predicted by small-signal Alfvén wave theory in both the step and steady-state responses. A comparison of behavior in uniform and nonuniform fields confirmed the theory developed in Section II; however, the precision was not sufficient to draw firm conclusions about which type of average was more correct.

Section V summarizes the present work and gives recommendations for further research.

II. THEORETICAL FOUNDATIONS OF THE EXPERIMENT

The propagation constant for a uniform hydromagnetic waveguide with finite conductivity will be studied first. Consideration of some nonideal properties such as viscosity, finite-conductivity walls, and transverse fields will be considered. The response of a hydromagnetic resonator under various kinds of excitation will then be examined. Finally, the effect of the Alfvén velocity varying as a function of radius will be studied.

2.1 PROPAGATION CONSTANT

Several investigators have examined the uniform hydromagnetic waveguide in some detail. Their analyses have included almost every possible effect that one could imagine to occur when the medium is plasma or liquid. The most general case, however, tends to obscure rather than illuminate the relevant issues. Experimental investigations have also been made indicating that the basic phenomena in the hydromagnetic waveguide may be explained by only a few of the possible physical processes taking place in a plasma or by rather gross averages of the microscopic phenomena in a plasma.

In this investigation, attention is fixed primarily on an experiment in which a liquid metal is used as the fluid conductor. Thus most of the bothersome properties of plasmas are eliminated from consideration. The remaining properties of interest are density, electrical conductivity, viscosity, and magnetic permeability. The electric permittivity is not important, because of the extremely low frequencies characterizing the Alfvén wave. No attempt will be made to cover all factors in one single formulation. Instead, the "ideal" hydromagnetic waveguide, that is with only density, conductivity, and permeability considered, will be examined in some detail. Then the principal neglected effects of viscosity and fringing fields will be examined to show their effect on the "ideal" situation.

a. Finite Conductivity Waveguide

Wave equations – We shall now be concerned with the "ideal" hydromagnetic waveguide. Consider a uniform hollow cylinder of arbitrary cross section as shown in

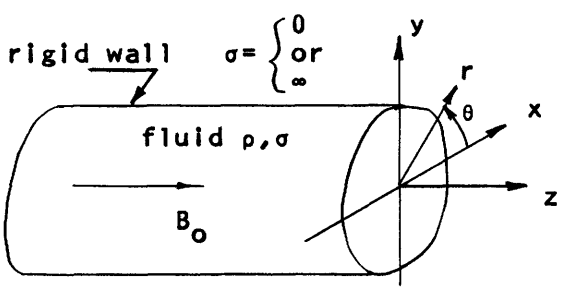

Fig. 1. Hydromagnetic waveguide.

Fig. 1. It is made of either perfectly conducting or perfectly insulating material, filled with a conducting fluid of density ρ and conductivity σ, and with its axis aligned with a

uniform steady magnetic field $\vec{B}_o = \vec{i}_z B_o$. The applicable laws are then Maxwell's equations

$$\nabla \times \vec{E} = -\frac{\partial \vec{B}}{\partial t} \tag{1}$$

$$\nabla \times \vec{B} = \mu_o \vec{J} + e_o \frac{\partial \vec{E}}{\partial t} \tag{2}$$

to which must be added the momentum equation and Ohm's law.

$$\rho \frac{D\vec{v}}{Dt} = -\nabla p + \vec{J} \times \vec{B} \tag{3}$$

$$\vec{J} = \sigma(\vec{E} + \vec{v} \times \vec{B}). \tag{4}$$

These equations can be linearized in the usual way by letting each quantity vary as

$$\vec{A} = \vec{A}_o + \vec{a} e^{i\omega t}, \tag{5}$$

where $|\vec{a}| \ll |\vec{A}|$, and with $\vec{B}_o$ the only nonzero constant term. Equations 1-4 then become

$$\nabla \times \vec{e} = -i\omega \vec{b} \tag{6}$$

$$\nabla \times \vec{b} = \mu_o \vec{j} \tag{7}$$

$$i\omega\rho\vec{v} = -\nabla p + \vec{j} \times \vec{B}_o \tag{8}$$

$$\vec{j} = \sigma(\vec{e} + \vec{v} \times \vec{B}_o), \tag{9}$$

where the displacement current term in Eq. 2 has been dropped through the assumption of low frequencies and high conductivity. For circular cylinder waveguides and transverse magnetic field modes Eqs. 6-9 may be reduced to a single equation in, for instance, b_θ. ($e^{in\theta}$ variation is assumed.)

$$\frac{d}{dr}\left[\frac{1}{r}\frac{d}{dr}(rb_\theta)\right] + \left\{\frac{\mu_o\sigma}{i\omega}\left[\omega^2 - k^2\left(\frac{B_o^2}{\mu_o\rho} + \frac{i\omega}{\mu_o\sigma}\right)\right] - \frac{n^2}{r^2}\right\} b_\theta = 0. \tag{10}$$

The resulting propagation constant is

$$k_{mn}^2 = \frac{\omega^2\mu_o\rho}{B_o^2} \frac{\left(\frac{a_{mn}}{a}\right)^2 + i\omega\mu_o\sigma}{1 + \frac{B_o^2\sigma}{i\omega\rho}}, \tag{11}$$

where a_{mn} is the m^{th} root of the n^{th}-order Bessel function and depends on the wall material (conducting or insulating), as well as on mode number. Equation 11 may be

rewritten in a simpler form as

$$k_{mn}^2 = \left(\frac{\omega}{c}\right)^2 \frac{1 + \frac{2\omega_1}{i\omega}}{1 + \frac{i\omega}{2\omega_2}}, \tag{12}$$

where

$$c = \frac{B_o}{\sqrt{\mu_o \rho}} \qquad \text{Alfvén speed} \tag{13}$$

$$\omega_1 = \frac{\alpha_{mn}^2}{2a^2 \mu_o \sigma} \qquad \text{Lower critical frequency} \tag{14}$$

$$\omega_2 = \frac{B_o^2 a}{2\rho}. \qquad \text{Upper critical frequency} \tag{15}$$

Propagation will take place only if

$$\omega_1 < \omega < \omega_2, \tag{16}$$

thereby dividing the range of possible frequencies into three regions. For $\omega \ll \omega_1$, k_{mn} approaches the asymptote

$$k_{mn} = \frac{\sqrt{\omega\ \omega_1}}{c}(1-i). \tag{17}$$

For $\omega \gg \omega_2$,

$$k_{mn} = \frac{\sqrt{\omega\ \omega_2}}{c}(1-i). \tag{18}$$

For $\omega_1 \ll \omega \ll \omega_2$,

$$k_{mn} = \left(\frac{\omega}{c}\right)\left[1 + \frac{1}{2}\left(\frac{-i\omega}{2\omega_2} + \frac{2\omega_1}{i\omega}\right)\right]. \tag{19}$$

Equation 19 may also be looked upon as having two asymptotes in the imaginary part for relatively low and relatively high frequencies. These several asymptotes are plotted in Fig. 2. Note that their intersections occur at the critical frequencies. For comparison, an exact evaluation of k_{mn} for NaK is also plotted in Fig. 2.

Inspection of Fig. 2 reveals that in order for low-attenuation Alfvén waves to exist, $\omega_2 \gg \omega_1$; this, in turn, means high conductivity σ, high magnetic field B_o, small density ρ, large radius a, and small mode number α_{mn}. The last means that the lowest order or simplest modes must be excited and that a conducting, rather than an insulating, wall should be used. In each case, then, the modes having the smallest

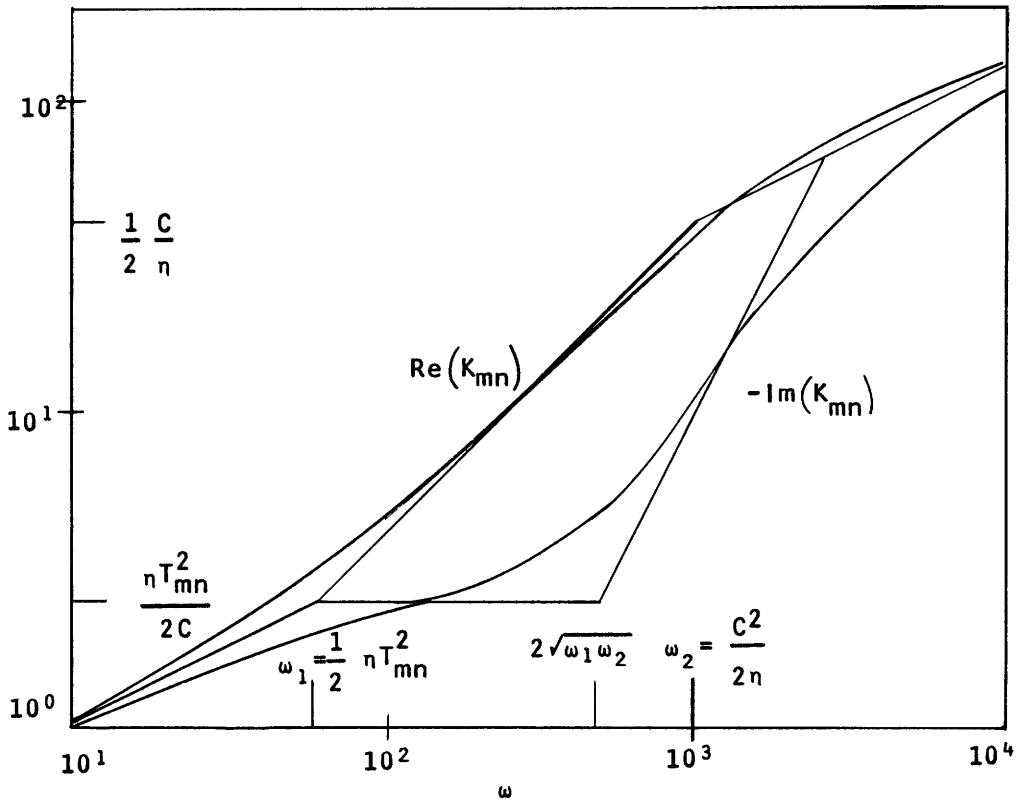

Fig. 2. K_{mn}-ω diagram for a liquid metal (NaK). $\sigma = 2.63 \times 10^6$ ℧/m; $\rho = 8.5 \times 10^2$ kgm/m^3; $B_o = 0.8$ w/m^2; a = 0.19 m; first axisymmetric mode; insulating wall.

attenuation are those with the simplest field configuration, that is, for rotational symmetry (n=0) and the smallest nonzero root of the Bessel function (m=1). The lowest attenuation for all modes is in the TM_{10} mode in a perfectly conducting cylinder.

Equations 17 and 18 are characteristic of diffusion phenomena. At low frequencies the magnetic field diffuses through the fluid in a time that is short compared with the period of the excitation. Thus the field is not convected by the fluid. At high frequencies the field cannot penetrate the fluid. Thus the fluid is not convected by the field. But if ω satisfies condition (16), there is a region in which mutual convection of the fluid and the field gives rise to the Alfvén wave.

Notice that the lower limit of the Alfvén region is controlled by conductivity and geometry, while the upper limit is controlled by conductivity, density, and applied field. The frequency below which, under condition (16), the waveguide is distortionless is twice the geometric mean of the upper and lower limits. Now,

$$\frac{\omega}{2\omega_1} = \frac{\mu_o \sigma \omega}{T_{mn}^2}$$ Magnetic Reynolds number

$$\frac{2\omega_2}{\omega} = \frac{\sigma B_o^2}{\omega\rho} \qquad \text{Lundquist number}$$

Thus, in order that an Alfvén wave exist, both the magnetic Reynolds and Lundquist numbers must be large compared with unity.

Listed below in tabular form is a comparison of a number of Alfvén wave experiments in terms of the critical frequencies.

	Experimenter	Medium	f_1	f_2
1.	Jephcott, Stocker, and Woods[6]	arc plasma	46.5 kc	51.3 Mc
2.	Wilcox, daSilva, Cooper, and Boley[5]	shock plasma	41.4 kc	111.0 Mc
3.	DeCourcy and Bruce[7]	irradiated gas	0 (TEM)	4.07 Mc
4.	Gothard,[8] and Jackson and Carson[10]	NaK	9.75 cps	158 cps
5.	Lundquist[4]	Hg	159 cps	10.3 cps
6.	Lehnert[3]	Na	21.5 cps	770 cps

The solutions to the hydromagnetic wave equations have been examined in some detail by Rook,[22] by utilizing vector potentials (Appendix D). He found that, in general, for an infinitely long cylinder of arbitrary cross section there are four possible solutions. One of these was identically zero, and a second was a potential flow in which the current density was identically zero and therefore not Alfvén. The remaining solutions are Alfvén, one consisting of a set of TE modes in which the perturbation electric field is transverse to $\vec{B}_o$, and the other a set of TM modes in which the perturbation magnetic field is transverse to $\vec{B}_o$.

If the waveguide is of a simple cross section such as a circle of radius a, the expressions for the various perturbation fields may be found closed form. Quoting Rook, we have the expressions for the TM waves with all quantities varying:

$$\vec{A} = \vec{a}\, e^{i(n\theta+kz+\omega t)} \tag{20}$$

$$\vec{v} = c_{TM}\left(1 + \frac{k^2}{T^2}\right)\left[\frac{in}{r}J_n(Tr)\,\vec{i}_r - TJ_n'(Tr)\,\vec{i}_\theta\right] \tag{21}$$

$$\vec{b} = \frac{ikB_o}{\omega}M_A^2\vec{v} \tag{22}$$

$$\vec{j} = c_{TM}\frac{kB_o}{\omega\mu_o}(T^2+k^2)M_A^2\left[\frac{ik}{T}J_n'(Tr)\,\vec{i}_r - \frac{kn}{T^2r}J_n(Tr)\,\vec{i}_\theta + J_n(Tr)\,\vec{i}_z\right] \tag{23}$$

$$\vec{e} = -c_{TM}ikB_o\left[-\frac{T}{k}\left(1+\frac{k^2}{T^2}M_A^2\right)J_n'(Tr)\vec{i}_r + \frac{n}{kr}\left(1+\frac{k^2}{T^2}M_A^2\right)J_n(Tr)\vec{i}_\theta - \left(1-M_A^2\right)J_n(Tr)\vec{i}_z\right] \tag{24}$$

$$p = 0, \tag{25}$$

where

$$M_A^2 = \frac{\omega^2}{k^2C^2} \tag{26}$$

$$C^2 = \frac{B_o^2}{\mu_o\rho} \tag{27}$$

$$-T^2 = k^2 + i\omega\sigma\mu_o\left(1 - \frac{k^2C^2}{\omega^2}\right), \tag{28}$$

and C_{TM} is an arbitrary constant.

The TE modes are

$$\vec{v} = c_{TE}\left[ikJ_n'(Tr)\,\vec{i}_r + \frac{k}{T}\frac{n}{r}J_n(Tr)\,\vec{i}_\theta + TJ_n(Tr)\,\vec{i}_z\right] \tag{29}$$

$$\vec{b} = \frac{ikB_o}{\omega}M_A^2\vec{v} \tag{30}$$

$$\vec{j} = +c_{TE}\frac{kB_o}{\omega\mu_o}(T^2+k^2)M_A^2\left[\frac{in}{Tr}J_n(Tr)\vec{i}_r - J_n'(Tr)\,\vec{i}_\theta\right] \tag{31}$$

$$\vec{e} = -c_{TE}ikB_o\left[M_A^2\frac{in}{Tr}J_n(Tr)\,\vec{i}_r - J_n'(Tr)\,\vec{i}_\theta\right] \tag{32}$$

$$p = -c_{TE}i\omega\rho\frac{T}{ik}J_n(Tr). \tag{33}$$

The potential modes are

$$\vec{v} = c_p\left[ikJ_n'(ik_r)\,\vec{i}_r + \frac{in}{r}J_n(ikr)\,\vec{i}_\theta + ikJ_n(ikr)\,\vec{i}_z\right] \tag{34}$$

$$\vec{b} = \frac{kB_o}{\omega}\vec{v} \tag{35}$$

$$\vec{j} = 0 \tag{36}$$

$$\vec{e} = -c_p ikB_o\left[\frac{n}{kr}J_n(ikr)\,\vec{i}_r - J_n'(ikr)\,\vec{i}_\theta\right] \tag{37}$$

$$p = c_p i\omega\rho J_n(ikr). \tag{38}$$

Boundary conditions – The assumption of a rigid-wall cylinder means that the normal component of velocity at the wall must be zero.

$$v_r(a) = 0. \tag{39}$$

Since viscosity has been neglected, there is no restriction on the tangential component of velocity. The effect of viscosity is considered in section 2.1b.

If the wall is assumed to consist of a perfectly conducting material ($\sigma=\infty$), the tangential component of electric field at the wall must be zero.

$$e_z(a) = e_\theta(a) = 0. \tag{40}$$

There is no restriction on the normal component, since a surface charge may exist on the interface. The tangential components of the magnetic field may be satisfied by surface currents, but the normal component must be zero.

$$b_r(a) = 0. \tag{41}$$

But since the perturbation magnetic and velocity fields are proportional, it is sufficient to require Eq. 39 only.

If the wall is assumed to consist of a perfectly insulating material ($\sigma=0$), the normal component of the current must be zero at the wall.

$$j_r(a) = 0. \tag{42}$$

There is no restriction on the tangential components of the electric field except continuity at the boundary; thus, there is a possibility of an external field structure. Again, as in the case of a perfectly conducting wall, the normal component of magnetic field will be zero if the normal component of velocity is zero. There is no restriction other than continuity on the tangential components which allow for the existence of an external magnetic field.

The rigid walls will make up whatever pressure is required by the various modes, if they exist, so that boundary conditions on the pressure need not be considered further.

Single mode propagation – An examination of Eqs. 21-38 for the field quantities and boundary conditions (39) to (42) reveals that while all of the individual modes may propagate in a perfectly conducting cylinder, only the n = 0 modes may propagate in a perfectly insulated cylinder. The difficulty comes in attempting to satisfy simultaneously the conditions on normal current and velocity. This point has not been generally recognized but was considered by Woods.[21] The problem of a general disturbance on a perfectly flexible cylinder has also been considered by Rook.[22]

If attention is restricted to those modes that may propagate singly, the propagation constant may be considered in more detail. For the TM and TE modes, application of the boundary conditions (39) and (40) for a perfectly conducting rigid cylinder of radius a yields:

$$J_n(Ta) = 0 \qquad \text{TM modes } (\sigma_{wall} = \infty) \tag{43}$$

$$J'_n(Ta) = 0 \qquad \text{TE modes } (\sigma_{wall} = \infty). \tag{44}$$

For a perfectly insulating rigid cylinder of radius a, application of the boundary conditions (39) and (42) yields for the n = 0, TM and TE modes:

$$J'_o(Ta) = 0 \qquad n = 0;\ (\sigma_{wall} = 0). \tag{45}$$

In each case, the boundary condition fixes the value of Ta and thus k. All modes except the TE_{m0} mode in an insulated cylinder have their fields confined to the region r < a. Continuity of the tangential magnetic field requires an external field to match the θ component in Eq. 29. If the m^{th} root of the n^{th}-order Bessel function or its derivative is denoted α_{mn}, then

$$Ta = \alpha_{mn}. \tag{46}$$

A mode factor T_{mn} similar to that used in ordinary waveguide theory would then be

$$T_{mn} = \frac{\alpha_{mn}}{a}. \tag{47}$$

Solving Eq. 28 for k^2 then yields, as before,

$$k_{mn}^2 = -\frac{\eta_\ell}{\eta_t} \frac{T_{mn}^2 + \frac{i\omega}{\eta_\ell}}{1 + \frac{c^2}{i\omega\eta_t}}, \tag{48}$$

where

$$\eta_{\ell,t} = \frac{1}{\mu_o \sigma_{\ell,t}} \tag{49}$$

are the longitudinal and transverse magnetic diffusivities corresponding to a conductivity tensor of the form

$$\overleftrightarrow{\sigma} = \begin{bmatrix} \sigma_t & 0 & 0 \\ 0 & \sigma_t & 0 \\ 0 & 0 & \sigma_\ell \end{bmatrix} \tag{50}$$

which results from a simpler derivation for the symmetric TM modes (Appendix E). Notice that the expression for k_{mn} is exactly the same for the TM_{mn} and TE_{mn} modes in a perfectly conducting cylinder and for the TM_{m0} and TE_{m0} modes in a perfectly insulating cylinder differing only in the value of T_{mn}. An examination of Eq. 48 shows that none of these modes is characterized by a cutoff frequency. In some studies, a cutoff in the TE modes has been reported. This was due to neglecting the pressure

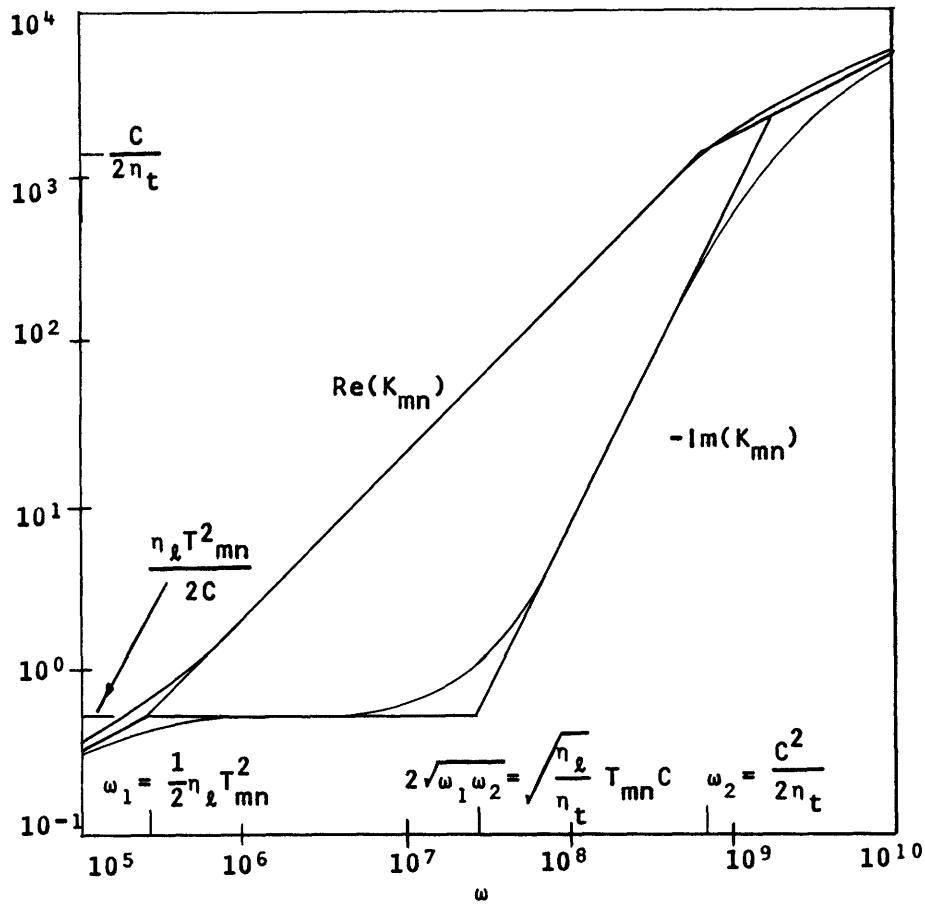

Fig. 3. K_{mn}-ω diagram for a shock-excited gas experiment. $\sigma_\ell = \sigma_t = 4.5 \times 10^3$ ℧/m (Te=3.5 eV); $\rho = 1.7 \times 10^{-5}$ kg/m^3 (n=1.5×10^{15}/cc H^+); $B_o = 1.6$ w/m^2; a = 0.07 m; first axisymmetric mode; insulating wall.

gradient improperly in the momentum equation (3). When the pressure is properly taken into account, it is seen that the perturbation pressure is indeed zero for the TM modes (Eq. 25) but nonzero and non-negligible for the TE modes (Eq. 33), unless the density is very small. For liquid metals, this is clearly not the case.

Figure 3 is a graph similar to Fig. 2, but for parameters suitable to a gaseous discharge experiment. It also shows the effect of differing transverse and longitudinal conductivities.

b. EFFECTS OF NONIDEAL CONDITIONS

Three important factors not considered in prior investigations are the effects of viscosity, finite conductivity walls and transverse fields.

Viscosity was considered by Blue[16] in attempting to account for inconsistencies in the Lundquist[4] and Lehnert[3] experiments in which the walls were made of insulating material. Because the ratio of electrical to viscous diffusivity is extremely large and the electromagnetic boundary conditions demand zero velocity at the walls, no significant

effect of viscosity was found. However, if the walls are perfectly conducting, the electromagnetic boundary conditions demand a maximum of velocity at the walls and some effect might then be expected. In Appendix A it is shown that again viscosity has no significant effect, the only alteration required being the addition of a thin (about 0.01 cm thick at the frequencies of interest) transition region at the wall.

In Appendix A the effect of a transverse component in the DC field is treated. There it is shown that the only effect is to introduce a highpass cutoff. If this cutoff occurs at a frequency less than ω_2 (i.e., the transverse field is less than the longitudinal field), it is given by

$$\omega_{co} = \frac{2\omega_2 \delta^2}{\sqrt{1 + \frac{\omega_2}{\omega_1}\delta^2}} \tag{51}$$

where δ is the ratio of transverse to longitudinal magnetic field. In Fig. 4 is shown an exact evaluation of the propagation constant for an NaK experiment, where $\delta = 0.1$ with the curves for $\delta = 0$ dashed in for comparison.

In Appendix A it is shown that a wall material of the same or lower conductivity as

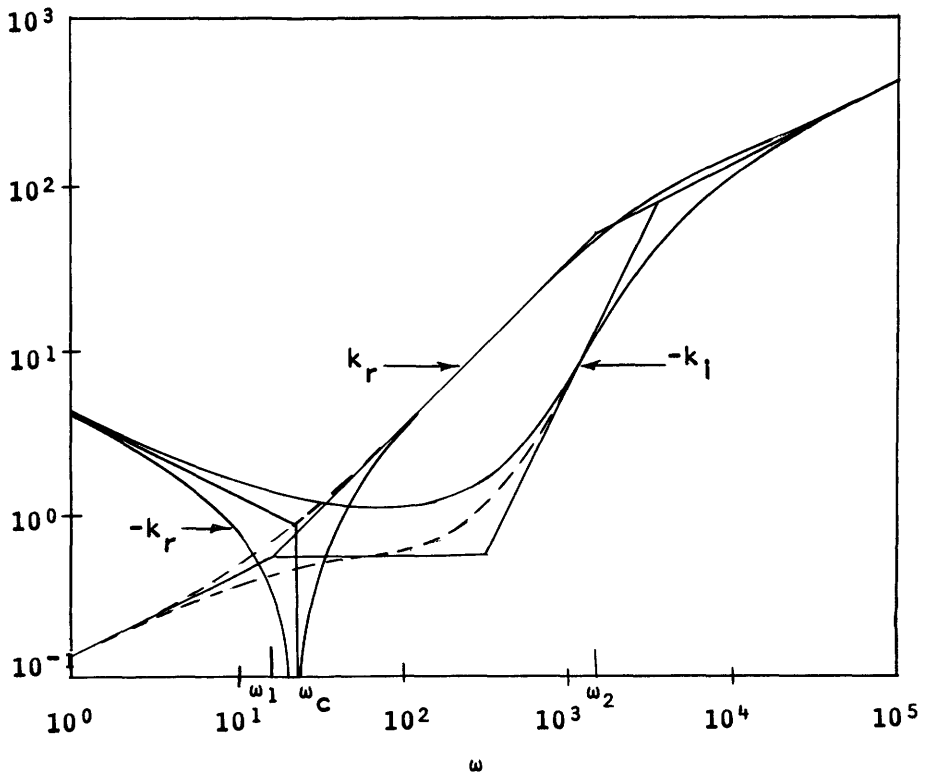

Fig. 4. Propagation constant with transverse field effect in NaK. $B_{oz} = 8$ kgauss; $a = 6$ in.; $\delta = 0.1$; $\sigma_2 = \infty$.

that of the fluid acts very much as if it were a perfect insulator. But if the wall conductivity is much greater than that of the fluid, it approximates a perfect conductor.

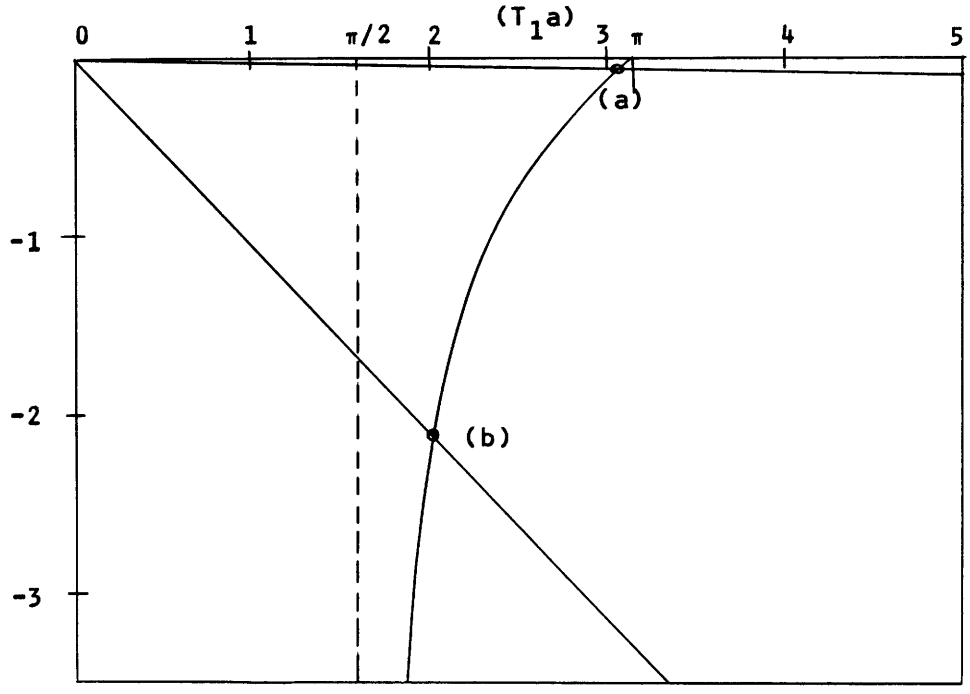

Fig. 5. Graphical solution of Eq. 52 for NaK.
(a) Stainless-steel wall, a = 7.5 in., b = 0.25 in.;
(b) Copper wall, a = 6 in., b = 0.25 in.

This is illustrated in Fig. 5 in which a plane parallel waveguide is considered. Figure 5 is the graphical solution of

$$\tan(\gamma_1 a) = -\frac{\sigma_2}{\sigma_1}\frac{b}{a}(\gamma_1 a), \tag{52}$$

in which γ_1 is the mode factor, a the half-width of the waveguide, b the wall thickness, σ_1 the fluid conductivity, and σ_2 the wall conductivity. If the wall is a perfect insulator (σ_2=0), $\gamma_1 a = \pi$; if it is a perfect conductor, $\gamma_1 a = \pi/2$. Two cases are shown, one for a stainless-steel wall (under the assumption of good electrical contact), and the other a copper wall.

2.2 LOSSY HYDROMAGNETIC RESONATOR

In general, when a hydromagnetic resonator is excited electrically, the current from the injector will spread through the fluid and excite both a bulk motion and an Alfvén wave. The division of energy between these two modes will depend on how close to a radial current sheet the exciting current is. This will, in turn, depend on both the

geometry of the electrode and the excitation frequency.

a. Small-Signal Waves

If, in Fig. 1, a length, ℓ, of the waveguide were cut out and terminated with insulating plates, it would act as a lossy half-wave resonator. It may be excited by a thin conducting ring set into one end as in Fig. 6. This situation may be approximated

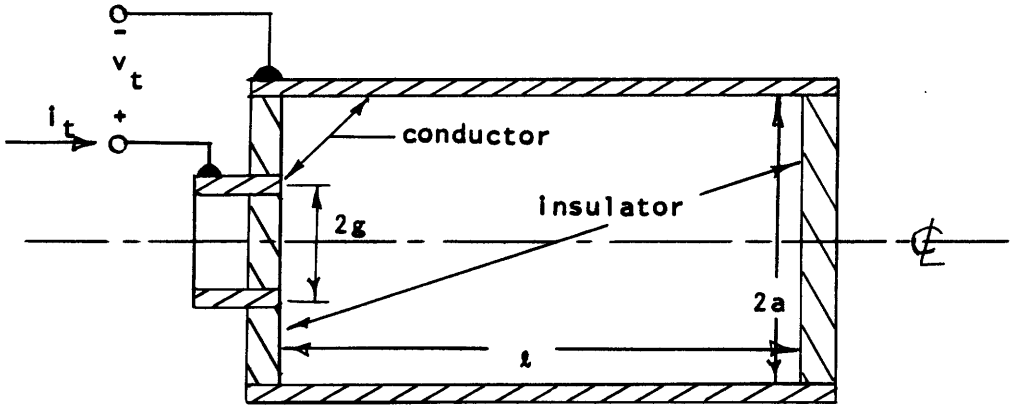

Fig. 6. Hydromagnetic resonator with electrical exciter.

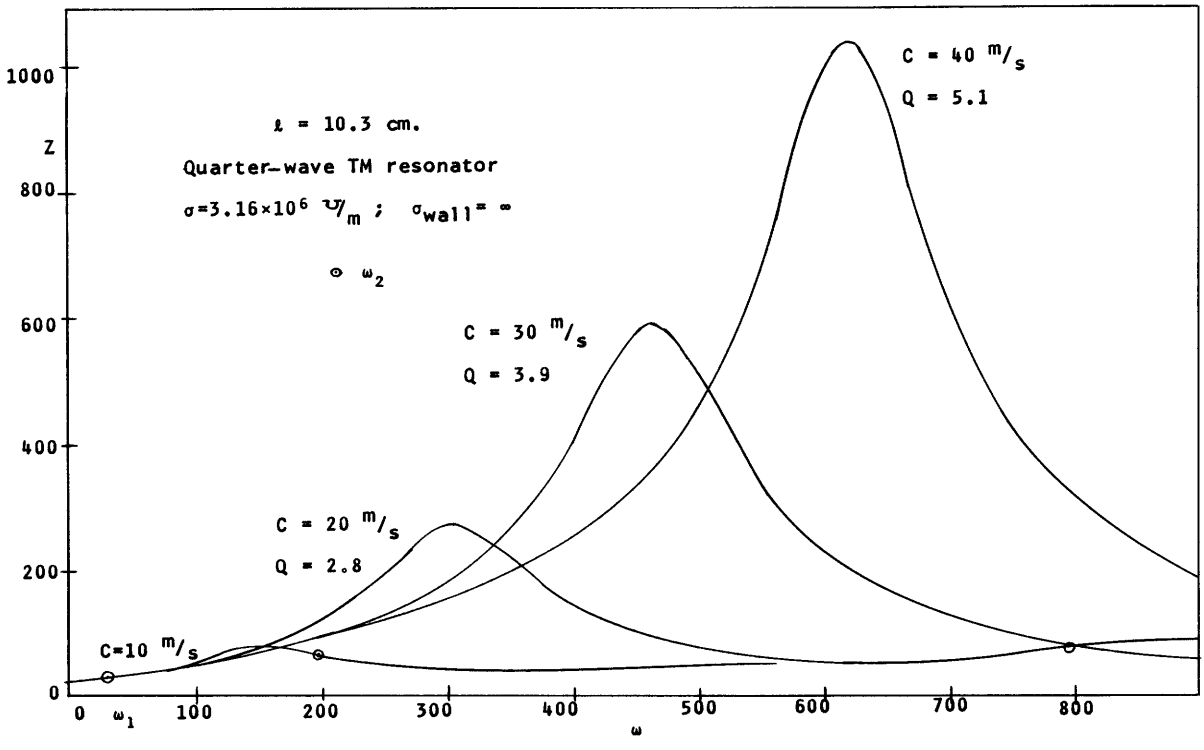

Fig. 7. Magnitude of Z as a function of frequency and Alfvén speed.

by a thin disk, insulated except for the edges. The exciting current will then be assumed to form a current sheet at the exciter end of the resonator, thereby exciting no bulk motion. Under these conditions, the electrical impedance seen at the terminals has been been found by Rink,[24] and is for the lowest order mode

$$Z = \frac{V_t}{I_t} = \frac{ik}{\pi a^2 \sigma} \left(1 + \frac{2\omega_2}{i\omega}\right) \frac{J_o^2\left(a\frac{g}{a}\right)}{J_1^2(a)} \cot k\ell. \tag{53}$$

A plot of the magnitude of this impedance as a function of frequency is shown in Fig. 7 for the conditions of an experiment in NaK. Notice that only one resonance

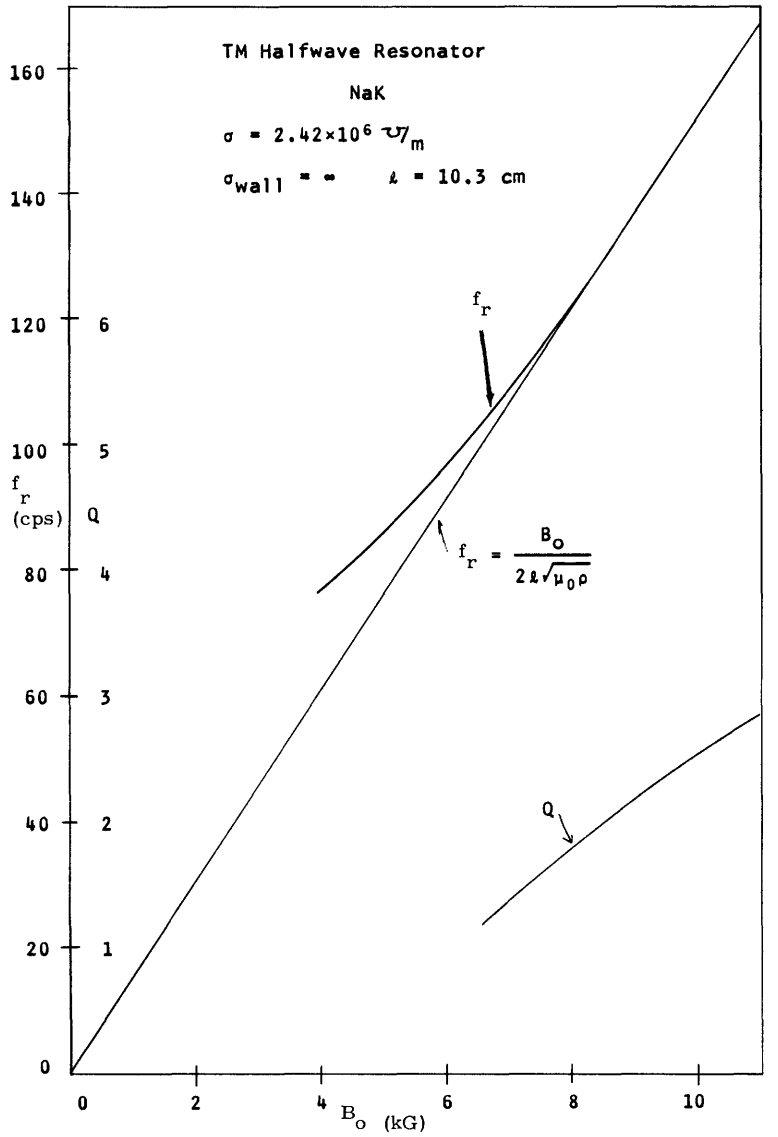

Fig. 8. Resonance frequency as a function of magnetic field.

occurs, and has a Q of, at most, approximately 5 for the conditions of a typical experiment. The resonance frequency and its Q are plotted as functions of magnetic field in Fig. 8 for the same conditions. The resonance frequency for $\sigma = \infty$ ($Q = \infty$) is also plotted. Notice that even though Q is quite low, the resonant frequency is quite close to the lossless case until one of the critical frequencies f_1 or f_2 is approached. If the resonance frequency is near f_2, it will be higher than the lossless case and lower if near f_1. This effect is clearly due to the variation of Re $[K_{mn}]$ from ω/c near the critical frequencies.

Near the resonance, an equivalent parallel RLC circuit may be found to approximate the terminal behavior. The parameters of this circuit (Appendix L) are

$$C_e = \frac{\pi \ell a^2 T^2 J_1^2(Ta)}{2\mu_o C^2 J_o^2(Tg)} \tag{54}$$

$$L_e = \frac{2\ell \mu_o J_o^2(Tg)}{\pi^3 b^2 T^2 J_1^2(Ta)} \tag{55}$$

$$R_e = \frac{C^2 J_o^2(Tg)}{2\sigma\pi\ell a^2 T^4 J_o^2(Ta)} \tag{56}$$

$$Q = \frac{\pi C \mu_o \sigma}{2\ell T^2}, \tag{57}$$

where $\omega_1 < \omega \ll \omega_2$. For the region $\omega_1 \ll \omega < \omega_2$, the expression for Q may be obtained only by solving a quadratic equation for ω_r; this results in a quite complex expression. The actual Q for all regions is presented in Figs. 7 and 8 from numerical evaluations of Z. For a typical set of data in an NaK experiment, C_ℓ is ~2200 farads, L_e is $\sim 5 \times 10^{-9}$ henry, and R_e is $\sim 2 \times 10^{-5}\ \Omega$.

b. Bulk Effects

If the bulk of the exciting current spreads out through the fluid and if the fluid reacts as if it were a rigid body (with frictionless contact at the walls), the equation of motion would be

$$\frac{\pi\rho a^4 \ell}{2} \frac{d^2\theta}{dt^2} = \int_0^\ell \int_0^{2\pi} \int_g^a r J_r(r,z)\, B_o r\, dr d\theta dz, \tag{58}$$

where g is the radius of the exciter.

The terminal voltage is given by

$$v_t = \int_g^a B_o r \frac{d\theta}{dt} dr. \tag{59}$$

Utilizing Eq. 58 and axisymmetry yield

$$v_t = \frac{2B_o^2(a^2-g^2)}{\rho a^4 \ell} \int_{-\infty}^{t} \int_{g}^{a} \int_{0}^{\ell} rJ_r(r,a)r\, drdzdt. \tag{60}$$

Thus, at the terminals, this appears to be a capacitor:

$$C_{HM} = \frac{\rho a^4 \ell}{2B_o^2(a^2-g^2) \int_{g}^{a} \int_{0}^{\ell} rJ_r r\, drdz}. \tag{61}$$

If J_r is assumed to be of the form

$$J_r = \frac{i_t}{(1-e^{\ell/L})\, 2\pi aL} \frac{e^{-(z/L)}}{r/a} \tag{62}$$

and if $\ell \approx L$, the result is

$$C_{HM} = \frac{2\pi a^4 \ell}{\mu_o C_o^2 (a^2-g^2)^2}. \tag{63}$$

It is demonstrated in Appendix K that if B_z is considered nonuniform, then this should be modified by replacing C_o^2 by the average C_o^2 on the cross section.

We have found that the equivalent circuit of a hydromagnetic resonator near resonance consists of a large capacitor and a small inductance. The inductance is of the order of the quasi-static inductance with zero magnetic field. The resonant capacitance, however, is approximately 30 times greater than the bulk hydromagnetic capacitance found in Appendix K.

$$C_{HM} = \frac{2\pi a^4 \ell}{\mu_o C_{Ave}^2}. \tag{64}$$

Notice that the functional dependence on dimensions and magnetic field is exactly the same for Eqs. 54 and 64. The bulk hydromagnetic capacitance of Eq. 64 assumes solid body rotation of the fluid and therefore represents an upper bound on the actual capacitance as seen from the terminals.

c. Step Response

Two cases may be distinguished in the response of a resonator to a step of current. The first case would occur if the losses are very low, that is, if conductivity is very high and viscosity is negligible. The exciting current would then tend to form a thin sheet near the exciter terminal and the principal effect would be an Alfvén wave. The voltage at the terminal would look very much as in Fig. 9.

On the other hand, if the medium were quite lossy, the terminal current would spread out over the column of the resonator and excite the whole mass of fluid

simultaneously. The principal effect would then be a hydromagnetic capacitance. Since some Alfvén wave would also be excited, the total response to a step of magnitude I at

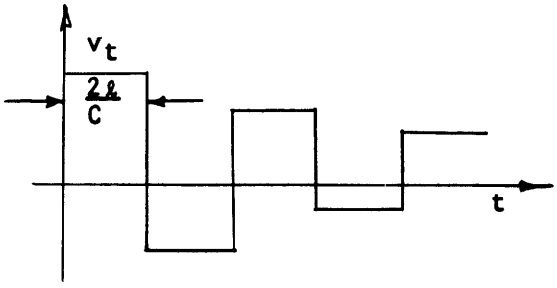

Fig. 9. Step response of a low-loss hydromagnetic resonator.

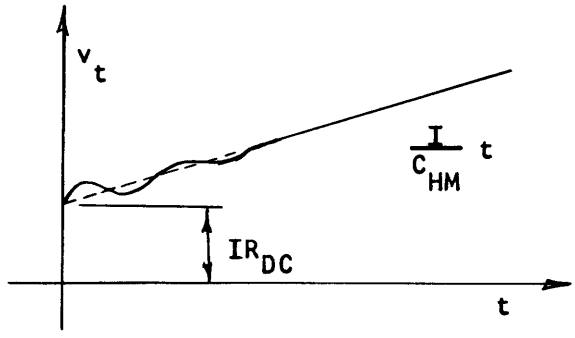

Fig. 10. Step response of a lossy hydromagnetic resonator.

the terminal should consist of a pedestal, because of the DC resistance, R_{DC}, of the fluid, a ramp attributable to the hydromagnetic capacitance, C_{HM}, and a damped sinusoid arising from the multiply reflected wave, as illustrated in Fig. 10.

2.3 NONUNIFORM MEDIA

Several types of nonuniform media problems may be considered. The conductivity, density, and magnetic field may be nonuniform, either singly or in combination. For example, several cases of nonuniformity may be considered for steady-state plasma experiments: (a) In a highly ionized gas of moderate density, the density distribution is governed by diffusion and therefore varies from a peak value near the center of a tube to a low value near the walls. The electron temperature and, therefore, the electrical conductivity is nearly constant except near the walls. (b) In a weakly ionized gas of moderate density, the ionized particle density is controlled by diffusion modified by the presence of neutrals. Neutral loading of the field lines by collision, however, tends to make the density appear nearly uniform. The electrical conductivity, on the other hand, is directly proportional to the electron density and, therefore, varies over the cross section. (c) In a partially ionized gas, both the effective density and conductivity may vary over the cross section.

All of these possibilities are important, to some extent, in various experiments. Here only two types of nonuniformity will be considered: (a) radial variation of density, and (b) radial variation of an axisymmetric longitudinal magnetic field. In both cases it is practical to limit discussion to only the axisymmetric, transverse, magnetic field modes. These are also the modes of greatest experimental interest.

a. Radial Variation of Density $\rho(r)$

Under the assumptions noted above, the equations for b_θ and e_z can be

found (Appendix B).

$$\frac{\partial}{\partial r}\left[\frac{1}{r}\frac{\partial}{\partial r}(rb_\theta)\right] + \frac{1}{i\omega\eta}\{\omega^2 - k^2[c^2(r)+i\omega\eta]\}b_\theta = 0 \tag{65}$$

$$e_z = \eta\frac{1}{r}\frac{\partial}{\partial r}(rb_\theta), \tag{66}$$

where

$$\eta = \frac{1}{\mu_o\sigma} \qquad \text{Magnetic diffusivity} \tag{67}$$

$$c^2(r) = \frac{B_o^2}{\mu_o\rho(r)} \qquad \text{Alfvén speed} \tag{68}$$

with the boundary conditions

$$b_\theta(a) = 0 \qquad \text{Insulating wall} \tag{69}$$

$$e_z(a) = 0 \qquad \text{Conducting wall} \tag{70}$$

Notice that Eq. 65 is the same as Eq. 10 with $n = 0$ and $\rho = \rho(r)$. Unless $\rho(r)$ is specified very simply, however, there is no known solution for (65).

b. Radial Variation of Longitudinal Magnetic Field $B_z(r)$

Since the various space derivatives of the magnetic field are related through the curl and divergence relations, a transverse component, B_r, must exist and both components must be functions of r and z.

$$\vec{B}_o(r,z) = \vec{i}_r B_{or}(r,z) + \vec{i}_z B_{oz}(r,z). \tag{71}$$

With σ and ρ constant, the equation for b_θ may again be found for axisymmetric TM modes (Appendix C).

$$\left(C_r^2+i\omega\eta\right)\frac{\partial}{\partial r}\left[\frac{1}{r}\frac{\partial}{\partial r}(rb_\theta)\right] + \left(C_r\frac{\partial C_r}{\partial r} + C_z\frac{\partial C_r}{\partial z}\right)\frac{1}{r}\frac{\partial}{\partial r}(rb_\theta)$$

$$+ C_rC_z\frac{1}{r}\frac{\partial}{\partial r}\left(r\frac{\partial b_\theta}{\partial z}\right) + \left(C_z\frac{\partial C_z}{\partial z} + C_r\frac{\partial C_z}{\partial r}\right)\frac{\partial b_\theta}{\partial z}$$

$$+ \left(C_z^2+i\omega\eta\right)\frac{\partial^2 b_\theta}{\partial z^2} + C_rC_z\frac{\partial^2 b}{\partial r\partial z} + \omega^2 b_\theta = 0, \tag{72}$$

where

$$C_r(r,z) = \frac{B_{or}(r,z)}{\sqrt{\mu_o\rho}} \tag{73}$$

$$C_z(r,z) = \frac{B_{oz}(r,z)}{\sqrt{\mu_o \rho}}. \tag{74}$$

Equation 72 appears to be extremely complex. Indeed it is not even separable. If, however, the magnetic field is assumed to be of a simple form with relatively weak variation, (72) may be considerably simplified (Appendix C).

The nonuniform magnetic field of the experiment was designed to be of the form (Appendix H)

$$B_{oz}(r,z) = B_o \sqrt{1 + (r/b)^2} \cos 2\pi \frac{z}{h} \tag{75}$$

$$B_{or}(r,z) = -\frac{B_o}{2\pi} \frac{h}{b} \frac{(r/b)}{\sqrt{1 + (r/b)^2}} \sin 2\pi \frac{z}{h} \tag{76}$$

which satisfies the curl relation exactly and the divergence relation approximately. With b and h suitably large compared with the range of r and z, and by making the assumption that the waveguide will respond in the main to some average property of the longitudinal magnetic field, we have

$$i\omega\eta \frac{\partial}{\partial r}\left[\frac{\partial}{\partial r}(rb_\theta)\right] + \left\{\omega^2 - k^2\left[C_z^2(r) + i\omega\eta\right]\right\} b_\theta = 0, \tag{77}$$

where effects due to the variation of C_z with z are also negligible (Appendix C). Notice that Eq. 77 is now identical to Eq. 65.

c. Perturbation Expansion

The solution of Eqs. 65 and 77 is quite difficult for even the simplest $c^2(r)$, since the result is complex hypergeometric functionals in which the unknown propagation constant, k, appears multiply. For more general $c^2(r)$, a closed-form solution is not possible. If, however, $c^2(r)$ may be expressed as a power series in r, then a perturbation expansion similar to those used in atomic physics[29] may be used. That is,

$$c^2(r) = c_o^2 \sum_{n=0}^{\infty} f_n \left(\frac{r}{b}\right)^n. \tag{78}$$

Thus, the $c^2(r)$ approximating the situation of (75) is given by $f_o = f_2 = 1$, $f_1 = 0$ and $f_n = 0$ for $n > 2$.

Since all boundary conditions will be evaluated at the radius, a, it is convenient to define an expansion parameter as

$$d = \frac{a}{b} \tag{79}$$

(so that d = 0 corresponds to a uniform field) and a normalized coordinate

$$x = \frac{r}{a}. \tag{80}$$

Then if the variables of interest are expanded,

$$c^2(x) = c_o^2 \sum_{n=0}^{\infty} f_n d^n x^n \tag{81}$$

$$b(x) = \sum_{n=0}^{\infty} b_n(x)\, d^n \tag{82}$$

$$e_z(x) = \sum_{n=0}^{\infty} e_n(x)\, d^n \tag{83}$$

$$k^2 = k_o^2 \sum_{n=0}^{\infty} P_n d^n. \tag{84}$$

Equating equal powers of d in (65) yields

$$\frac{i\omega\eta}{a^2} L(b_n) = k_o^2 \sum_{k=1}^{k} \left\{ b_{n-k} \left[\sum_{m=0}^{k} c_o^2 f_{m-k} P_m x^{k-m} + i\omega\eta P_k \right] \right\} \tag{85}$$

The equations represented by (85) are uncoupled from below, and thus may be solved sequentially. L is a linear differential (Bessel) operator defined as

$$L(b_n) = \frac{d}{dx}\left[\frac{1}{x}\frac{d}{dx}(xb_n)\right] + \frac{a^2}{i\omega\eta}\left[\omega^2 - k_o^2\left(f_o c_o^2 + i\omega\eta\right)\right] b_n. \tag{86}$$

Since $c^2(r)$ is symmetrical, $f_n = 0$ for n odd. It may then be shown that b_n, e_n, and p_n are also zero for n odd. Thus, for $c^2(r)$, by approximating Eq. 75, Eq. 85 becomes

$$\frac{i\omega\eta}{k_o^2 c_o^2 a^2} L(b_{2n}) = \sum_{k=0}^{n} b_{2(n-k)} \left[P_{2(k-1)} x^2 + P_{2k}\left(1 + \frac{i\omega\eta}{c_o^2}\right)\right]. \tag{87}$$

The expressions for k^2 derived from this expansion have been worked out to fourth order. For insulated walls,

$$k^2 = k_o^2 \left\{ 1 + \frac{\frac{1}{3} d^2}{\left(1 + \frac{i\omega}{2\omega_2}\right)} + \frac{\frac{1}{9} d^4}{\left(1 + \frac{i\omega}{2\omega_2}\right)^2} \left[1 + \frac{1}{5}\left(1 - \frac{24}{a^2}\right)\left(1 + \frac{i\omega}{2\omega_1}\right)\right] \right\}, \tag{88}$$

and for conducting walls,

$$k^2 = k_o^2 \left\{ 1 - \frac{\frac{1}{3} d^2}{\left(1 + \frac{i\omega}{2\omega_2}\right)} \left(1 + \frac{4}{a^2}\right) + \frac{\frac{1}{9} d^4}{\left(1 + \frac{i\omega}{2\omega_2}\right)^2} \left[\left(1 + \frac{8}{a^2} + \frac{16}{a^4}\right) - \frac{1}{5} \left(1 + \frac{7}{a^2} - \frac{192}{a^4}\right) \left(1 + \frac{i\omega}{2\omega_1}\right) \right] \right\}. \tag{89}$$

The form of these expansions strongly suggests that they derive from expanding an expression of the form

$$k^2 = \left(\frac{\omega}{c_o}\right)^2 \frac{1 + \frac{2\omega_1}{i\omega}}{f_\ell^2 + \frac{i\omega}{2\omega_{02}}}, \tag{90}$$

where

$$f_\ell^2 = \frac{1}{c_o^2 \pi a^2 \ell} \int_0^a \int_0^{2\pi} \int_0^\ell c^2(r) \frac{a}{2} \, dr d\theta dz. \tag{91}$$

That is, f_ℓ is a weighting factor on the field at r = 0 which represents taking a "linear" mean-square average of the field based on one-half the waveguide radius, rather than the volume mean-square average of the field given by

$$f_v^2 = \frac{1}{c_o^2 \pi a^2 \ell} \int_0^a \int_0^{2\pi} \int_0^\ell c^2(r) \, r \, dr d\theta dz. \tag{92}$$

An exact numerical evaluation of the expression (Eq. 88) for insulated walls agrees very closely with the linear type average (within 1%) over the entire frequency range of interest for an NaK experiment. Equation 89 diverges, however. This difficulty was traced to a singularity in the differential equation for e_z. The position of this singularity in frequency, radius, and expansion parameter may be predicted with accuracy by use of the "linear" average rms Alfvén speed to compute k. This was verified by an exact numerical evaluation of (89). Thus it may be concluded that for moderately nonuniform density or field, a liquid-metal Alfvén waveguide with either conducting or insulating walls behaves very much as if it were a uniform waveguide having linear average properties. In the final analysis, however, the correctness of linear averaging vs space averaging can only be settled by an experiment that must be precise, since the difference between the two kinds of averaging process should not amount to more than 4-6%.

III. EXPERIMENT

3.1 DESCRIPTION OF THE APPARATUS

Since the first prediction of magnetohydrodynamic waves by Alfvén,[2] in 1942, there has not been an experiment that demonstrated in a precise and unequivocal manner the properties of these waves. There has been no shortage of theoretical papers, but the formidable difficulties facing any experimenter in this area have kept the number of experiments small. These difficulties, such as those inherent in plasmas and the marginal electrical properties and reactivity of liquid metals, have limited these experiments to demonstrations rather than precise verifications of the properties of Alfvén waves. The experiment described here was undertaken as an attempt to rectify this situation. This experiment also provided a tool for verifying the results of the nonuniform field theory presented in Section II.

3.1.1 Resonator

The objective of the resonator design was to provide a cylindrical waveguide of large diameter and long wavelength. These objectives were, of course, subject to limitations imposed by the magnet that would be used and the pole tips that would be used in forming the nonuniform field. Basically the resonator structure is a cylinder, 12 inches in diameter and 4 inches deep, with provisions for filling with NaK (78% potassium, 22% sodium) and for injecting currents in order to excite the various waves of interest.

The shell of the resonator, Figs. 11 and 12 (shown with the nonuniform-field pole tips), was constructed of 1/4" thick, nonmagnetic stainless steel, Heliarc welded throughout to eliminate the possibility of NaK leaking out or air leaking in. It was built in two almost identical mating parts in order to be compatible with the nonuniform pole tips (Figs. 11 and 12). The two halves of the resonator are sealed with a neoprene O-ring on the rim. The interior cylindrical wall is lined with a sheet of oxygen-free copper, 1/8" thick, to approximate a perfectly conducting boundary condition for the wave. The end walls are coated with a layer of cured "Eco-Bond" epoxy, 1/16" thick, to provide an insulated (open-circuit) termination at either end of the resonator. Filling and draining of the NaK is accomplished through two dry seat stainless-steel valves mounted at opposite sides of the shell on the rim. Pipes from the valves are welded into the wall at one end and directly opposite one another.

Electrical contact with the conducting fluid is made through ceramic and stainless-steel stand-off connectors (ADVAC 450-ES) welded into the shell at each end. An oxygen-free copper rod welded to the end of each connector extends through the steel wall and epoxy layer. It is threaded to accommodate various types of exciters. In this experiment, a disk, 1/16" thick and 2" in diameter, insulated except for the edge, was used on each end. Two copper bars, insulated from the shell, terminating near the rim, conduct the excitation current to the center post of the connector and to the shell around the connector to ensure a symmetric current distribution. Current injected by the disk

Fig. 11. Resonator and nonuniform field pole tips.

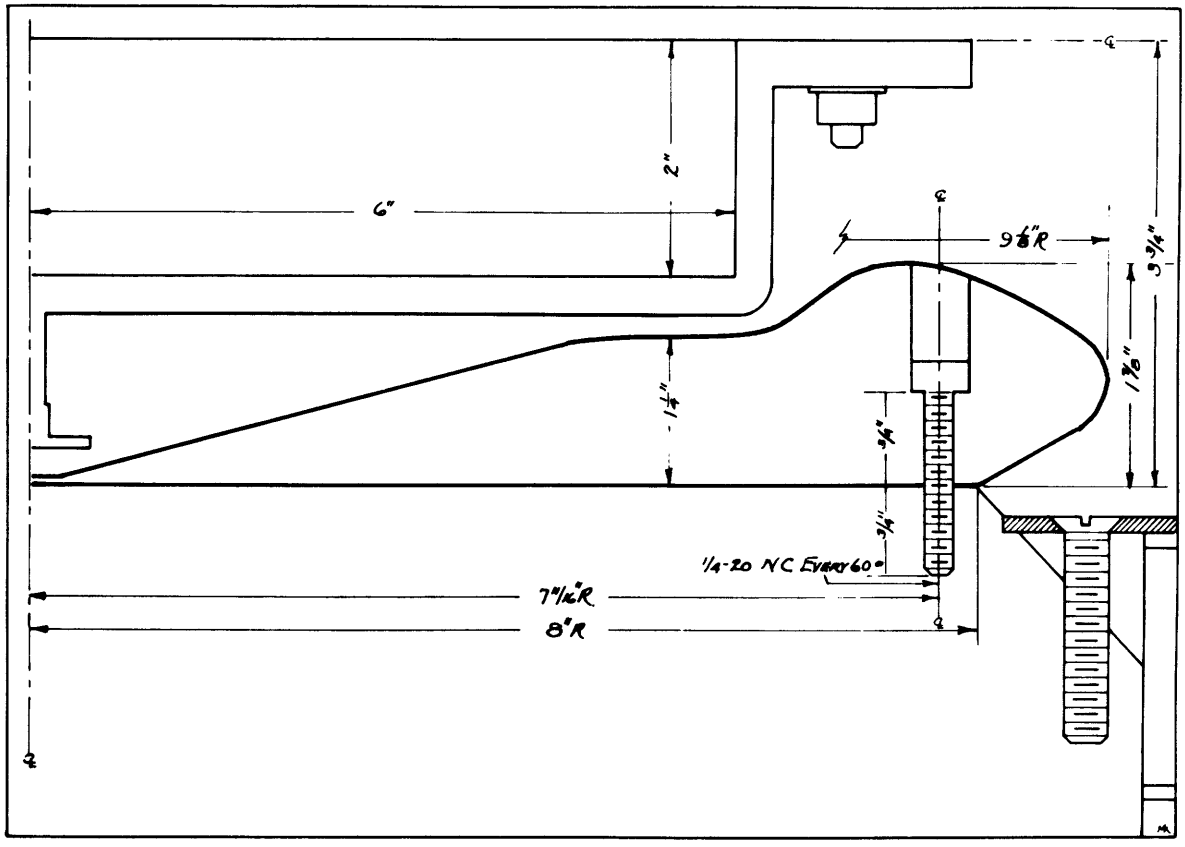

Fig. 12. Cross section of the magnet pole, nonuniform field pole, tips, and the resonator.

is collected on the copper wall and returned through the steel shell.

3.1.2 Electronic Systems

The arrangement of the main components of the electronics systems are diagrammed in Fig. 13. The physical layout is shown in Fig. 14. The primary excitation of the entire system is provided by an HP 202A low-frequency function generator whose frequency is monitored by a Berkely "EPUT" meter counting on a crystal-controlled 10-second interval. Thus for the range of interesting frequencies, measurements may be made to ±0.1 cps or less than ±0.1%. When the apparatus had been warmed up for 30 minutes, the combined drift of the oscillator and counter could not be detected in a 1-hour interval. The counter itself was calibrated against an oven-stabilized HP 524B counter and was found to have no detectable long-time drift.

The output of the oscillator is the input of a high-current, low-voltage amplifier specially designed and built for this application. This amplifier will provide a current of approximately 200 amps peak-to-peak to a load of 200 mΩ, or less, over a frequency range of 1-2000 cps. The amplifier output section consists of 18 power transistors, in two banks of 9 each, operating in class B push-pull. Power supplies for the amplifier

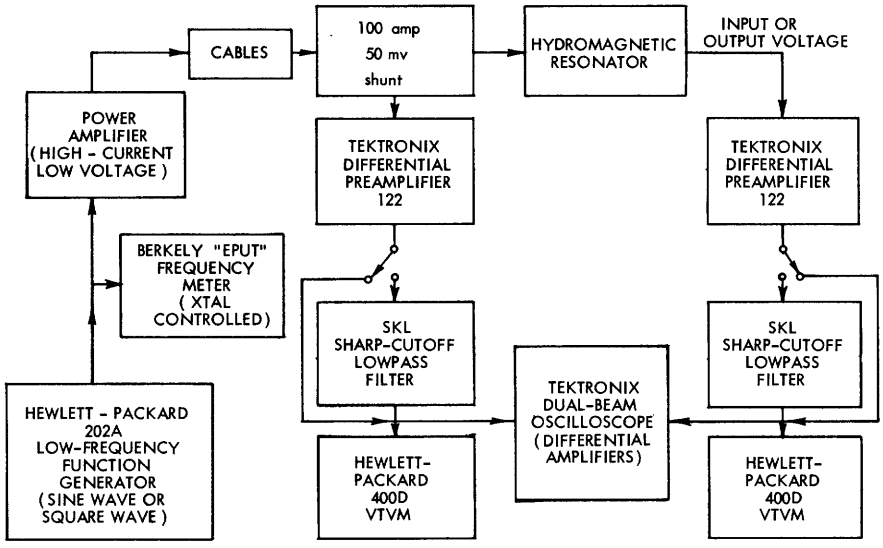

Fig. 13. Electronic systems block diagram.

were a set of four 2-volt marine storage batteries and two electronically regulated low-voltage power supplies for the input stages. The storage batteries were sufficiently robust to allow full-power operation of the amplifier continuously for several hours. The output of the amplifier is fed to the resonator through two cables made of paralleled lengths of copper braid. The combined output resistance of the amplifier and the resistance of the cables and contacts amounted to some 5 mΩ. The DC resistance of the resonator input $\approx$0.1 mΩ. Thus for direct-current operation the amplifier and cables appear to the waveguide to be a current source. The wave impedance computed from Eq. 53 is in the vicinity of 1-10 $\mu\Omega$. Therefore, for Alfvén waves, the driving system appears to be a quite good current source (within 0.2%, at worst).

The driving current is measured with a standard 100-amp, 50-mv instrument shunt inserted in one of the cables. The shunt voltage and the input or output voltage of the resonator are both monitored with Tektronix Type 122 differential preamplifiers. Differential inputs are used to minimize the effects of ground loops, stray currents, 60-cycle pickup, commutator hash from the magnet generator, lead vibration and potential differences on the resonator case. To reduce the effects of lead vibration in the intense magnetic fields required for the existence of Alfvén waves, the high-current leads were bound together as tightly as possible and wrapped with vibration damping material. The voltage pickup contacts were made directly on the connectors at the center of the resonator and rigidly taped down while inside the field.

The single-ended output of the differential preamplifiers is then fed through Spencer-Kennedy Laboratories 200-cps sharp cutoff lowpass filters, displayed on a dual-beam Tektronix oscilloscope and measured with Hewlett-Packard 400D vacuum tube voltmeters. When step excitation is being used, the SKL filters are by-passed. With all units operating, the residual effective noise level was approximately 50 μv of 120 cps,

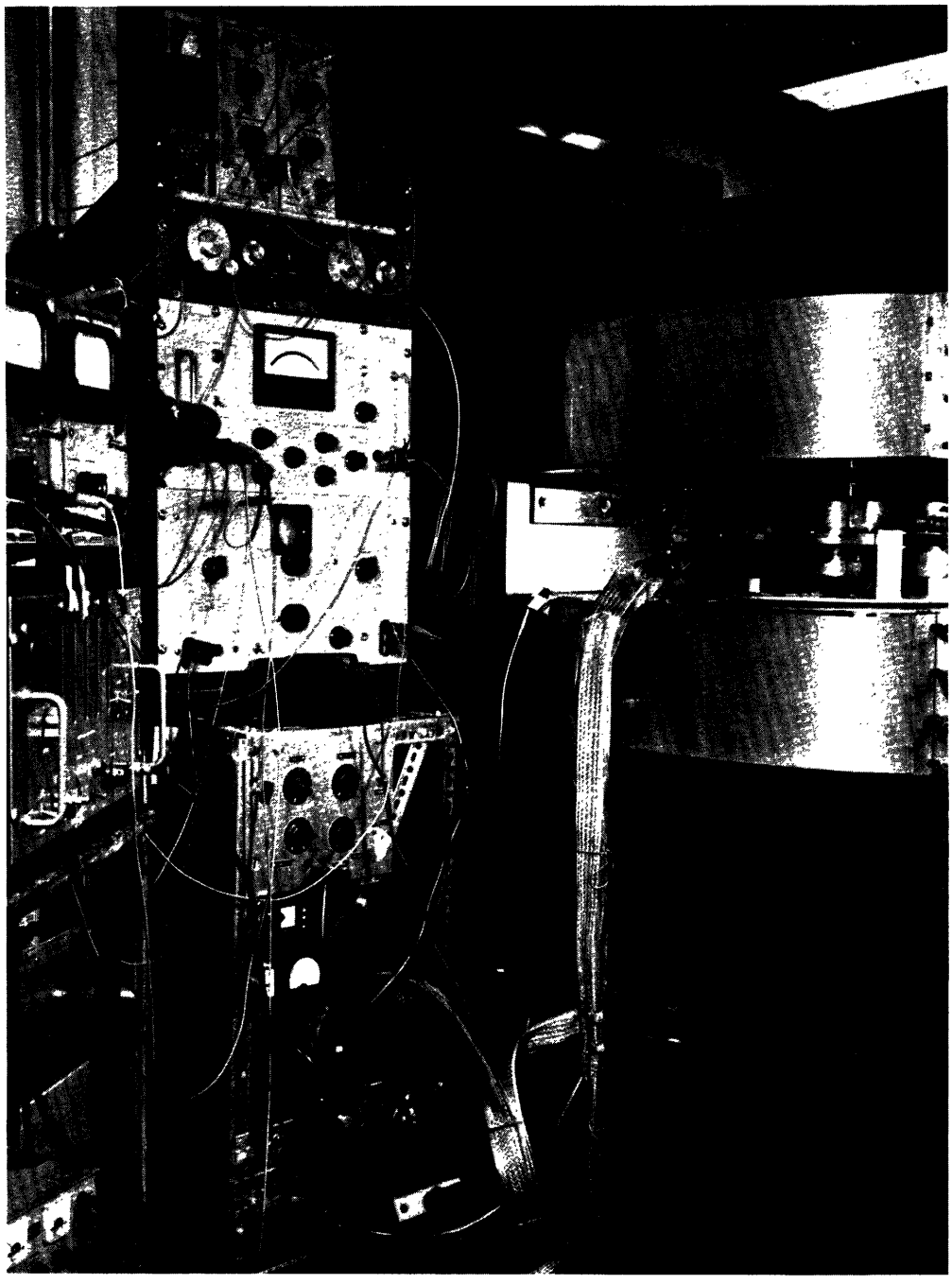

Fig. 14. Physical arrangement of the apparatus.

which was apparently due entirely to the preamplifier power supplies. Thermal noise was negligible. The SKL filters are used to reduce the effect of third-harmonic cross-over distortion in the power amplifier.

3.1.3 Magnetic Field

The magnetic field was supplied by a Pacific Electric Motor Company iron core magnet. The working volume of the magnet is a cylinder, 16" in diameter and 7 1/2" deep. The principal field is aligned parallel to the axis and is vertical. The cross section of a pole face is shown in Fig. 11. The magnet was designed to provide a maximum field of approximately 8500 gauss without pole tips for short periods with water cooling. Safety considerations dictated that kerosene be used as a coolant with some degradation of performance. A field current of 400 amps was required and was supplied by a rebuilt motor-generator set which was available. This field strength is enough to be in the region of Alfvén waves. It was found, however, that by precooling the coils and pushing the generator to a maximum output of approximately 525 amps, a field of up to 10,700 gauss could be obtained for a few minutes. Heating was so strong at these power levels that the coil resistance increased rapidly, thereby reducing the current. A plot of magnetic

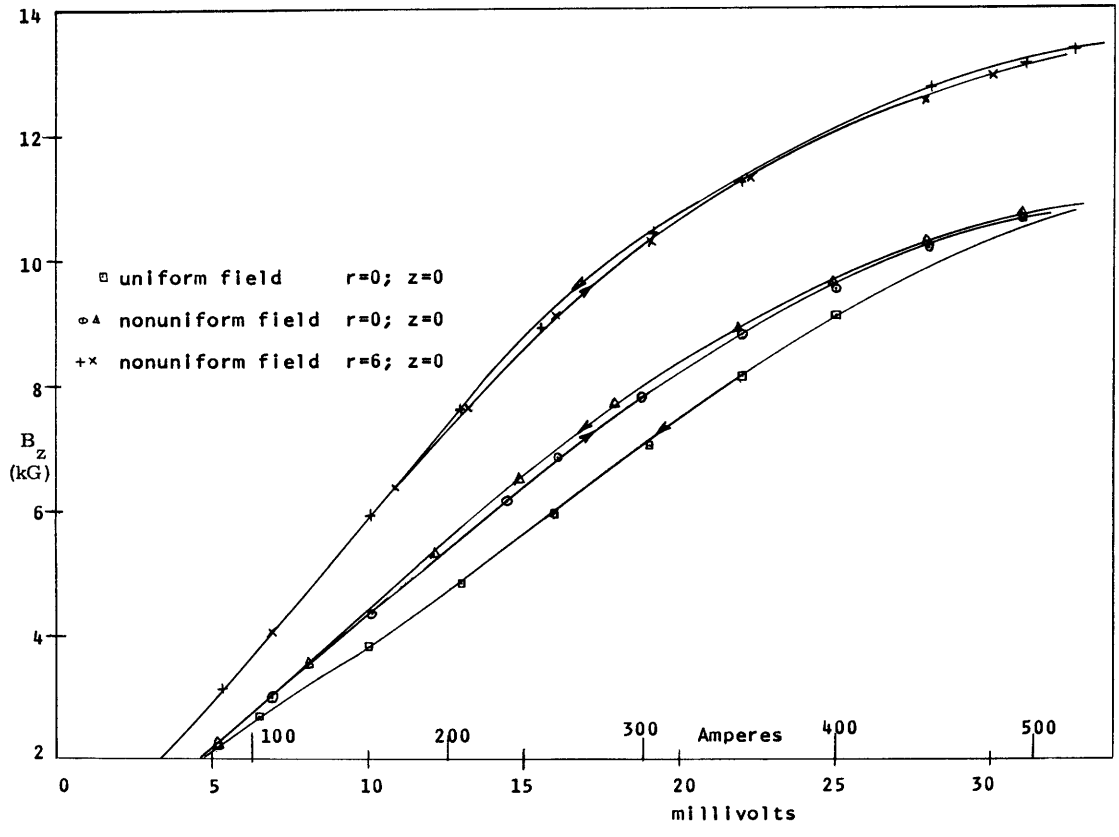

Fig. 15. Saturation curves for uniform and nonuniform fields.

field as a function of current is presented in Fig. 15 (also millivolts across an 800-amp, 50-mv shunt). Over the central region of the field ($0 < r < 6"$, $-2" < z < +2"$) it varies less than 5% in radius and less than 0.9% in height. The effect of the iron yoke was examined and found to be negligible.

The nonuniform field was obtained by the use of shaped pole tips made of 100% pure iron (Armco) to minimize saturation effects. The contour of the pole tips was selected to yield a longitudinal (B_z) field that varied as in Eq. 75, with the smallest possible variation in the z direction and a minimal radial (B_r) field, while keeping the largest possible variation of B_z in the radial direction. Typical results are illustrated in Fig. 16 with the fitted prediction of Eqs. 75 and 76 for comparison. A plot of B_z at r = 0" and at r = 2" as a function of magnet current is shown in Fig. 15. The hysteresis effect is also shown.

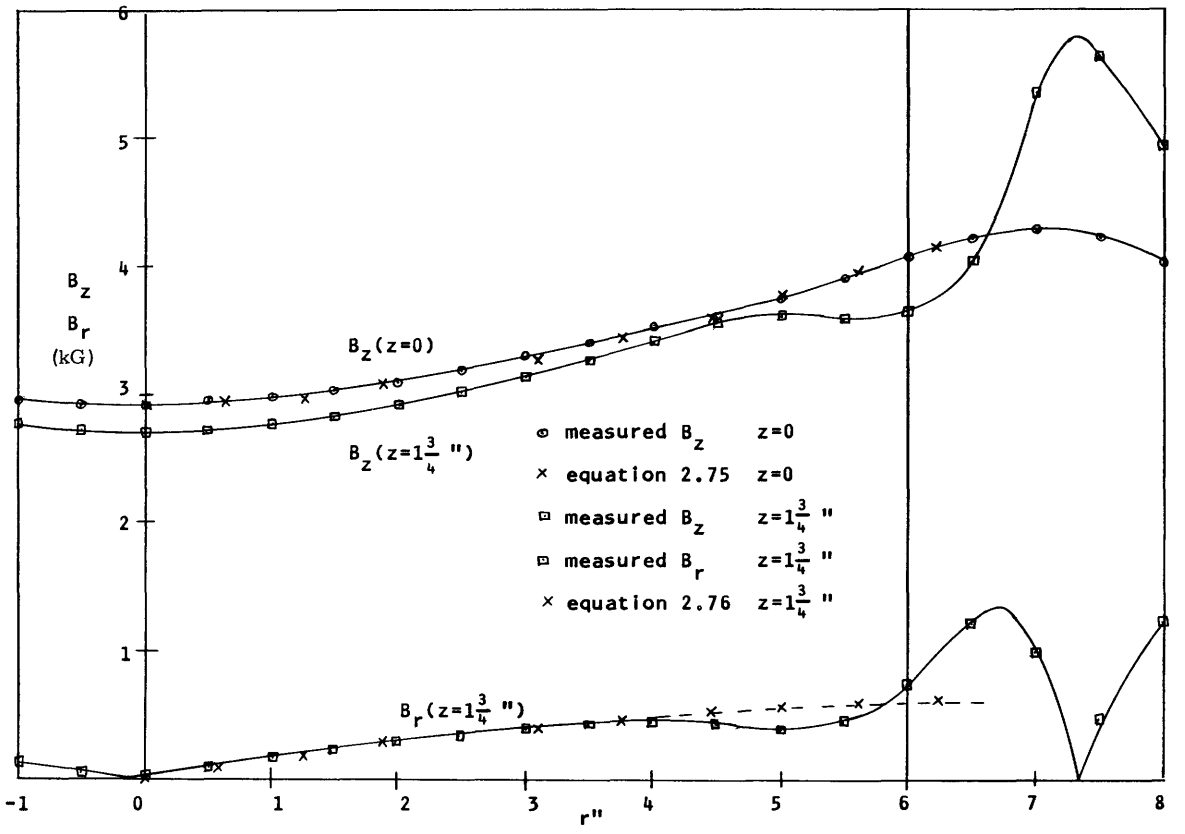

Fig. 16. Radial variation of B_z and B_r.

When uniform fields were being used, the resonator was mounted on an aluminum stand so that its center was exactly at the center of the field volume. That is, z = 0, r = 0 was 3 3/4" from the pole faces. When a nonuniform field was being used, the resonator was held by brass screw jacks bearing on the pole tip mounting screws. Magnet current was measured by a Leeds and Northrup

potentiometer and an 800-amp, 50-mv shunt.

3.2 EXPERIMENTAL PROCEDURES

3.2.1 Resonance Measurements

Before starting a resonance frequency measurement, the magnet was precooled from 1 1/2 to 2 hours to make certain that the copper coils had reached minimum temperature. All electronic systems were turned on, allowed to warm up, and thoroughly checked for malfunctions and drift.

To start a run, the resonator drive current was set to 22 amps rms and monitored to be sure it remained constant during the run. The magnet was turned on a allowed to stabilize at the highest possible current. The current was then reduced to 31.05 mv as indicated on the potentiometer, and allowed to drift downward to 30.95 mv as the coils heated. This meant that approximately 15 seconds were available in which to find the peak of the resonance curve in the output voltage by scanning the HP function generator frequency. The current was then reduced to 29.05 mv, and the measurement repeated. This procedure was repeated until a resonance could no longer be detected. Smaller steps were not taken, because of a total time limitation imposed by the temperature rise of the magnet. In order to eliminate the effects of hysteresis, the current was always reduced in a continuous fashion so that only the upper branch of the hysteresis curve was used.

These runs were repeated in a period of 3 days with several hours between runs. This was done to allow for adequate precooling of the magnet, to make sure that chance circumstances were not affecting the data and to get a measure of how much all of the indeterminate factors contributed to scattering of the data.

3.2.2 Step Response

Step response was obtained by using the square-wave output of the function generator at low frequency (≈10 cps). Polaroid Land camera photographs were taken of the input and output voltage waveforms for decreasing magnetic fields.

In order to examine the Alfvén wave part of the waveform more closely, the output signal was fed to one side of the oscilloscope differential amplifier and a highpass filtered version of the current waveform was fed to the other. By adjusting the time constant of the filter (incorporated into the Tektronix preamplifier) and its amplitude, the ramp could be subtracted out. The remaining damped sinusoid was then expanded and amplified for close observation and recording.

3.2.3 Field Measurements

All field measurements were made with a Rawson-Lush rotating-coil gaussmeter. The curves presented in Fig. 15 were obtained by carefully centering and aligning the gaussmeter probe and rigidly fixing it in the magnetic field. The field was then varied as in the resonance measurements. Complete profiles of the magnetic field were made

by sliding the gaussmeter along a calibrated wooden track aligned on a radius, wedged and levelled at various heights. The precision of the magnet current setting was relaxed to ±0.1 mv, because of the necessity for a longer measurement interval and the low sensitivity of the gaussmeter indicator, as compared with the digital-frequency measurement. Small resetting of the current was allowed, but hysteresis did not show up in the data.

3.3 SUMMARY OF RESULTS

The results of the experiments fall into several distinct groups: resonance frequencies, total step response, Alfvén wave part of the step response, and

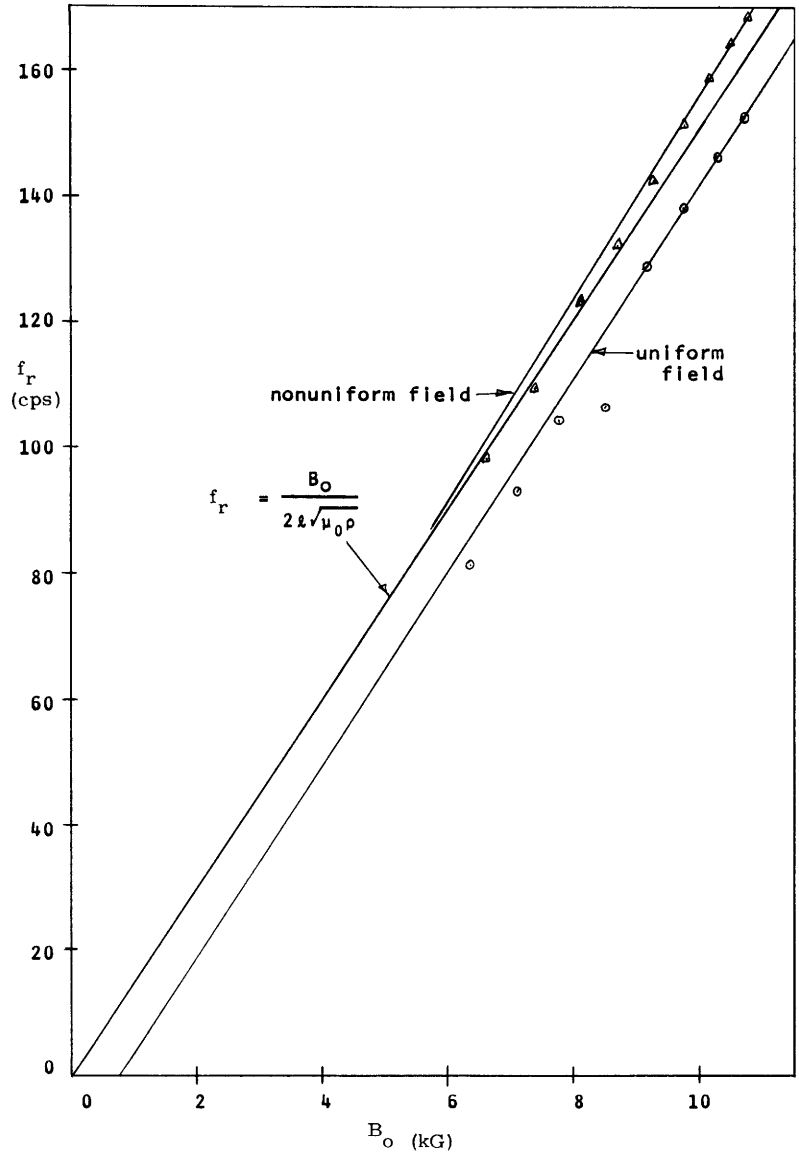

Fig. 17. Half-wave resonance frequencies as measured.

Table 1. Data for Uniform Field.

B_o (kgauss)	f_r (cps)	Average deviation (%)
10.70	152.9 ± 0.5	0.3
10.25	146.3 ± 0.4	0.3
9.72	138.0 ± 0.3	0.2
9.16	129.0 ± 0.8	0.6
8.50	106.2 ± 0.8	0.7
7.85	104.1 ± 0.4	0.4
7.10	93.0 ± 0.3	0.3
6.35	81.1 ± 0.6	0.7
	Run Average	0.4%

Table 2. Data for Nonuniform Field.

B_o (kgauss)	f_r (cps)	Average deviation (%)
10.76	168.8 ± 0.7	0.4
10.50	164.7 ± 0.7	0.4
10.13	158.8 ± 1.0	0.6
9.72	151.7 ± 0.7	0.5
9.25	142.2 ± 1.2	0.8
8.70	132.8 ± 0.7	0.5
8.10	123.4 ± 0.9	0.7
7.38	109.5 ± 1.2	1.1
6.60	98.0 ± 0.6	0.6
	Run Average	0.6%

magnetic-field maps.

The half-wave resonant frequency is plotted in Fig. 17 for both uniform and nonuniform magnetic fields. For nonuniform fields, the abscissa is the longitudinal field at r = 0, z = 0. Each point represents the average of data from 5 runs taken over a period of 3 days and spaced several hours apart. The data used in Fig. 17 are also given in Tables 1 and 2. The average deviations referred to in these tables are computed as linear average magnitude differences between the individual measurements and their linear average.

Several examples of step (square-wave) response are shown with their exciting

currents in Fig. 18. Figure 18a displays some typical input voltages. The pedestal, ramp and damped oscillation are clearly visible. Figure 18b is similar, but for output

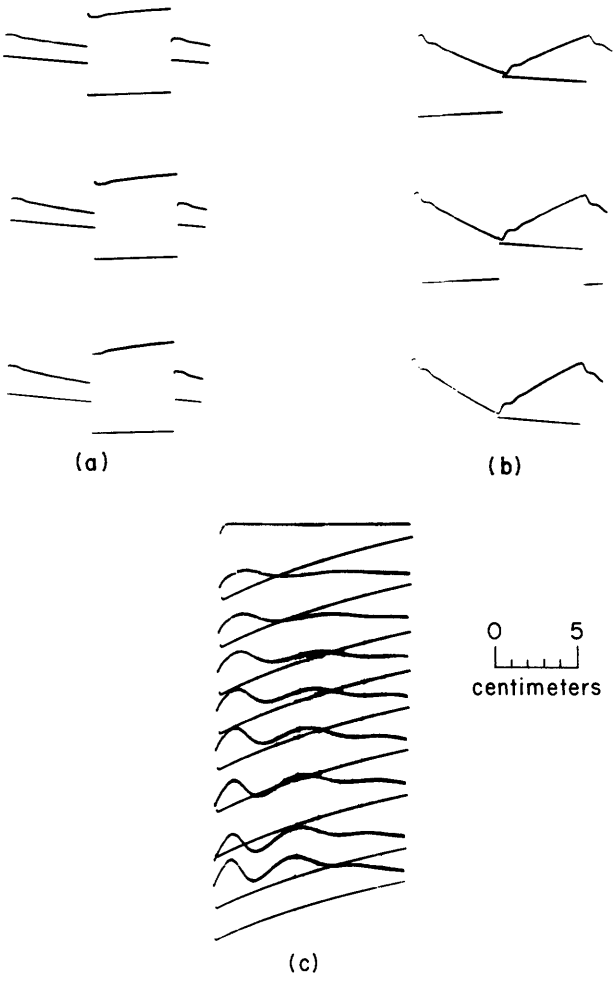

Fig. 18. Step response at various magnetic fields (see Table 3). (a) Input voltage. (b) Output voltage. (c) Output voltage with ramp subtracted.

voltages. In this case no pedestal is observed because the diffusion of the driving current did not reach the output terminals in any significant amounts. Figure 18c shows a set of the step responses at the output terminals with the ramp part approximately subtracted out, the resultant signal being greatly expanded and amplified. The first nine from the bottom were taken at intervals of 2 mv, as indicated on the magnet potentiometer, starting with a maximum of 31. The top trace is for zero field. The arrival time of the wave front is the first negative dip after the step. Data pertaining to Fig. 18 are given in Table 3. All of the samples shown are for uniform fields. Pictures taken with nonuniform fields are identical in character, differing only in some of

Table 3. Step-excitation data.

Figure 18a

Vertical 3.62 mv/cm. Horizontal 10 msec/cm.

Trace 1	B_o = 10.58 kgauss
2	10.00
3	9.15

Figure 18b

Vertical 1.45 mv/cm. Horizontal 10 msec/cm.

Trace 1	B_o = 10.00 kgauss
2	9.15
3	8.15

Figure 18c

Vertical 0.362 mv/cm. Horizontal 2 msec/cm.

Trace 1	B_o = 10.68 kgauss
2	10.48
3	9.73
4	9.15
5	8.53
6	7.82
7	7.18
8	6.35
9	0.00

the relative dimensions. The drive current is 44 amps peak-to-peak in all cases.

Data relating to the magnetic fields consist of Figs. 15 and 16, and several field maps that are shown in Appendix H.

IV. ANALYSIS OF THE RESULTS

4.1 COMPARISON OF EXPERIMENT AND THEORY

The results of the experiment summarized in Figs. 17 and 18 reveal quite strikingly the ability of small-signal hydromagnetic theory to predict the qualitative and quantitative aspects of the hydromagnetic waveguide performance. Since the step-response measurements were made primarily to give assurance that an Alfvén wave did indeed exist rather than to obtain precision data, step response will be dealt with first.

4.1.1 Step Response

If the slope of the voltage ramp in Fig. 18a and the given driving current is used in Eq. 93, which describes the terminal behavior of the resonator,

$$V_t = IR_{dc} + \frac{I}{C_{HM}} t, \tag{93}$$

the hydromagnetic capacitance may be computed as 86 farads. Since this value depends on lengths scaled from the photograph, this must be taken as an indication of the range of the capacitance, rather than as an accurate or reliable figure. The field for this measurement was 1.07 webers/m^2, corresponding to an Alfvén speed of 32.5 m/sec. If this value of Alfvén speed is used in Eq. 64, the "rigid-body" hydromagnetic capacitance is C_{HM} = 475 farads. This predicted capacitance is 5.5 times the measured value. It must be borne in mind, however, that the rigid body C_{HM} is only an upper bound and must be reduced to account for inefficiency of coupling between strongly excited parts of the fluid and weakly excited parts both in radius and in length. It was also assumed that, because of considerations of electromagnetic skin depth relative to the resonator length, a reasonable fraction (e^{-1}) of the exciting current reached the opposite end. The evidence of Fig. 18b indicates that this is not the case. Thus only a fraction of the fluid is directly excited.

Figure 19 is a log-log plot of transit time of an Alfvén waveguide of various lengths and of Alfvén speed as a function of magnetic field. The measured length of the resonator is 10.32 cm. At a field of 10.68 kgauss, as in trace 1 of Fig. 18c, the transit time is approximately 3.4 msec. In Fig. 18c, the time from the initiation of the step to the peak of the signal arriving at the opposite end is almost exactly 4 msec. An examination of Fig. 9 indicates that the arrival time of the leading edge of the step should be assigned, more properly, to the zero crossing rather than to the peak, and this occurs at approximately 3.2 msec. The succeeding traces show the peak (and zero crossings) occurring at proportionately later times as the field is decreased. Note also that the peaks become rapidly dispersed as the field decreases, in harmony with the theoretical prediction that the upper critical frequency, ω_2, rapidly approaches the lower critical frequency, ω_1, thereby erasing the Alfvén region.

The evidence of the step-response measurements quite conclusively affirms the

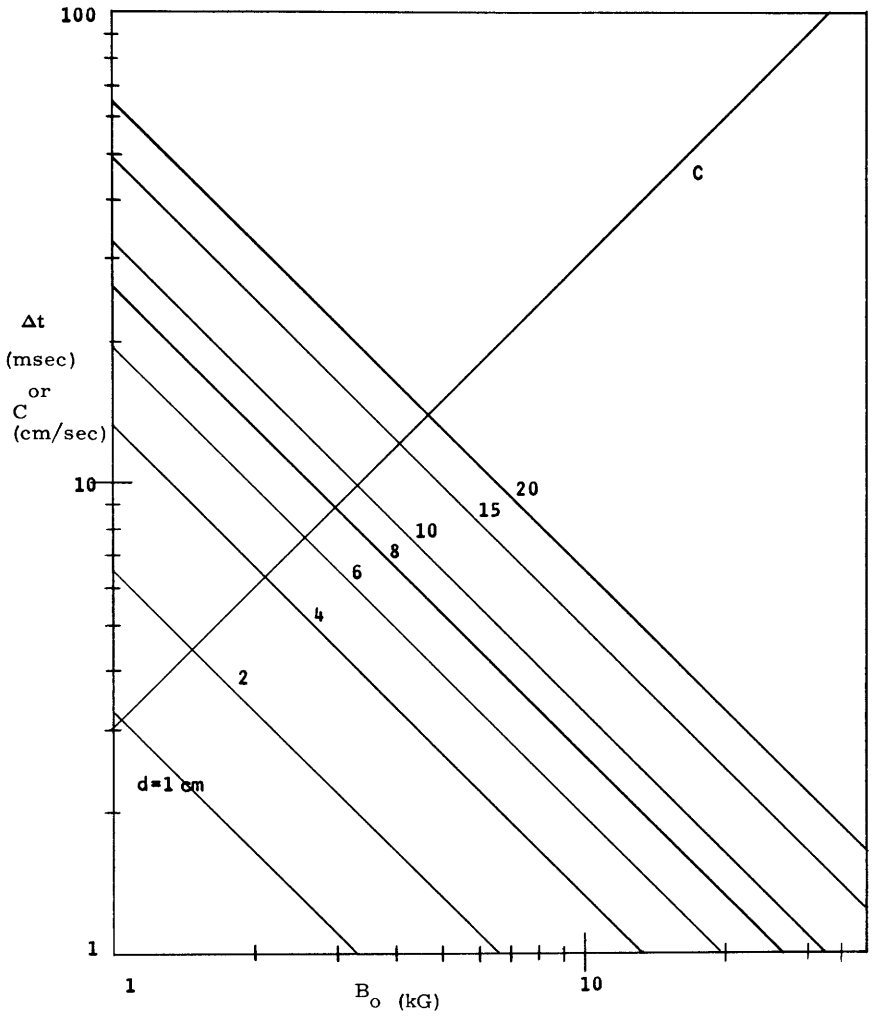

Fig. 19. Transit times and Alfvén speed for NaK (22-78).

existence of a hydromagnetic capacitor and an Alfvén wave both qualitatively and quantitatively. These measurements are, however, clearly not of sufficient precision to be used for comparison with the resonance measurements.

4.1.2 Resonance

In the plots of Fig. 17, there are several features of interest. First, the slope of the f_r vs B_o line for uniform fields is undoubtedly straight and parallel to the line based on the lossless case ($\sigma=\infty$).

$$f_r = \frac{c}{2\ell} = \frac{B_o}{2\ell\sqrt{\mu_o \rho}}. \tag{94}$$

Second, it is offset by a constant 10 cps. Third, the deviation from a straight line because of the proximity of f_1 (or f_2) occurs sooner than predicted. Before continuing

with detailed comparisons of theory and experiment, it is necessary to examine the physical constants used to obtain the theoretical predictions.

Unfortunately, physical data on NaK (22% sodium, 78% potassium) is sparse and conflicting. The only sources of data are the Liquid Metals Handbook[31] and the only present supplier of NaK. Data in the Liquid Metals Handbook (LMH) comes principally from the supplier, Mine Safety Appliances Corp., Callery Division. Figure 20 is a plot of density of

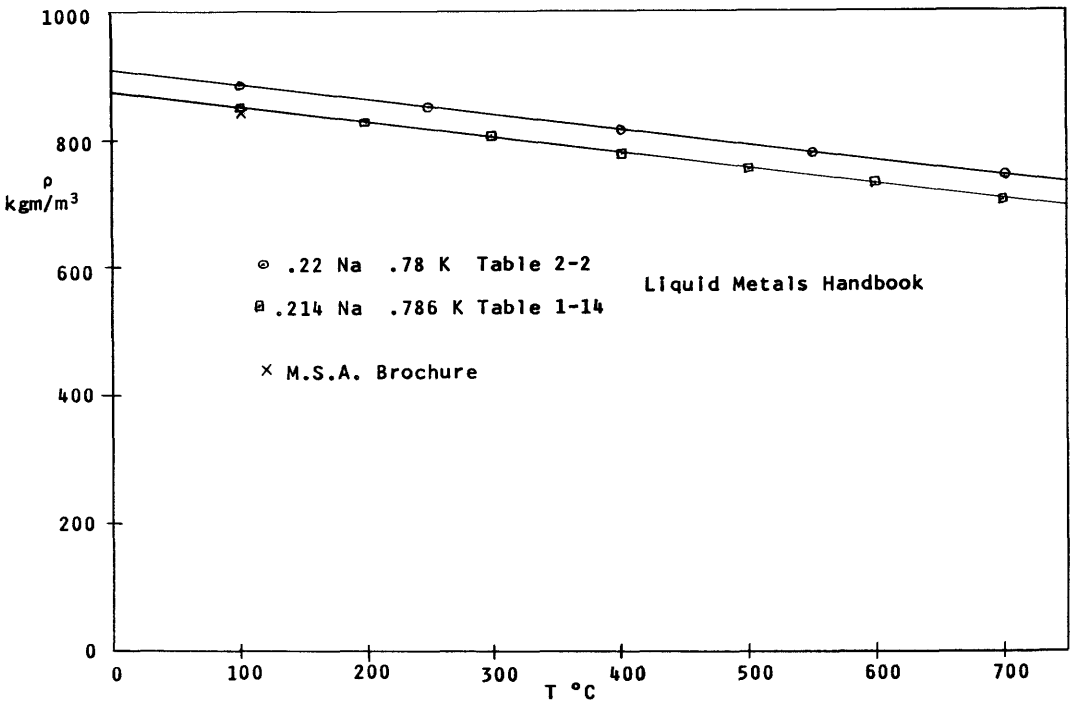

Fig. 20. Density of NaK as a function of temperature.

NaK (22-78) as a function of temperature. Figure 21 is a semi-log plot of electrical conductivity as a function of temperature. It is evident that although the precision of these measurements is high, there are constant differences and no criteria for determining which set of data might be correct. In a brochure, the supplier gives the values indicated in Figs. 20 and 21 by an "x." Since the x-value corresponds to the lower line in Fig. 20, it is assumed that this leads to the correct density, which is taken to be 868 kgm/m^3 at 20°C. The situation in regard to conductivity is not as clear, as the manufacturer's data falls midway between those given in LMH which differ by 25% at room temperature. All calculations were made on the basis of the poorest conductivity, $\sigma = 2.41 \times 10^6$ ℧/m at 20°C.

Referring to Fig. 17, the slope of f_r as a function of B_o agrees closely with that predicted. The only physical parameter involved is the density for which two of three published values agree. Thus it may be concluded that this aspect of the theory is proved within a precision of ±1/2%.

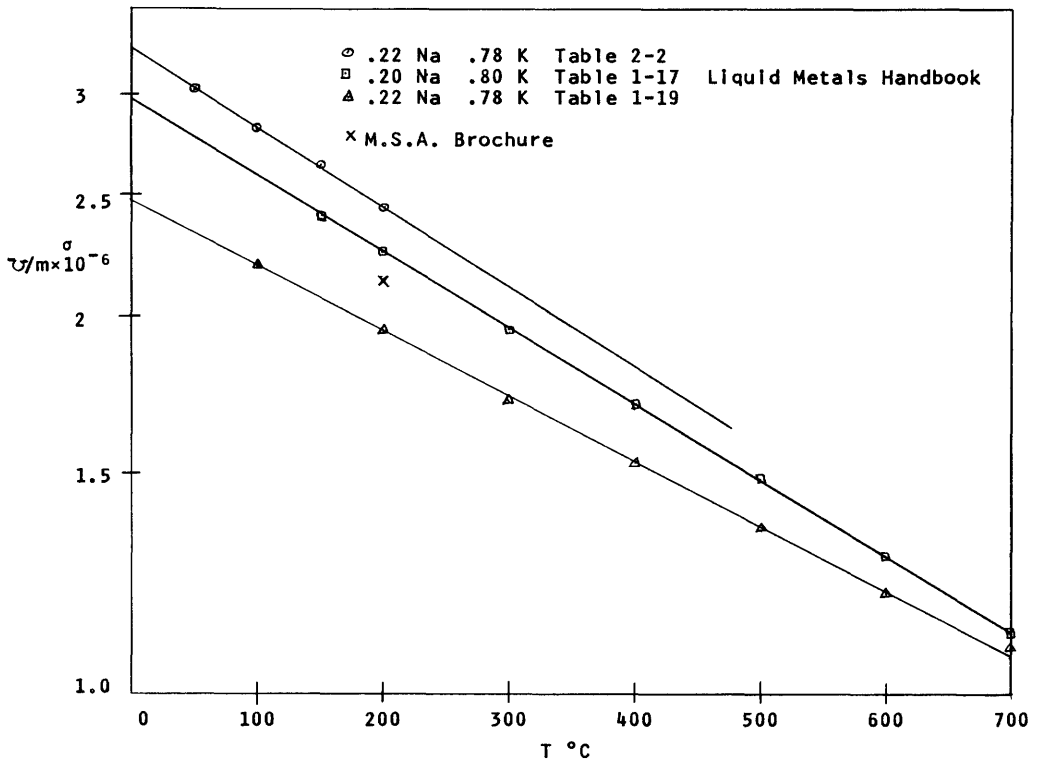

Fig. 21. Electrical conductivity of NaK as a function of temperature.

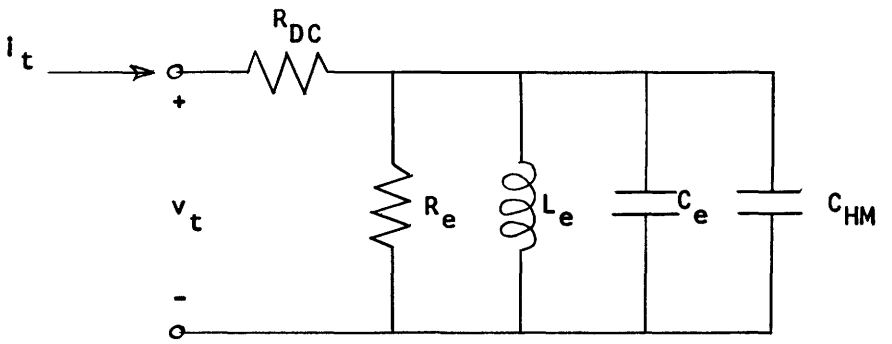

Fig. 22. Total resonator equivalent circuit.

To account for the constant offset, recall that two phenomena are taking place in the resonator simultaneously: the Alfvén wave, and hydromagnetic bulk energy storage as a capacitor. Since this is the case and currents resulting from each phenomenon add at the terminals, it is reasonable to take the equivalent circuit of the total resonator as shown in Fig. 22. Now the resonant frequency f_r is given by

$$f_r = \frac{1}{2\pi \sqrt{L_e(C_e+C_{HM})}}, \tag{95}$$

where L_e, C_e, and C_{HM} are given by Eqs. 54, 55 and 64. The effect of the hydromagnetic capacitance, C_{HM}, is then to decrease the resonant frequency as observed. It is important to note that the Alfvén and hydromagnetic capacitances depend in exactly the same way on the magnetic field and fluid density. If it were otherwise, the offset could not possibly be constant as observed. Subtracting the hydromagnetic capacitance as computed from Eq. 64 predicts a resonance frequency that is much too high, but using the measured value of C_{HM} brings the measured resonance frequency within 3 cps of that predicted. Closer agreement should not be expected, because of the uncertainties in the measurement of C_{HM}.

The deviation from a straight-line characteristic of the approach of f_2 with decreasing field does not occur. A deviation more like the proximity of f_1 does occur, and at a higher frequency than expected from the most pessimistic conductivity figure. The apparent contradiction of this qualitative aspect may be due to a small jump in the data at 7.7 kgauss, which at present is unexplained. A similar effect occurs in the nonuniform field measurements at 9.5 kgauss.

4.2 COMPARISON OF UNIFORM AND NONUNIFORM FIELD RESULTS

The perturbation expansion method for solving the wave equation with variable Alfvén speed suggested that, under the stated assumptions, an Alfvén waveguide with nonuniform properties would behave as if it were uniform with averaged physical parameters, these averages not being the normal space average but a "linear" average based on one half of the waveguide radius. Figure 17 demonstrates that the resonator in a nonuniform magnetic field is indeed responding to an average of the longitudinal field. The apparent lack of offset in the nonuniform field curve is due to using the field at $r = 0$ as the abscissa, rather than the average field, since the proper average has yet to be determined.

In order to differentiate between the two kinds of averages, the following procedures were used in the treatment of the data. Direct comparison of experiment and theory was not advisable, because of uncertainties in the available physical data on NaK. Also, there is a certain amount of variation of the nonuniform field distribution in space resulting from approaching saturation in the pole tips. To eliminate or minimize the problems of uncertain physical parameters, the nonuniform field measurements are

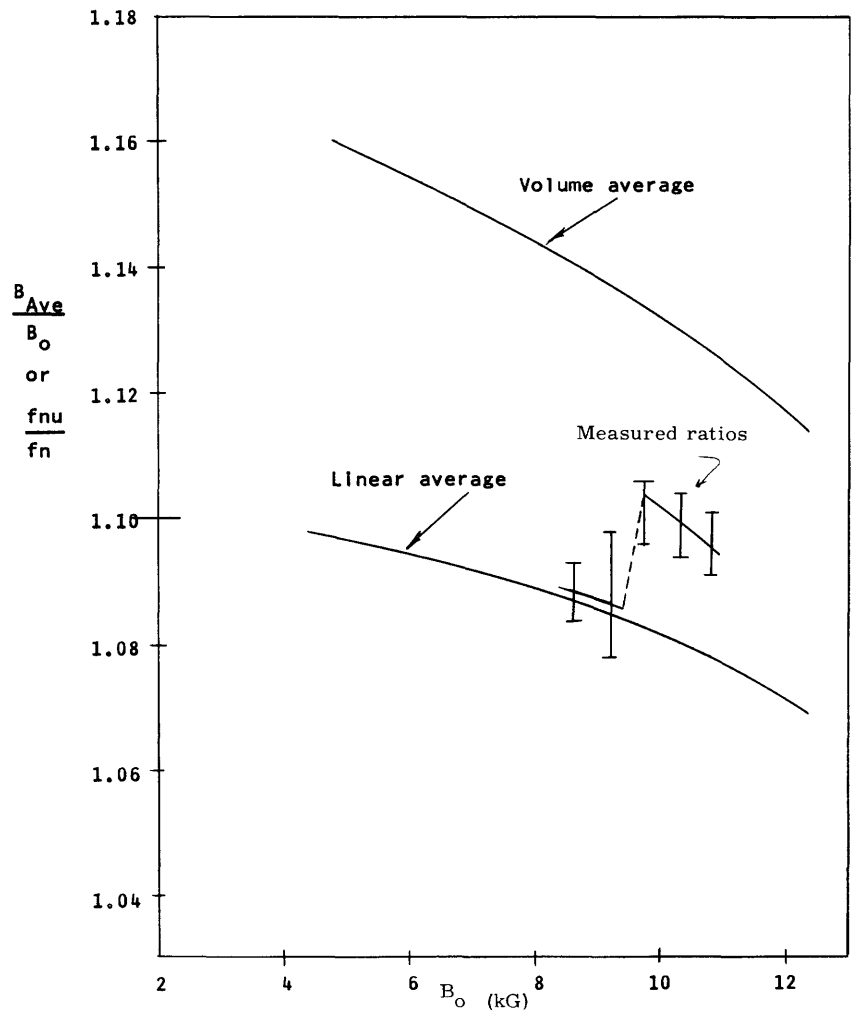

Fig. 23. Ratio of nonuniform to uniform resonance frequencies and average fields.

compared with uniform field measurements made at a field strength equal to that at r = 0, z = 0 in the nonuniform field. Thus the ratio of the resonant frequencies should be in the same ratio as the proper average field to the field at r = 0, z = 0. Since, on account of saturation, the fields are not exactly described by Eqs. 75 and 76, the actual measured field distributions were numerically integrated by Simpson's rule according to the two kinds of averages (Eqs. 91 and 92). The ratios of the average field to the field at r = 0, z = 0 (B_o) are plotted in Fig. 23 as a function of B_o. Both curves dip downward because saturation tends to make the field more uniform.

The ratio of the resonant frequencies in nonuniform and uniform fields from the measurements is also plotted in Fig. 23. These ratios are not derived from actual data points, but from curves faired in between them to make a "best fit." This was done because the data points do not correspond exactly to the same central field. Error flags corresponding to dispersion in the data of Tables 1 and 2 and the estimated precision of the field measurement (≈1%) are attached to the resonance frequency ratios. (Notice that the ordinate zero is suppressed.) The two most interesting features of this plot are that the measured ratios correspond more closely to the "linear" average than to the space average, and there appears to be a marked discontinuity in the data. In these plots, only data for central fields over 8 kgauss was used. This was done because, according to the theory, an Alfvén wave does not exist for much lower fields, and the propagation constant in this region becomes very conductivity-dependent.

A closer examination of Fig. 17 reveals the source of the discontinuity in Fig. 23 as a jump in the data for nonuniform fields at approximately 9.5 kgauss. To facilitate close examination of the data, the upper portion of Fig. 17 is expanded in Fig. 24. The averaged values are shown as circles with attached error flags, and the data used to compute them are shown as dots.

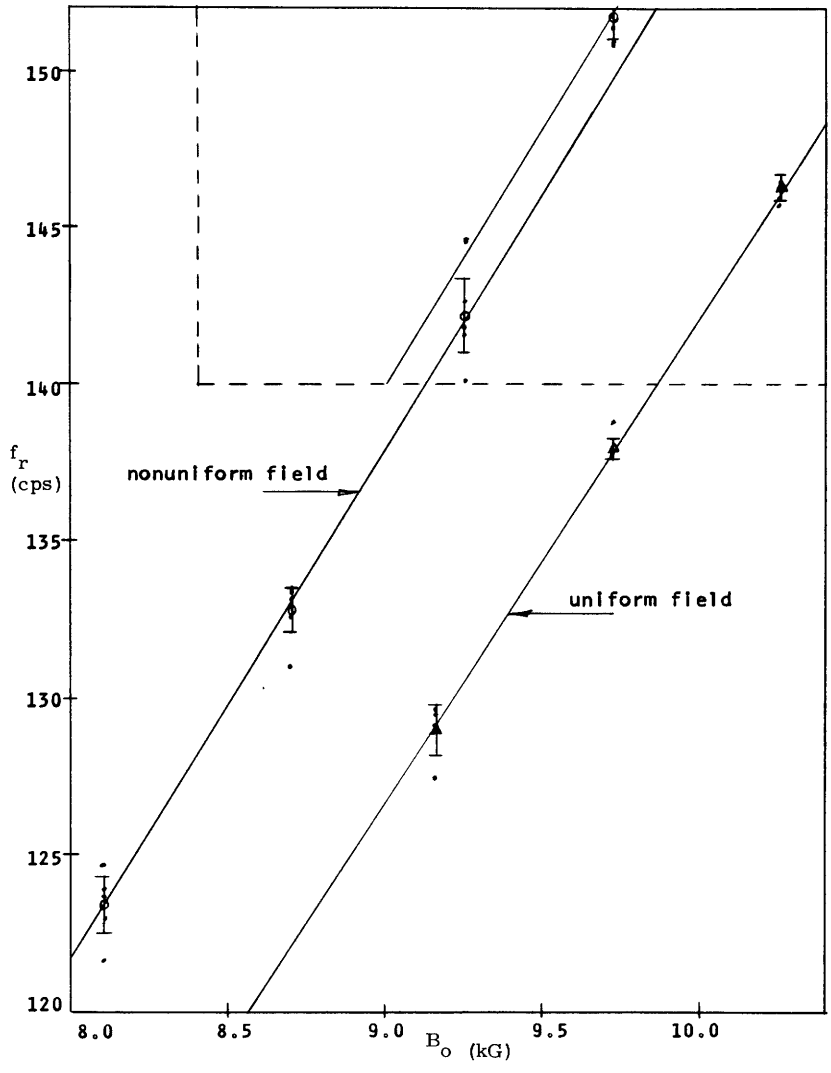

Fig. 24. Section of Fig. 17 expanded.

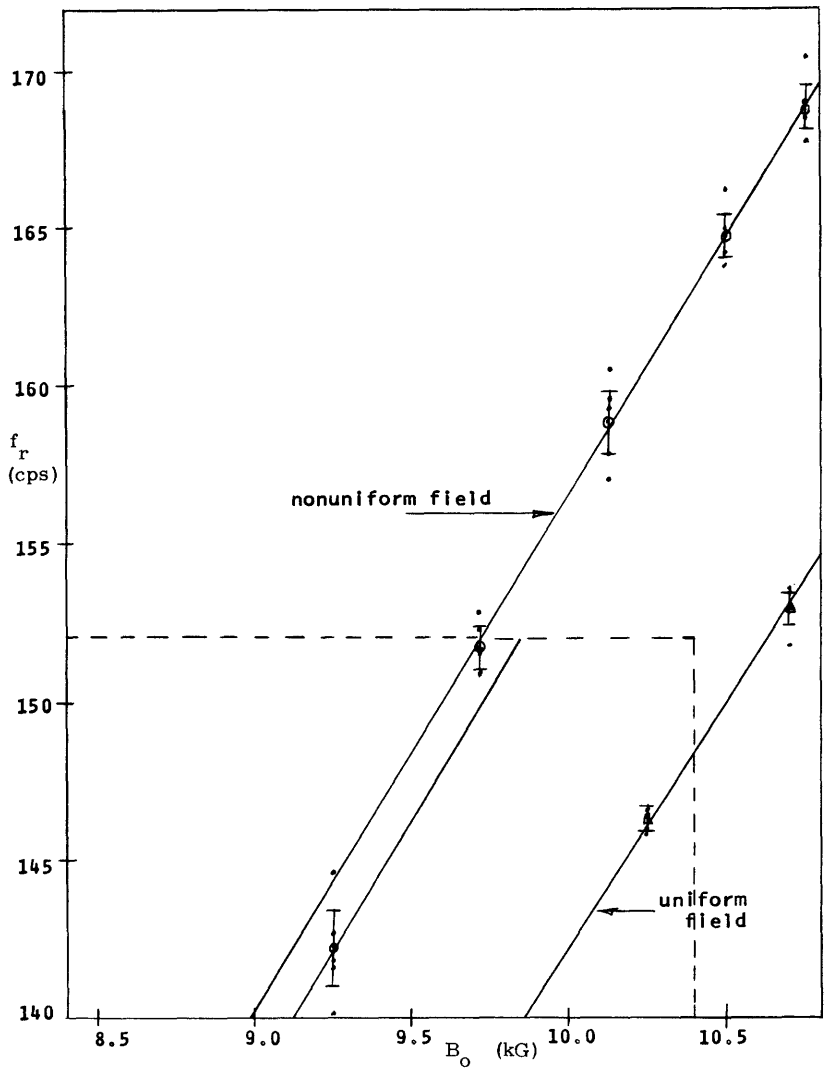

Fig. 24 continued.

V. CONCLUSIONS AND RECOMMENDATIONS

The conclusions of this report may be divided into three groups. The first concerns the experiment which has conclusively proved the validity of small-signal hydromagnetic wave theory. The second comprises a series of theoretical developments filling in a number of gaps in the theory of uniform hydromagnetic waveguides. The third is a theoretical development, with experimental verification, of the effects of nonuniform density or magnetic field.

5.1 EXPERIMENT

In this experiment, great care was taken in the design of the resonator, electronic equipment, and procedures to achieve the maximum possible accuracy, precision, and stability. The results are summarized in Fig. 17. This measurement was the first of sufficient precision to demonstrate the effect of the bulk hydromagnetic capacitance on the resonance frequency. In its close (within 0.5%) correspondence with theoretical predictions, it also provides the first proof of the validity of small-signal hydromagnetic wave theory, rather than a simple demonstration of the existence of a wave phenomenon.

During the trouble-shooting part of the experiment, measurement of the step response of the resonator was developed as a technique of quickly observing the existence or nonexistence of an Alfvén wave. Data from these measurements provided important corroboration of the steady-state resonator results and interpretations, as well as being interesting for their own sake.

Novel features of the resonator itself lay in the total elimination of rigid bodies in the volume, precision of construction, and construction to vacuum-system standards. The results were a vastly improved precision in the measurements and the capability of maintaining the experiment for long periods of time without danger of contamination or leakage. Use of a copper liner yielded lower losses than were previously thought to be attainable.

The resonator and associated electronic equipment then provided a tool for the verification of the theory for nonuniform media which had been developed. Associated with this part of the experiment was the semiempiric design of the Armco pole tips to give a specified field distribution in the magnet gap.

5.2 THEORY OF UNIFORM HYDROMAGNETIC WAVEGUIDES

While a great deal of attention had been given to the subject of hydromagnetic waveguides, still many gaps remained. These gaps consisted in a lack of theoretical developments in some areas and incomplete or inconvenient interpretations of existing developments.

The propagation constant k_{mn}, where conductivity and density were the only important physical parameters, had been known for some time, but its properties were not

fully understood. Indeed, an entire frequency region ($2\sqrt{\omega_1\omega_2} < \omega < \omega_2$) had been ignored. The $k_{mn} - \omega$ diagram (Fig. 2) summarizes and displays (simply) all of the properties of the propagation constant k_{mn} in terms of the two critical frequencies and the Alfvén speed.

In prior investigations, the hydromagnetic waveguide was assumed to have perfectly conducting or perfectly insulating walls. The experimental fact was that the wall conductivity was somewhere between these extremes. An analysis of this problem revealed that when the walls were of almost the same conductivity as the fluid (for instance, with NaK against stainless steel) it appeared to be an insulator. This result led to the insertion of a copper liner in the stainless-steel resonator case.

The behavior of a waveguide when the DC magnetic field did not coincide with its axis was investigated for simple geometries. It was found that the effect of the transverse component of the field was to introduce a low-frequency, highpass cutoff. The theory also showed that this cutoff would not affect the nonuniform field experiment.

The effect of viscosity had been investigated previously with insulating walls and found to have no significant effect. In that case, the velocity of the fluid goes to zero at the walls even when viscosity is zero. An investigation of the use of a perfectly conducting wall, where the velocity must be a maximum, showed that, for liquid metals, there was no significant effect.

5.3 NONUNIFORM MEDIA

The differential equation for hydromagnetic waveguides with uniform longitudinal field and densities that are functions of radius was derived. A perturbation technique was developed to solve this equation. The solution so obtained indicated that the waveguide was behaving as if it were uniform and had an Alfvén speed corresponding to a linear rms average of the Alfvén speed distribution rather than the usual volume average.

Since it is difficult to obtain variable-density liquids, an experiment was proposed and developed in which the Alfvén speed varied by virtue of a spatial variation in the magnetic field, rather than in the density. Since such a field necessarily has radial, as well as longitudinal, components both varying in space, a complete analysis was made of this situation. For moderately varying fields, it was shown that the governing differential equation reduced to the nununiform-density case.

Armco tips were designed to fit onto the magnet poles and around the resonator to produce a field in the resonator to match that treated in the nonuniform-field theory. Steady-state resonance and step-response measurements were made with the use of the previously developed techniques. Comparison of nonuniform and uniform field behavior showed that the resonator was indeed behaving as if it had a uniform field corresponding to the linear average. The precision of the experiment was not sufficient, however, to draw a firm conclusion about which average was actually most correct.

5.4 RECOMMENDATIONS FOR FURTHER RESEARCH

5.4.1 Experiment

The most pressing need for further work is in the experiment and here the most important item is the magnet. The data of this experiment was severely restricted by the maximum available field of 10.7 kilogauss and by the short times available for measurement at high power levels. Experiments should be run in magnetic fields up to 20 kilogauss in a magnet that can be stabilized at the highest power levels. An electronic stabilizer operating directly on the magnetic field would eliminate the hysteresis problem. The increased time available will then allow measurement of Q at the resonance.

In instrumentation, an oscillator of higher resolution in frequency would provide the greatest increase in precision of the data. A general cleanup in the electronics to reduce noise levels and distortion would also help to improve the precision. In the step response measurements, apparatus for automatically substracting out the pedestal and ramp portions of the signal would make the measurement not only more convenient, but would allow a more precise determination of the transit time and the hydromagnetic capacitance. An informative series of experiments could be done with the addition of an amplitude modulator to examine the response to pulsed sinusoids.

Improvements must be made in the method of mounting the high current leads to minimize vibrations. Routing and stabilization of the signal pickup leads should also be studied to reduce the effects of vibration.

Many more experiments need to be run on the apparatus in its present configuration to support, with statistical data, the conclusions of this study. The unexplained jumps observed in the available data series must be investigated to determine their origin and, if possible, to eliminate them.

Experiments with various permutations of the internal structure may be carried out. Some possible studies are 1.) changing the diameter or thickness of the disk exciters, 2.) quarter wave resonance by installing a copper plate to cover one end of the resonator, 3.) conversion to a coaxial resonator by the addition of a copper cylinder electrode to allow the study of TEM modes, 4.) insulating walls by the insertion of a plastic sheet, 5.) the design of exiter for TE modes, 6.) non-axisymmetric modes with suitable exciters, 7.) lumped and distributed terminations to achieve approximate matching conditions, and 8.) the addition of probes to sample the internal fields.

With a new structure, the completed and proposed experiments should be redone in waveguides of rectangular cross-section having various aspect ratios.

5.4.2 Theory

The behavior of the exciter disk poses an important problem. This problem has already been looked at with drastic simplifications,[24] but a more exact treatment is needed to include the effects of current spread. The optimization of exciter design and placement should come out of such studies. In the same area, a study is needed of the

hydromagnetic capacitor to include the effects of viscosity.

A thorough numerical study of the waveforms to be expected at the input and output terminals under step and pulsed sine-wave excitation should be carried out, taking into consideration the exact frequency behavior of the input impedance and propagation constant.

In regard to hydromagnetic waveguides in general, the present derivations of the effects of viscosity, finite conductivity walls, and transverse fields should be repeated in cylindrical coordinates. The dispersion equation for a finite-conductivity wall must be solved numerically to find the range of validity of the approximate solutions used in the present study. It would be of interest to extend all of the theoretical studies to materials of simply anisotropic conductivity (Hall effect) and to rectangular waveguides of arbitrary aspect ratio.

The most important problem to be solved in the nonuniform-media theory is that concerned with the perfectly conducting wall. A promising approach that has produced results in other problems is the WKB method,[29] which should be applied to both insulating and conducting walls. In the perturbation solution, the sixth-order terms should be worked out to check the convergence of the solution for insulating walls and to see if there might be a pattern to the higher order coefficients. The effects of terms neglected in Eq. 72 also need to be examined more closely.

To extend the present work, studies should be made of the coaxial hydromagnetic waveguide with nonuniform density or magnetic field. Other studies might be made for simultaneous variation of density and magnetic field where significant simplifications may be possible by cancellation of variation in the Alfvén speed. Finally, the restriction of axisymmetry could be removed, possibly by use of Rook's method.

APPENDIX A

Effects of Factors Usually Neglected

In the analysis of hydromagnetic waveguides, the effects of viscosity, fringing fields, and finite-conductivity walls are usually neglected. An example of each factor will be given separately, in infinite plane parallel geometry and the lowest attenuation mode, for the sake of simplicity. The waveguide geometry is given in Fig. A-1.

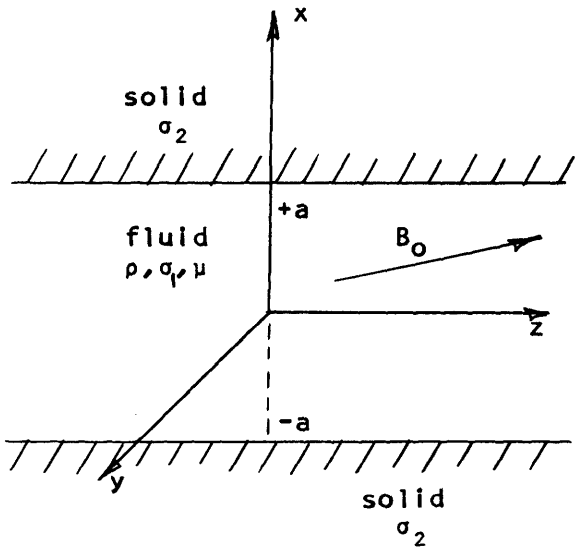

Fig. A-1. Plane parallel waveguide geometry $\frac{\partial}{\partial y} = 0$.

The waveguide is formed by two semi-infinite regions of conductivity, σ_2, spaced a distance 2a apart with faces parallel to the y-z plane. The fluid between the planes has density ρ, conductivity σ_1, and absolute viscosity μ. The imposed uniform DC magnetic field is given by

$$\vec{B}_o = \vec{i}_x B_{ox} + \vec{i}_z B_{oz}. \tag{A.1}$$

The wave will be assumed to be TM (principal mode) and to vary as

$$A(x,z,t) = a(x)\, e^{i(\omega t + kz)}. \tag{A.2}$$

The relevant equations in the fluid may now be written in components as

$$i\omega\rho v_y = -j_x B_{oz} + j_z B_{ox} - \mu k^2 v_y + \mu \frac{d^2 v_y}{dx^2} \qquad \text{Navier-Stokes} \tag{A.3}$$

$$j_x = \sigma_1(e_x + v_y B_{oz}) \qquad \text{(A. 4)}$$

Ohm's law

$$j_z = \sigma_1(e_z - v_y B_{ox}) \qquad \text{(A. 5)}$$

$$ike_x - \frac{de_z}{dx} = -i\omega b_y \qquad \text{curl e} \qquad \text{(A. 6)}$$

$$-ikb_y = \mu_o j_x \qquad \text{(A. 7)}$$

curl b

$$\frac{db_y}{dx} = \mu_o j_z \qquad \text{(A. 8)}$$

A. 1 EFFECT OF VISCOSITY ($B_{ox} = 0$)

Equations A. 3-A. 8 may now be reduced to a single fourth-order equation in v_y.

$$\nu\eta \frac{d^4 v_y}{dx^4} - \left[\eta(k^2\nu + i\omega) + \nu(k^2\nu + i\omega)\right] \frac{d^2 v_y}{dx^2} + \left[(k^2\nu + i\omega)(k^2\eta + i\omega) + k^2 c_{oz}^2\right] v_y = 0, \qquad \text{(A. 9)}$$

where

$$\nu = \frac{\mu}{\rho} \qquad \text{viscous diffusivity} \qquad \text{(A. 10)}$$

$$\eta = \frac{1}{\mu_o \sigma_1} \qquad \text{magnetic diffusivity} \qquad \text{(A. 11)}$$

$$c_{oz} = \frac{B_{oz}}{\sqrt{\mu_0 \rho}} \qquad \text{longitudinal Alfvén speed} \qquad \text{(A. 12)}$$

Note the symmetry of the magnetic and viscous diffusivities in (A. 9).

The solution of (A. 9) has been investigated by Blue[16] for $\sigma_2 = 0$. In this case, the electromagnetic boundary condition required that the velocity be zero at the walls quite independently of viscosity. He found that for liquid metals viscosity played no significant part. For a perfectly conducting wall $\sigma_2 = \infty$, however, the electromagnetic boundary condition requires a velocity that is maximum at the walls if $\mu = 0$. Viscosity might then be expected to have a significant effect.

The antisymmetric solution of (A. 9) is

$$v_y = A_1 \sin \gamma_1 x + A_2 \sinh \gamma_2 x. \qquad \text{(A. 13)}$$

The boundary conditions for $\sigma_2 = \infty$ are

$$v_y(a) = 0 \qquad \text{(A. 14)}$$

$$e_z(a) = 0, \tag{A.15}$$

where

$$e_z = -\frac{\eta B_o}{ikc_{oz}^2}\left[\nu\frac{d^3v_y}{dx^3} - (k^2\nu+i\omega)\frac{dv_y}{dx}\right] \tag{A.16}$$

and

$$\gamma^2 = -\left(k^2+i\omega\frac{\nu+\eta}{2\nu\eta}\right) \pm \sqrt{i\omega\left(\frac{\nu-\eta}{2\nu\eta}\right)^2 - \frac{k^2c_{oz}^2}{\nu\eta}}. \tag{A.17}$$

Here, γ_1 is associated with the plus sign and γ_2 with the minus sign.

Since in a typical liquid metal (NaK) at room temperature $\nu = 9.7 \times 10^{-8}$ m^2/sec and $\eta = 0.3$ m^2/sec, the limiting forms of γ_1 and γ_2 as $\nu \to 0$ are

$$\gamma_1^2 = \frac{\omega^2 - k^2\left(c_{oz}^2+i\omega\eta\right)}{i\omega\eta} \tag{A.18}$$

and

$$\gamma_2^2 = -\frac{i\omega}{\nu}. \tag{A.19}$$

Notice that γ_1^2 is just what would have been obtained if viscosity had been neglected at the outset. The velocity and tangential electric fields then become

$$v_y = A_1\left[\sin\gamma_1 x - 2\, e^{-(1-i)\sqrt{\frac{\omega}{2\nu}}(a-x)}\right] \tag{A.20}$$

$$e_z = A_1\frac{\omega\eta B_o}{kc_{oz}^2}\cos\gamma_1 x. \tag{A.21}$$

The effect of the second term in (A.20) decays away from the wall with a characteristic distance

$$\delta = \sqrt{\frac{2\nu}{\omega}} \qquad \text{viscous skin depth} \tag{A.22}$$

In NaK at $\omega = 400$ (a frequency near the lower end of the Alfvén region) $\delta = 0.002$ cm and decreases with increasing frequency. Summarizing these results, it is seen that the addition of viscosity only introduces a thin boundary layer near the wall in the velocity and does not effect the tangential electric field, as illustrated in Fig. A-2, in which the relative thickness of the boundary layer has been exaggerated.

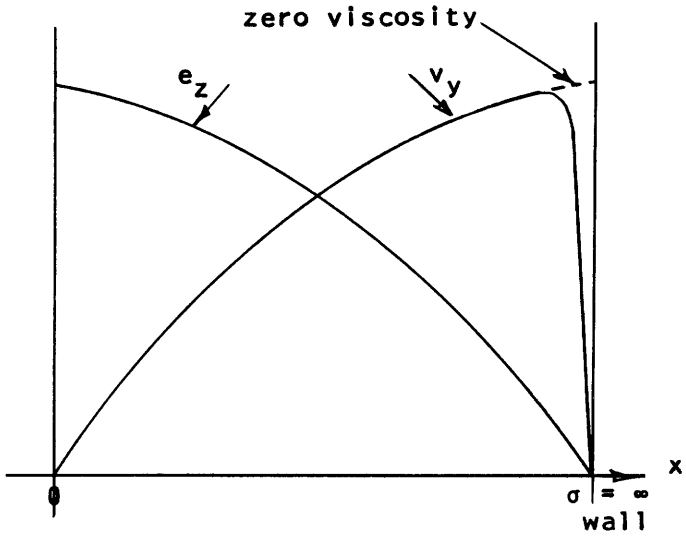

Fig. A-2. The effect of viscosity on e_z and v_y.

A.2 EFFECT OF FINITE WALL CONDUCTIVITY ($B_{ox} = \mu = 0$ and $\eta_1 = \eta$)

In this case the fields in the fluid are given by setting $\nu = 0$, and are

$$b_{y1} = A_1 \sin \gamma_1 x \tag{A.23}$$

and

$$e_{z1} = A_1 \eta_1 \gamma_1 \cos \gamma_1 x, \tag{A.24}$$

where γ_1 is given by (A.18). In the walls

$$b_{y2} = A_2 e^{-\gamma_3 x} \tag{A.25}$$

$$e_{z2} = - A_2 \eta_2 \gamma_3 e^{-\gamma_3 x}, \tag{A.26}$$

where

$$\eta_2 = \frac{1}{\mu_o \sigma_2} \tag{A.27}$$

and

$$\gamma_3^2 = \frac{\omega^2 - i\omega\eta_2 k^2}{i\omega\eta_2} \tag{A.28}$$

Setting the tangential electric and magnetic fields equal at the walls yields

$$\tan \gamma_1 a = -\frac{\sigma_2}{\sigma_1}\frac{\gamma_1}{\gamma_3}. \tag{A.29}$$

It is evident that γ_1 and γ_3 must now be complex, thereby making the solution of Eq. A.29 for k^2 quite difficult. Approximate solutions may be obtained for σ_2 very large and very small, but they are not very useful.

If the wall is assumed to be of finite thickness, b, much less than an electromagnetic skin depth so that the wall current may be considered constant in x, then (A.29) becomes

$$\tan \gamma_1 a = -\frac{\sigma_2}{\sigma_1}\frac{b}{a}\gamma_1 a. \tag{A.30}$$

This assumption will good for b = 0.25 inch and frequencies in the NaK-Alfvén region for stainless-steel walls, and even for copper walls. Equation A.30 may be solved graphically (as in Fig. 5) for γ_1 and thus k.

Notice in Fig. 5 that an NaK waveguide constructed of stainless steel (even if good electrical contact could be made) is almost equivalent to a perfect insulator, while copper approaches reasonably close to being perfect conductor.

A.3 EFFECT OF TRANSVERSE FIELDS ($\mu = 0$)

After some reduction, Eqs. A.3-A.8 become

$$-\left(c_o^2+i\omega\eta_1\right)ik\eta_1 b_y = \left(c_{ox}^2+i\omega\eta_1\right)e_x + c_{ox}c_{oz}e_z \tag{A.31}$$

$$\left(c_o^2+i\omega\eta_1\right)\eta_1\frac{db_y}{dx} = c_{ox}c_{oz}e_x + \left(c_{oz}^2+i\omega\eta_1\right)e_z, \tag{A.32}$$

where

$$c_{ox} = \frac{B_{ox}}{\sqrt{\mu_o\rho}} = \quad \text{transverse Alfvén speed} \tag{A.33}$$

$$c_o^2 = c_{ox}^2 + c_{oz}^2. \tag{A.34}$$

Equations A.31 and A.32 may now be combined to give

$$\left(c_{ox}^2+i\omega\eta_1\right)\frac{d^2b_y}{dx^2} + 2ikc_{ox}c_{oz}\frac{db_y}{dx} + \left[\omega^2-k^2\left(c_{oz}^2+i\omega\eta_1\right)\right]b_y = 0 \tag{A.35}$$

$$e_z = \frac{1}{i\omega}\left[\left(c_{ox}^2+i\omega\eta_1\right)\frac{db_y}{dx} + ikc_{ox}c_{oz}b_y\right]. \tag{A.36}$$

The antisymmetric solution of (A.35) is

$$b_y = A_1 e^{-iT_1 x} \sin T_2 x \tag{A.37}$$

$$e_z = A_1 \frac{T_2\left(c_{ox}^2 + i\omega\eta_1\right)}{i\omega} e^{-iT_1 x} \cos T_2 x, \tag{A.38}$$

where

$$T_1 = \frac{k c_{ox} c_{oz}}{c_{ox}^2 + i\omega\eta_1} \tag{A.39}$$

and

$$T_2 = \frac{1}{c_{ox}^2 + i\omega\eta_1}\left[\omega^2\left(c_{ox}^2 + i\omega\eta_1\right) - i\omega\eta_1 k^2\left(c_o^2 + i\omega\eta_1\right)\right]^{1/2}. \tag{A.40}$$

Application of the boundary condition for either an insulated wall $b_y(a) = 0$ or an infinite conductivity wall $e_z(a) = 0$ fixes T_2 and thus k^2.

$$k^2 = \left(\frac{\omega}{c_{oz}}\right)^2 \frac{1 + \frac{2\omega_1}{i\omega} + \frac{2\omega_1}{i\omega}\frac{2\omega_2}{i\omega}\delta^2}{1 + \frac{i\omega}{2\omega_2} + \delta^2}\left(1 + \frac{2\omega_2}{i\omega}\delta^2\right), \tag{A.41}$$

where ω_1 and ω_2 are the critical frequencies as defined in section 2.1, and

$$\delta = \frac{c_{ox}}{c_{oz}}. \tag{A.42}$$

An exact evaluation of (A.41) is shown in Fig. 4 (log-log coordinates) for an NaK experiment, $\delta = 0.1$, with the curve for $\delta = 0$ dashed for comparison. Notice that the real part of k goes to zero at frequency ω_c. If $\delta < 1$, this frequency is given by

$$\omega_c = \frac{2\omega_2\delta^2}{\sqrt{1 + \frac{\omega_2}{\omega_1}\delta^2}}, \tag{A.43}$$

and is due to an ordinary cutoff in the transverse field. As the transverse field component is made smaller, $\delta \to 0$, this cutoff recedes to zero frequency.

APPENDIX B

Nonuniform Density and the Perturbation Expansion

The behavior of a hydromagnetic waveguide with a radially nonuniform density will now be investigated. It is assumed that the fluid is inviscid and of finite conductivity. Furthermore, attention is restricted to the axisymmetric transverse magnetic modes. For simplicity, the walls of the rigid confining cylinder are taken to be either a perfect insulator or a perfect conductor.

B.1 WAVE EQUATION

The geometry of the hydromagnetic waveguide is as shown in Fig. 1. It consists of a hollow, rigid cylinder with radius, a, made of either perfectly conducting ($\sigma = \infty$) or perfectly insulating ($\sigma = 0$) material with its axis of symmetry aligned parallel to the z-axis and the applied uniform, steady magnetic field $\vec{B}_o = \vec{i}_z B_o$. The governing equations are Maxwell's equations

$$\nabla \times \vec{E} = -\frac{\partial \vec{B}}{\partial t} \tag{B.1}$$

$$\nabla \times \vec{B} = \mu_o \vec{J} \tag{B.2}$$

in which it has been assumed that the frequencies of interest are low enough that displacement currents may be neglected. The momentum equation and the Ohm's Law are also required:

$$\rho \frac{D\vec{V}}{Dt} = -\nabla P + \vec{J} \times \vec{B} \tag{B.3}$$

$$\vec{J} = \sigma(\vec{E} + \vec{V} \times \vec{B}). \tag{B.4}$$

These equations may be linearized in the usual way by assuming that all of the variables may be written

$$\vec{A} = \vec{A}_o + \vec{a}\, e^{i\omega t}, \tag{B.5}$$

where $|\vec{a}| \ll |\vec{A}_o|$ and the only nonzero zero-order term is that for the magnetic field. Thus Eqs. B.1-B.4, with $\rho = \rho(r)$, become

$$\nabla \times \vec{e} = -i\omega \vec{b} \tag{B.6}$$

$$\nabla \times \vec{b} = \mu_o \vec{j} \tag{B.7}$$

$$i\omega\rho\vec{v} = -\nabla p + \vec{j} \times \vec{B}_o \tag{B.8}$$

$$\vec{j} = \sigma(\vec{e} + \vec{v} \times \vec{B}_o). \tag{B. 9}$$

The assumption of an axisymmetric TM mode leads to the following simplifications:

$$\nabla p = 0; \quad e_\theta = 0; \quad b_r = b_z = 0; \quad v_r = v_z = 0; \quad j_\theta = 0; \quad \frac{\partial}{\partial \theta} = 0. \tag{B. 10}$$

Notice that the equations are linear in z. Thus the following substitution may be made:

$$\vec{a} = \vec{a}_o \, e^{ikz}. \tag{B. 11}$$

Utilizing (B. 10) and (B. 11), we may now rewrite (B. 6-B. 9) in components:

$$ike_r - \frac{\partial e_z}{\partial r} = -i\omega b_\theta \tag{B. 12}$$

$$-ikb_\theta = \mu_o j_r \tag{B. 13}$$

$$\frac{1}{r}\frac{\partial}{\partial r}(rb_\theta) = \mu_o j_z \tag{B. 14}$$

$$i\omega\rho v_\theta = -j_r B_o \tag{B. 15}$$

$$j_r = \sigma(e_r + v_\theta B_o) \tag{B. 16}$$

$$j_z = \sigma e_z. \tag{B. 17}$$

From (B. 13) and (B. 15) it is seen that

$$v_\theta = \frac{KC^2}{\omega}\frac{b_\theta}{B_o}, \tag{B. 18}$$

where

$$C^2 = \frac{B_o^2}{\mu_o \rho} \qquad \text{local Alfvén speed.} \tag{B. 19}$$

From (B. 14) and (B. 17), b_θ may be related to e_z. Thus

$$e_z = \eta \frac{1}{r}\frac{\partial}{\partial r}(rb_\theta), \tag{B. 20}$$

where

$$\eta = \frac{1}{\mu_o \sigma} \qquad \text{magnetic diffusivity.} \tag{B. 21}$$

This relation will be useful in applying the boundary condition for a perfectly conducting wall.

Now if (B. 12-B. 17) are reduced to a single equation in b_θ, Eq. B. 22 results.

$$\frac{\partial}{\partial r}\left[\frac{1}{r}\frac{\partial}{\partial r}(rb_\theta)\right] + \frac{1}{i\omega\eta}[\omega^2 - K^2(C^2 + i\omega\eta)]b_\theta = 0. \tag{B. 22}$$

Since C is an arbitrary function of radius, the solution of this equation is not apparent.

B. 2 BOUNDARY CONDITIONS

If the wall is a perfect conductor, application of the induction law yields immediately

$$e_z(\text{wall}) = 0. \tag{B. 23}$$

The conditioning for an insulating wall is obtained by noting that since j_r must be continuous at the wall and zero in the wall, then

$$j_r(\text{wall}) = 0. \tag{B. 24}$$

From (B. 23), if $K \neq 0$,

$$b_\theta(\text{wall}) = 0. \tag{B. 25}$$

B. 3 PERTURBATION SOLUTION

Since in most cases of interest the variation of Alfvén speed with radius is a smoothly and usually slowly increasing or decreasing function of radius, c^2 may be expanded in a series of the form

$$c^2(r) = c_o^2 \sum_{n=0}^{\infty} f_n (r/b)^n. \tag{B. 26}$$

Here, the f_n are numerical coefficients dependent on the exact shape of the variation, and the parameter b is an indicator of how fast the Alfvén speed is varying with radius.

With a technique similar to those used in atomic physics for the solution of Schrödinger's equation,[29] the dependent variables, such as b_θ and e_z, will also be expanded in a similar series. As the boundary conditions will be evaluated at r = a, it is convenient to rewrite (B. 26) in terms of a nondimensional expansion parameter

$$d = \frac{a}{b} \tag{B. 27}$$

and a normalized coordinate

$$x = \frac{r}{a}. \tag{B. 28}$$

Equations B. 22 and B. 26 then become

$$\frac{\partial}{\partial x}\left[\frac{1}{x}\frac{\partial}{\partial x}(xb_\theta)\right] + \frac{a^2}{i\omega\eta}[\omega^2 - K^2(c^2 + i\omega\eta)]b_\theta = 0 \tag{B. 29}$$

$$c^2(x) = c_o^2 \sum_{n=0}^{\infty} f_n d^n x^n, \tag{B. 30}$$

where the boundary conditions are to be evaluated at x = 1. Similarly, let

$$b_\theta(x) = \sum_{n=0}^{\infty} b_n d^n \tag{B. 31}$$

$$e_z(x) = \sum_{n=0}^{\infty} e_n d^n \tag{B. 32}$$

$$K^2 = K_o^2 \sum_{n=0}^{\infty} p_n d^n, \tag{B. 33}$$

where K_o is the propagation constant that would be obtained if d = 0.

Substituting (B. 31-B. 33) in (B. 29) and equating terms of equal powers in the expansion parameter d yields for n = 0, 1, 2, . . . , n

$$i\omega \frac{\eta}{a^2} L(b_o) = 0 \tag{B. 34}$$

$$\frac{i\omega\eta}{a^2} L(b_1) = \left[C_o^2 f_1 P_o x + P_1\left(f_o C_o^2 + i\omega\eta\right)\right] K_o^2 b_o \tag{B. 35}$$

$$\begin{aligned}\frac{i\omega\eta}{a^2} L(b_2) = &\left[C_o^2 f_1 P_o x + P_1\left(f_o C_o^2 + i\omega\eta\right)\right] K_o^2 b_1 \\ &+ \left[C_o^2 f_2 P_o x^2 + C_o^2 f_1 P_1 x + P_2\left(f_o C_o^2 + i\omega\eta\right)\right] K_o^2 b_o\end{aligned} \tag{B. 36}$$

$$\begin{aligned}\frac{i\omega\eta}{a^2} L(b_3) = &\left[C_o^2 f_1 P_o x + P_1\left(f_o C_o^2 + i\omega\eta\right)\right] K_o^2 b_2 \\ &+ \left[C_o^2 f_2 P_o x^2 + C_o^2 f_1 P_1 x + P_2\left(f_o C_o^2 + i\omega\eta\right)\right] K_o^2 b_1 \\ &+ \left[C_o^2 f_3 P_o x^3 + C_o^2 f_2 P_1 x^2 + C_o^2 f_1 P_2 x + P_3\left(f_o C_o^2 + i\omega\eta\right)\right] K_o^2 b_o \\ &\vdots\end{aligned} \tag{B. 37}$$

$$\frac{i\omega\eta}{a^2} L(b_n) = K_o^2 \sum_{k=1}^{n} b_{n-k} \left\{\left[\sum_{m=0}^{k} C_o^2 f_{m-k} P_m x^{k-m}\right] + i\omega\eta P_K\right\}, \tag{B. 38}$$

where

$$L(b_n) = \frac{d}{dx}\left[\frac{1}{x}\frac{d}{dx}(x b_n)\right] + \frac{a^2}{i\omega\eta}\left[\omega^2 - K_o^2\left(f_o C_o^2 + i\omega\eta\right)\right] b_n. \tag{B. 39}$$

The expanded equations (B. 34-B. 38) are seen to be uncoupled from below. They may be solved by first finding the solution to (B. 34), and then using that as the driving function for (B. 35) and so on through the complete set as far as required.

Two properties may be noticed immediately. First, the solution to Eq. B. 34 is just that for a waveguide having a uniform Alfvén speed of $\sqrt{f_o}C_o$. The solution is

$$b_o = AJ_1(T_k x) + BN_1(T_k x). \tag{B. 40}$$

Since b_o must be finite at x = 0, then B = 0. Similarly, the solutions of the remaining equations may not contain N_1. The constant T_k is determined from the boundary condition at x = 1 and is given by

$$T_k^2 = \frac{a^2}{i\omega\eta}\left[\omega^2 - K_{ok}^2\left(f_o C_o^2 + i\omega\eta\right)\right]. \tag{B. 41}$$

Thus the K_{ok} are determined by the various allowed values of T_k. In further developments it will be assumed that only the lowest order mode (smallest T_k) is being considered. This would be the mode of lowest attenuation in the uniform case. Therefore T and K_o will not have further subscripts.

Second, if the solution to (B. 34) satisfies the boundary condition at x = 1, then the homogeneous solutions to all of the remaining equations also satisfy the boundary condition at x = 1. The remaining particular integrals must then satisfy the conditions at x = 0 and x = 1 individually. The condition at x = 0 is automatically satisfied for all equations by setting B = 0 in Eq. B. 40.

B. 4 A CASE OF INTEREST

For an axisymmetric density distribution, the density must be an even function of radius. Therefore, in (B. 26),

$$f_n = 0 \qquad n = 1, 3, 5, 7, \ldots . \tag{B. 42}$$

Thus (B. 34-B. 38) may be rewritten

$$L(b_o) = 0 \tag{B. 43}$$

$$G^{-1}L(b_1) = P_1\left(f_o + i\omega\eta/C_o^2\right)b_o \tag{B. 44}$$

$$G^{-1}L(b_2) = P_1\left(f_o + i\omega\eta/C_o^2\right)b_1 + \left[f_2 P_o x^2 + P_2\left(f_o + i\omega\eta\right)\right]b_o \tag{B. 45}$$

$$G^{-1}L(b_3) = P_1\left(f_o+i\omega\eta/C_o^2\right)b_2$$

$$+\left[f_2P_ox^2+P_2\left(f_o+i\omega\eta/C_o^2\right)\right]b_1$$

$$+\left[f_2P_1x^2+P_3\left(f_o+i\omega\eta/C_o^2\right)\right]b_o \qquad \text{(B. 46)}$$

$$\vdots$$

etc.

where

$$G^{-1} = \frac{i\omega\eta}{a^2K_o^2C_o^2}. \qquad \text{(B. 47)}$$

At this point, it is convenient to note that since L is a linear differential operator, the right-hand side of each of the equations (B. 34-B. 38) consists of a sum of terms of the form

$$C_{in}r^kJ_\ell(Tx), \qquad \text{(B. 48)}$$

where C_{in} is a complex constant, k and ℓ real integers, and T a real constant determined by the zero-order equation. Taking advantage of the linearity of L allows us to form the solution of an equation of any order by a sum of the solutions for each term of the driving function taken one at a time. Thus

$$b_n = G\sum_i C_{in}R_{in}(x), \qquad \text{(B. 49)}$$

where the C_{in} are those in B. 48, and $R_{in}(x)$ is the particular integral of

$$L(R_{in}) = r^kJ_\ell(Tx). \qquad \text{(B. 50)}$$

Notice that all quantitites in (B. 50) are real.

By using the notation (B. 49), the solutions to (B. 43-B. 45) become

$$b_o = R_{oo} \qquad \text{(B. 51)}$$

$$G^{-1}b_1 = P_1\left(f_o+i\omega\eta/C_o^2\right)R_{10} \qquad \text{(B. 52)}$$

$$G^{-1}b_2 = GP_1^2\left(f_o+i\omega\eta/C_o^2\right)^2R_{20} + f_2P_oR_{21} + P_2\left(f_o+i\omega\eta/C_o^2\right)R_{23}. \qquad \text{(B. 53)}$$

One of the two possible boundary conditions may now be applied, that is, a perfectly insulating wall (Eq. B. 25, $b_\theta = 0$) or a perfectly conducting wall (Eq. B. 23, $e_z = 0$).

Taking, first, the condition for an insulating wall and requiring each particular integral to meet this condition, we obtain

$$R_{oo}(T) = 0 \tag{B.54}$$

$$P_1\left(f_o+i\omega\eta/C_o^2\right)R_{10}(T) = 0. \tag{B.55}$$

Equation B.54, as before, determines the allowable values of T. Since the R_{in} are Bessel functions, they will not have the same zeros if they are of different order. Therefore if $R_{oo}(T) = 0$, then $R_{10}(T) \neq 0$. Thus $P_1 = 0$ and $b_1 = 0$. The second-order equation (B.45) then becomes

$$G^{-1}L(b_2) = \left[f_2P_ox^2+P_2\left(f_o+i\omega\eta/C_o^2\right)\right]b_o, \tag{B.56}$$

thereby yielding

$$G^{-1}b_2 = f_2P_oR_{21} + P_2\left(f_o+i\omega\eta/C_o^2\right)R_{22}. \tag{B.57}$$

Setting $b_2(1) = 0$ gives the required value of P_2.

$$P_2 = -\frac{R_{22}(T)}{R_{21}(T)}\,\frac{f_2P_o}{f_o + i\omega\eta/C_o^2}. \tag{B.58}$$

The third-order equation (B.46) now becomes

$$G^{-1}L(b_3) = P_3\left(f_o+i\omega\eta/C_o^2\right)b_o,$$

which is formally identical to (B.44). This application of the condition $b_3(1) = 0$ results in $P_3 = 0$ and $b_3 = 0$. This pattern carries through all orders and results in

$$\begin{aligned} P_n &= 0 \\ b_n &= 0 \end{aligned} \qquad n = 1,3,5,7,\ldots. \tag{B.59}$$

In this case, then, original equations (B.34-B.38) may now be simplified to

$$L(b_o) = 0 \tag{B.60}$$

$$G^{-1}L(b_2) = \left[P_of_2x^2+P_2\left(f_o+i\omega\eta/C_o^2\right)\right]b_o \tag{B.61}$$

$$\begin{aligned} G^{-1}L(b_4) = &\left[P_of_2x^2+P_2\left(f_o+i\omega\eta/C_o^2\right)\right]b_2 \\ &+ \left[P_of_4x^4+P_2f_2x^2+P_4\left(f_o+i\omega\eta/C_o^2\right)\right]b_o \end{aligned} \tag{B.62}$$

$$\vdots$$

$$G^{-1}L(b_{2n}) = \sum_{k=0}^{n} b_{2(n-k)}\left\{\left[\sum_{m=0}^{k} P_{2m}f_{2(k-m)}x^{2(k-m)}\right] + \frac{i\omega\eta}{C_o^2}P_{2k}\right\}. \tag{B. 63}$$

To apply the condition for a perfectly conducting wall ($e_z = 0$), recall that

$$e_z = \sum e_n d^n$$

and

$$e_z = \eta\frac{1}{r}\frac{d}{dr}(rb_\theta).$$

Then, with the use of the notation of Eq. B. 49, the orders of e_z become

$$ae_o = \eta\frac{1}{x}\frac{d}{dx}(xR_{oo}) \tag{B. 64}$$

$$aG^{-1}e_1 = P_1\left(f_o+i\omega\eta/C_o^2\right)\eta\frac{1}{x}\frac{d}{dx}(xR_{10}) \tag{B. 65}$$

$$aG^{-1}e_2 = GP_1^2\left(f_o+i\omega\eta/C_o^2\right)^2\eta\frac{1}{x}\frac{d}{dx}(xR_{20}) + f_2P_o\,\eta\frac{1}{x}\frac{d}{dx}(xR_{21}) + P_2\left(f_o+i\omega\eta/C_o^2\right)\eta\frac{1}{x}\frac{d}{dx}(xR_{23}). \tag{B. 66}$$

The same argument as that for the insulating wall case may now be used to deduce that

$$\begin{aligned} P_n &= 0 \\ e_n &= 0 \end{aligned} \qquad n = 1,3,5,7,\ldots . \tag{B. 67}$$

B. 5 APPLICATION TO THE EXPERIMENT

In the experimental apparatus it will be found that the variation of Alfvén speed over the cross section of the waveguide is very close to

$$C(r) = C_o\sqrt{1 + (r/b)^2}, \tag{B. 68}$$

or in Eq. B. 42,

$$\begin{aligned} f_o &= f_2 = 1 \\ f_n &= 0 \qquad n = 1 \text{ and } n > 2. \end{aligned} \tag{B. 69}$$

Now Eqs. B. 60-B. 63 may be further simplified to

$$L(b_o) = 0 \tag{B. 70}$$

$$G^{-1}L(b_2) = \left(P_o x^2 + P_2 D\right) b_o \tag{B. 71}$$

$$G^{-1}L(b_4) = \left(P_o x^2 + P_2 D\right) b_2 + \left(P_2 x^2 + P_4 D\right) b_o \tag{B. 72}$$

$$G^{-1}L(b_6) = \left(P_o x^2 + P_2 D\right) b_4 + \left(P_2 x^2 + P_4 D\right) b_2 + \left(P_4 x^2 + P_6 D\right) b_o \tag{B. 73}$$

$$\vdots$$

$$G^{-1}L(b_{2n}) = \sum_{k=0}^{n} b_{2(n-k)} \left(P_{2(k-1)} x^2 + P_{2k} D\right), \tag{B. 74}$$

where

$$D = 1 + i\omega\eta/C_o^2. \tag{B. 75}$$

The various component solutions of

$$L(R_{in}) = r^k J_\ell(Tx) \tag{B. 50}$$

have been worked out in Appendix J.

To fourth order, for insulating walls, the propagation constant K is given by

$$K^2 = K_o^2 \left[1 - \frac{\frac{1}{3} d^2}{D} + \frac{\frac{1}{9} d^4}{D^2} - \frac{\frac{1}{45} d^4}{D} G \frac{a^2}{\alpha^2} \left(1 - \frac{24}{\alpha^2}\right)\right]. \tag{B. 76}$$

For perfectly conducting walls

$$K^2 = K_o^2 \left[1 - \frac{\frac{1}{3} d^2}{D} \left(1 + \frac{4}{\alpha^2}\right) + \frac{\frac{1}{9} d^4}{D^2} \left(1 + \frac{8}{\alpha^2} + \frac{16}{\alpha^4}\right) - \frac{\frac{1}{45} d^4}{D} G \frac{a^2}{\alpha^2} \left(1 + \frac{7}{\alpha^2} - \frac{192}{\alpha^2}\right)\right], \tag{B. 77}$$

where α is the root of the Bessel function J_o or J_1 to satisfy the zero-order equation appropriate to insulating or to perfectly conducting walls.

It may be noted that the two solutions are identical in general outline, differing only in the detail of the coefficients related to the geometry, α and K_o. This corresponds very closely to the case of a uniform waveguide.

B. 6 INTERPRETATION OF THE EXPANSIONS

Equations B. 76 and B. 77 may be rewritten, by substituting the expression for G, in terms of the critical frequencies ω_1 and ω_2 (Eq. A. 41) based on the d = 0 field. First, for insulating walls, Eq. B. 76 becomes

$$K^2 = K_o^2\left\{1 - \frac{\frac{1}{3}d^2}{1 + \frac{i\omega}{2\omega_2}} + \frac{\frac{1}{9}d^4}{\left(1 + \frac{i\omega}{2\omega_2}\right)^2}\left[1 + \frac{1}{5}\left(1 + \frac{i\omega}{2\omega_1}\right)\left(1 - \frac{24}{a^2}\right)\right]\right\}. \tag{B. 78}$$

For conducting walls, Eq. B. 77 becomes

$$K^2 = K_o^2\left\{1 - \frac{\frac{1}{3}d^2}{1 + \frac{i\omega}{2\omega_2}}\left(1 + \frac{4}{a^2}\right) + \frac{\frac{1}{9}d^4}{\left(1 + \frac{i\omega}{2\omega_2}\right)^2} \times \left[\left(1 + \frac{8}{a^2} + \frac{16}{a^4}\right) - \frac{1}{5}\left(1 + \frac{i\omega}{2\omega_1}\right)\left(1 + \frac{7}{a^2} - \frac{192}{a^4}\right)\right]\right\}. \tag{B. 79}$$

Note that in each case K^2 is a function only of the physical parameters and the expansion parameter. The forms of (B. 78) and (B. 79) suggest that there may be an equivalent "average" Alfvén speed which, as a function of d and C_o, may account for the principal properties of the propagation constant.

First, consider the volume rms Alfvén speed

$$C_{rms}^2(d) = \frac{1}{\pi a^2 \ell}\int_0^a \int_0^\ell \int_0^{2\pi} C^2(r) r\, dr d\theta dz. \tag{B. 80}$$

By using Eq. B. 68 for C(r), we obtain

$$C_{rms}^2 = C_o^2\left(1 + \frac{1}{2}d^2\right). \tag{B. 81}$$

Using C_{rms} in Eq. 12 for K^2 in a uniform waveguide, we obtain

$$K^2 = \left(\frac{\omega}{C_o}\right)^2 \frac{1 + \frac{2\omega_1}{i\omega}}{1 + \frac{1}{2}d^2 + \frac{i\omega}{2\omega_2}}. \tag{B. 82}$$

If Eq. B. 82 is now expanded in powers of d, we have

$$K^2 = K_o^2\left[1 - \frac{\frac{1}{2}d^2}{1 + \frac{i\omega}{2\omega_2}} + \frac{\frac{1}{4}d^4}{\left(1 + \frac{i\omega}{2\omega_2}\right)^2} - \frac{\frac{1}{8}d^6}{\left(1 + \frac{i\omega}{2\omega_2}\right)^3} + \ldots + \left(\frac{-\frac{1}{2}d^2}{1 + \frac{i\omega}{2\omega_2}}\right)^n\right] \qquad n = 0, 1, 2, 3, \ldots \tag{B. 83}$$

which bears a very strong family resemblance to Eqs. B. 78 or B. 79, except that the principal coefficients have the wrong base and some parts of the coefficients are missing. On the other hand, consider a linear rms of the Alfvén speed:

$$C^2_{rms}(d) = \frac{1}{\pi a^2 \ell} \int_0^a \int_0^\ell \int_0^{2\pi} C^2(r) \frac{a}{2} dr d\theta dz. \tag{B.84}$$

Again, using (B.88) for C(r), we obtain

$$C^2_{rms} = C_o^2\left(1 + \frac{1}{3}d^2\right), \tag{B.85}$$

which when put into Eq. 12 and expanded gives

$$K^2 = K_o^2\left[1 - \frac{\frac{1}{3}d^2}{1 + \frac{i\omega}{2\omega_2}} + \frac{\frac{1}{9}d^4}{\left(1 + \frac{i\omega}{2\omega_2}\right)^2} - \frac{\frac{1}{27}d^6}{\left(1 + \frac{i\omega}{2\omega_2}\right)^3} + \ldots + \left(\frac{-\frac{1}{3}d^2}{1 + \frac{i\omega}{2\omega_2}}\right)^n\right]$$

$$n = 0, 1, 2, 3, \ldots \tag{B.86}$$

in which the coefficients now match those of Eqs. B.78 and B.79 much more closely. The matter of the extra terms in the coefficients remains. When the appropriate value for a is used, (B.78) and (B.79) become

$$K^2 = K_o^2\left\{1 - \frac{\frac{1}{3}d^2}{1 + \frac{i\omega}{2\omega_2}} + \frac{\frac{1}{9}d^4}{\left(1 + \frac{i\omega}{2\omega_2}\right)^2}\left[1 - 0.127\left(1 + \frac{i\omega}{2\omega_1}\right)\right]\right\} \tag{B.87}$$

$$K^2 = K_o^2\left\{1 - 1.692\frac{\frac{1}{3}d^2}{1 + \frac{i\omega}{2\omega_2}} + 2.862\frac{\frac{1}{9}d^4}{\left(1 + \frac{i\omega}{2\omega_2}\right)^2}\left[1 + 0.247\left(1 + \frac{i\omega}{2\omega_1}\right)\right]\right\}. \tag{B.88}$$

At high frequencies ($\omega \to \infty$), Eqs. B.87 and B.88 reduce identically to the first three terms of (B.86). This means that in the limit of very high frequencies, where there is no hydromagnetic effect in the uniform case, the nonuniformity has no effect. Each term of higher order than zero in any of Eqs. B.86, B.87 or B.88 goes to zero as the frequency approaches infinity and leaves $K = K_o$. At low frequencies ($\omega \to 0$), (B.87) and (B.88) become

$$K^2 = K_o^2(1 - 1/3d^2 + 1.127 \times 1/9d^4) \tag{B.89}$$

and

$$K^2 = K_o^2(1 - 1.692 \times 1/3d^2 + 3.569 \times 1/9d^4). \tag{B.90}$$

By taking d = 1, Eq. B.89 yields a value of K^2 differing from the linear average by approximately 0.15% because of the extra terms. This increases to approximately 0.7% (with the effect of ω_2 neglected) at the upper end of the frequency range of interest. On the other hand, taking d = 1 in Eq. B.90 yields a difference of approximately 20%, which

also increases with frequency. An exact evaluation of the perturbation expansion and the propagation constant based on the linear average shows that (B. 86) and (B. 87) agree to better than 1. 0%. Equation B. 88 blows up and gives totally unrealistic results over the middle range of frequencies.

The reason for the nonconvergence of (B. 88) may be seen by solving Eqs. B. 12-B. 17 for e_z instead of b_θ. Utilizing the special form for the Alfvén speed variation (Eq. B. 68) and normalizing, as before, yields

$$\frac{\partial^2 e_z}{\partial x^2} + \frac{\omega^2 - K^2\left[C_o^2(1-d^2x^2)+i\omega\eta\right]}{\omega^2 - K^2\left[C_o^2(1+d^2x^2)+i\omega\eta\right]} \frac{1}{x} \frac{\partial e_z}{\partial x}$$

$$+ \frac{a^2}{i\omega\eta}\left\{\omega^2 - K^2\left[C_o^2(1+d^2x^2)+i\omega\eta\right]\right\} e_z = 0. \qquad \text{(B. 91)}$$

The direct-expansion solution of this equation again yields exactly Eq. B. 88. It is now clear that singularities may exist at some $0 < x < 1$ for some frequencies. An estimate of this point may be obtained by using the linear average Alfvén speed to compute K^2. Setting the real and imaginary parts of the denominator of the second term of Eq. B. 91 equal to zero gives the location of the singularity as

$$x^2 = \frac{1/3}{d^2} \frac{d^4 + \left(1 - \frac{\omega_1}{\omega_2}\right)\frac{d^2}{3} - \frac{2}{9}\frac{\omega_1}{\omega_2}}{d^2 + \frac{1}{3}\frac{\omega_1}{\omega_2}} \qquad \text{(B. 92)}$$

and

$$\omega^2 = \frac{4\omega_1\omega_2(1+d^2x^2)\left(1 + \frac{1}{3}d^2\right)}{\frac{\omega_1}{\omega_2} - d^2\left(\frac{1}{3} - x^2\right)}. \qquad \text{(B. 93)}$$

Setting $d = 1$ and using ω_1 and ω_2 appropriate to the experiment yields $x = 0.380$ and $\omega = 2 \times 10^3$ which fall within the range of interest.

APPENDIX C

Inhomogeneous Magnetic Field

The behavior of a hydromagnetic waveguide with a radially inhomogeneous magnetic field and uniform density will now be investigated. It is assumed that the fluid is inviscid and of finite conductivity. Furthermore, attention is restricted to the axisymmetric transverse magnetic modes because these are the most important experimentally. For simplicity, the walls of the rigid confining cylinder forming the waveguide are taken to be either perfectly insulating or perfectly conducting.

C.1 WAVE EQUATION

The geometry of the nonuniform hydromagnetic waveguide is as shown in Fig. 1. It consists of a hollow, rigid cylinder of radius a, made of either perfectly conducting ($\sigma=\infty$) or perfectly insulating ($\sigma=0$) material, with its axis of symmetry aligned parallel to the z-axis. The applied nonuniform, but axisymmetric and steady, magnetic field is given by

$$\vec{B}_o(r,z) = \vec{i}_r B_{or}(r,z) + \vec{i}_z B_{oz}(r,z) \tag{C.1}$$

with

$$\nabla \times \vec{B}_o = 0 \tag{C.2}$$

$$\nabla \cdot \vec{B}_o = 0. \tag{C.3}$$

The governing physical laws are Maxwell's equations

$$\nabla \times \vec{E} = -\frac{\partial \vec{B}}{\partial t} \tag{C.4}$$

$$\nabla \times \vec{B} = \mu_o \vec{J} \tag{C.5}$$

in which it has been assumed that the frequencies of interest are low enough that displacement currents may be neglected. The momentum equation and the Ohm's law equation are also required.

$$\rho \frac{D\vec{V}}{Dt} = -\nabla P + \vec{J} \times \vec{B} \tag{C.6}$$

$$\vec{J} = \sigma(\vec{E} + V \times B). \tag{C.7}$$

These equations may be linearized in the usual way by assuming that all of the variables may be written as

$$\vec{A} = \vec{A}_o + \vec{a}\, e^{i\omega t}, \tag{C.8}$$

where $|\vec{a}| \ll |\vec{A}_o|$ and the only nonzero zero-order term is that for the magnetic field. Thus Eqs. C.4-C.7, by using the distributive property of the curl, become

$$\nabla \times \vec{e} = -i\omega\vec{b} \tag{C.9}$$

$$\nabla \times \vec{b} = \mu_o\vec{j} \tag{C.10}$$

$$i\omega\rho\vec{v} = -\nabla p + \vec{j} \times \vec{B}_o \tag{C.11}$$

$$\vec{j} = \sigma(\vec{e} + \vec{v} \times \vec{B}_o). \tag{C.12}$$

The assumption of an axisymmetric TM mode leads to the following simplifications:

$$\nabla p = 0; \quad e_\theta = 0; \quad b_r = b_z = 0; \quad v_r = v_z = 0; \quad j_\theta = 0; \quad \frac{\partial}{\partial\theta} = 0 \tag{C.13}$$

Equations C.9-C.12 may now be rewritten in components:

$$-\frac{\partial b_\theta}{\partial z} = \mu_o j_r \tag{C.14}$$

$$\frac{1}{r}\frac{\partial}{\partial r}(rb_\theta) = \mu_o j_z \tag{C.15}$$

$$\frac{\partial e_r}{\partial z} - \frac{\partial e_z}{\partial r} = -i\omega b_\theta \tag{C.16}$$

$$j_r = \sigma(e_r + v_\theta B_{oz}) \tag{C.17}$$

$$j_z = \sigma(e_z - v_\theta B_{or}) \tag{C.18}$$

$$i\omega\rho v_\theta = -j_r B_{oz} + j_z B_{or} \tag{C.19}$$

It may be seen that the assumption of a TM wave is consistent. After some manipulation, Eqs. C.14 and C.15 and C.17-C.19 may be condensed:

$$-(c^2 + i\omega\eta)\eta\frac{\partial b_\theta}{\partial z} = \left(c_r^2 + i\omega\eta\right)e_r + c_r c_z e_z \tag{C.20}$$

$$(c^2 + i\omega\eta)\eta\frac{1}{r}\frac{\partial}{\partial r}(rb_\theta) = c_r c_z e_r + \left(c_z^2 + i\omega\eta\right)e_z, \tag{C.21}$$

where

$$c_r^2(r,z) = \frac{B_{or}^2(r,z)}{\mu_o\rho} \tag{C.22a}$$

$$c_z^2(r,z) = \frac{B_{oz}^2(r,z)}{\mu_o\rho} \tag{C.22b}$$

$$\eta = \frac{1}{\mu_o \sigma} \tag{C.22c}$$

$$c^2 = c_r^2 + c_z^2. \tag{C.22d}$$

Equations C.20, C.21 and C.16 may now be combined to obtain a single equation in b_θ

$$\left(c_r^2 + i\omega\eta\right)\frac{\partial}{\partial r}\frac{1}{r}\frac{\partial}{\partial r} r b_\theta + \left(c_r \frac{\partial c_r}{\partial r} + c_z \frac{\partial c_r}{\partial z}\right)\frac{1}{r}\frac{\partial}{\partial r} r b_\theta$$
$$+ c_r c_z \frac{1}{r}\frac{\partial}{\partial r} r \frac{\partial b_\theta}{\partial z} + \left(c_z \frac{\partial c_z}{\partial z} + c_r \frac{\partial c_z}{\partial r}\right)\frac{\partial b_\theta}{\partial z}$$
$$+ \left(c_z^2 + i\omega\eta\right)\frac{\partial^2 b_\theta}{\partial z^2} + c_r c_z \frac{\partial^2 b_\theta}{\partial r \partial z} + \omega^2 b_\theta = 0. \tag{C.23}$$

This appears to be extremely complex, since c_r and c_z are functions of both r and z. Because of the simple variation of the DC magnetic field in the related experiment, however, some simplifications may be made.

C.2 PROPERTIES OF THE MAGNETIC FIELD

Figure 16 is made from measurements taken on the actual magnetic field of the experiment. The objective of the magnetic-field design process was to achieve a variation of Alfvén speed over the cross section of the form

$$c_z = c_o \sqrt{1 + (r/b)^2}, \tag{C.24}$$

in order to take advantage of the considerable simplifications described in Appendix B.

Since the density and permeability of the fluid in (C.22b) are constants, only the magnetic field may be varied to achieve this result. The spatial derivatives of $\vec{B}_o$ are, however, related through the curl and divergence so that a radial component of the DC magnetic field must be present. Also, both components must be functions of r and z as in Eq. C.1, which results eventually in the complexity of Eq. C.23.

The solution of the Laplace equation in cylindrical coordinates in this situation may be formed from combinations of functions of the form

$$I_o\left(\frac{r}{b}\right) \cos 2\pi \frac{z}{h}. \tag{C.25}$$

Inspection of I_o reveals that it is very close to the form of Eqs. C.24. This suggests that B_{oz} may be written approximately

$$B_{oz}(r,z) = B_o \sqrt{1 + (r/b)^2} \cos 2\pi \frac{z}{h}, \tag{C.26}$$

where b and h are parameters to be determined from fitting (C.6) to the measurements presented in Fig. C-2. In this case b = 6.22" and h = 27.6". The divergence relation

may be satisfied by relating the constants b and h in Eq. C. 25. The curl relation, under the assumption of axisymmetry, reduces to

$$\frac{\partial B_{or}}{\partial z} - \frac{\partial B_{oz}}{\partial r} = 0 \tag{C. 27}$$

from which an expression for B_{or} may be deduced:

$$B_{or}(r,z) = -\frac{B_o}{2\pi}\frac{h}{b}\frac{(r/b)}{\sqrt{1+(r/b)^2}}\sin 2\pi\frac{z}{h}. \tag{C. 28}$$

Equations C. 26 and C. 28 are plotted in Fig. 16 for comparison with the measured fields. It may be seen that these forms fit the data almost exactly for most points. Notice that when a departure from the data occurs it is in the direction of overestimation of the relative magntiude of the radial component and the variation of the c_z component with z. Thus the longitudinal and radial Alfvén speeds in (C. 23) may be represented as

$$c_z(r,z) = c_o\sqrt{1+(r/b)^2}\cos 2\pi\frac{z}{h} \tag{C. 29}$$

$$c_r(r,z) = -\frac{c_o}{2\pi}\frac{h}{b}\frac{(r/b)}{\sqrt{1+(r/b)^2}}\sin 2\pi\frac{z}{h}. \tag{C. 30}$$

C. 3 SIMPLIFICATION OF THE WAVE EQUATION

In the experiment the region of interest in the DC magnetic field extends over the volume enclosed by the cylinder r = 6" and the planes z = ±2". Here the various terms in (C. 23) will be compared, to determine their relative magnitudes in the volume of interest as a measure of their effect on the solution. The expressions developed in section C. 2 for the magnetic field and Alfvén speeds will be used with b = 6. 22" and h = 27. 6".

The ratio of the two components of the second term is

$$\frac{c_r\frac{\partial c_r}{\partial r}}{c_z\frac{\partial c_r}{\partial z}} = -\left(\frac{h}{2\pi b}\right)^3\frac{\left(\frac{r}{b}\right)}{\left[1+\left(\frac{r}{b}\right)^2\right]^3}\tan 2\pi\frac{z}{h}. \tag{C. 31}$$

This ratio is zero at r = 0, at r = ∞, and at z = 0, with a maximum of 0.04 at r = 1.6" and z = 2".

The ratio of the two components of the fourth term is

$$\frac{c_r\frac{\partial c_z}{\partial r}}{c_z\frac{\partial c_z}{\partial z}} = \frac{2}{(2\pi)^3}\left(\frac{h}{b}\right)^2\frac{\left(\frac{r}{b}\right)^2}{\left[1+\left(\frac{r}{b}\right)^2\right]^3}. \tag{C. 32}$$

This ratio is zero at r = 0 and at r = ∞, with a maximum of 0.024 at r = 4.4" independent of z.

Since c_z varies only approximately 10% over the entire range of z under consideration, it is reasonable to expect that the waveguide will behave, in the main, as if there were no variation of c_z with z. This assumption will be examined in more detail below. The perturbation magnetic field may then be taken to vary as e^{ikz}. Equation C.23 may now be rewritten

$$\left(c_r^2+i\omega\eta\right)\frac{\partial}{\partial r}\frac{1}{r}\frac{\partial}{\partial r}rb_\theta + c_z\left(\frac{\partial c_r}{\partial z}+ikc_r\right)\frac{1}{r}\frac{\partial}{\partial r}rb_\theta$$

$$+ ikc_rc_z\frac{\partial b_\theta}{\partial r}+\left[\omega^2-k^2\left(c_z^2+i\omega\eta\right)+ikc_z\frac{\partial c_z}{\partial z}\right]b_\theta = 0. \qquad (C.33)$$

The ratio of the two components of the second term in (C.33) is

$$\frac{kc_r}{\frac{\partial c_r}{\partial z}} = \frac{kh}{2\pi}\tan 2\pi\frac{z}{h}. \qquad (C.34)$$

If the waveguide were responding mainly to the bulk field as if it were uniform, then $|k| \approx 40$ for a representative frequency. By using this value for the magnitude of k, the right side of Eq. C.34 is zero at z = 0, with a maximum of 86 at z = 2" independent of r. Thus the second component of the second term is much larger than the first, except in a region approximately 0.1" thick in z near z = 0. But it is precisely here that the second component becomes zero.

Comparing the principal components of the last term in (C.33) yields

$$\frac{kc_z\frac{\partial c_z}{\partial z}}{k^2c_z^2} = \frac{2\pi}{kh}\tan 2\pi\frac{z}{h}. \qquad (C.35)$$

This ratio is zero at z = 0, with a maximum of 0.0028 at z = 2" independent of r. Equation C.33 may then be reduced to

$$\left(c_r^2+i\omega\eta\right)\frac{\partial}{\partial r}\frac{1}{r}\frac{\partial}{\partial r}rb_\theta + ikc_rc_z\left(\frac{1}{r}\frac{\partial}{\partial r}rb_\theta+\frac{\partial b_\theta}{\partial r}\right)+\left[\omega^2-k^2\left(c_z^2+i\omega\eta\right)\right]b_\theta = 0. \qquad (C.36)$$

Notice that (C.36) is formally identical, in cylindrical coordinates, to (C.34), which was concerned with the effect of a transverse component of the DC magnetic field. Recall that, in the uniform case, the only effect of the transverse field was to introduce a low-frequency cutoff. For a transverse field which was 10% of the main field and other conditions similar to the experiment, the transverse field cutoff was near or below the low-frequency end of the Alfvén region. In this case the transverse field or c_r is zero at r = 0 and at z = 0, with a maximum of c_r/c_z at z = 2", r = 6" of 0.17, as in Eq. C.37.

$$\frac{c_r}{c_z} = -\frac{1}{2\pi}\frac{h}{b}\frac{(r/b)}{1+(r/b)^2}\tan 2\pi\frac{z}{h}. \tag{C.37}$$

The average value of $|c_r/c_z|$ in the volume is

$$\left|\frac{c_r}{c_z}\right|_{aver.} = \left[\frac{h^2 b}{2\pi^2 a^2 \ell}\right]\left[\frac{a}{b}-\tan^{-1}\frac{a}{b}\right]\left[-\ln\cos 2\pi\frac{z}{h}\right]. \tag{C.38}$$

For the conditions of the experiment this value is 0.022, the actual average being zero, because of the symmetry of the DC field. In Appendix B it was demonstrated that the propagation constant depended principally on the average value of the DC field. Thus for the frequencies of interest, the effects of the transverse component c_r may be dropped from (C.36) to leave

$$i\omega\eta\frac{\partial}{\partial r}\frac{1}{r}\frac{\partial}{\partial r}rb_\theta + \left[\omega^2 - k^2\left(c_z^2 + i\omega\eta\right)\right]b_\theta = 0 \tag{C.39}$$

which is identical to Eq. B. 22 for a waveguide having a uniform magnetic field and non-uniform density.

C.4 EFFECTS OF LONGITUDINAL NONUNIFORMITY

We have claimed that if the field varied only approximately 10% over the range of z under consideration, the waveguide would behave, in the main, as if there were no variation with z. From measurements of the magnetic field, it is found that C_z varies as $\cos 2\pi\frac{z}{27.6''}$ (Eq. C.29) over the range z = ±2". This is plotted as a solid line in Fig. C-1.

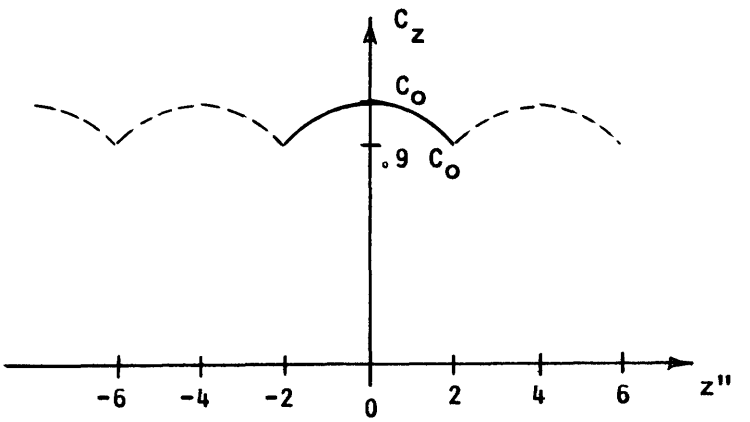

Fig. C-1. Variation of C_z in z.

But this segment of the z axis must be considered as part of an infinite continuum on z if the results are to be related to the behavior of an infinitely long waveguide. Another way of looking at this is to consider the progress of a wave launched at z = -2". It will

propagate in some manner to z = +2" where it will be reflected, propagate back to z = -2", be reflected again, and so on. Thus, to the wave, the 4"-segment of the z-axis appears to be like an infinitely long waveguide with C_z varying as the dashed lines in Fig. C-1. Thus, in order to estimate the effect of this variation, a good approximation is

$$C_z = C_o\left(0.95 + 0.05 \cos 2\pi\frac{z}{4}\right). \tag{C.40}$$

Consider now a lossless waveguide in which the longitudinal wave velocity is given by (C.40). In an infinite plane parallel geometry the wave equation (with x as the transverse direction) would be

$$\frac{\partial^2 u}{\partial x^2} + \frac{\omega^2}{C_z^2} u = 0. \tag{C.41}$$

By using C_z as given by (C.40) and expanding in terms of the small variation (C.41) becomes

$$\frac{\partial^2 u}{\partial x^2} + \frac{\omega^2}{0.9\, C_o^2}\left(1 - 0.1 \cos 2\pi\frac{z}{2}\right) u = 0. \tag{C.42}$$

This is one form of the well-known Mathieu equation. Equation C.42 may be put into the standard form

$$\frac{d^2 u}{d\zeta^2} + (\eta - \gamma \cos 2\zeta) u = 0 \tag{C.43}$$

by setting

$$z = \frac{2}{\pi}\zeta \tag{C.44}$$

$$\gamma = \frac{\omega^2 \pi^2}{3.6\, C_o^2} \tag{C.45}$$

$$\eta = \frac{\omega^2 \pi^2}{0.36\, C_o^2}. \tag{C.46}$$

Note that $\gamma = 0.1\ \eta$.

The diagram showing the various regions of the solution of Eq. C.43 is reproduced from Brillouin[30] as Fig. C-2. The bounded regions near the positive η-axis represent passing bands (unattenuated waves), and the remainder of the space represents stopping bands (attenuated waves). The line $\gamma = 0.1\ \eta$ is drawn in Fig. C-2. It is seen that while there are stopping bands existing in the limit as $\gamma \to 0$ (no

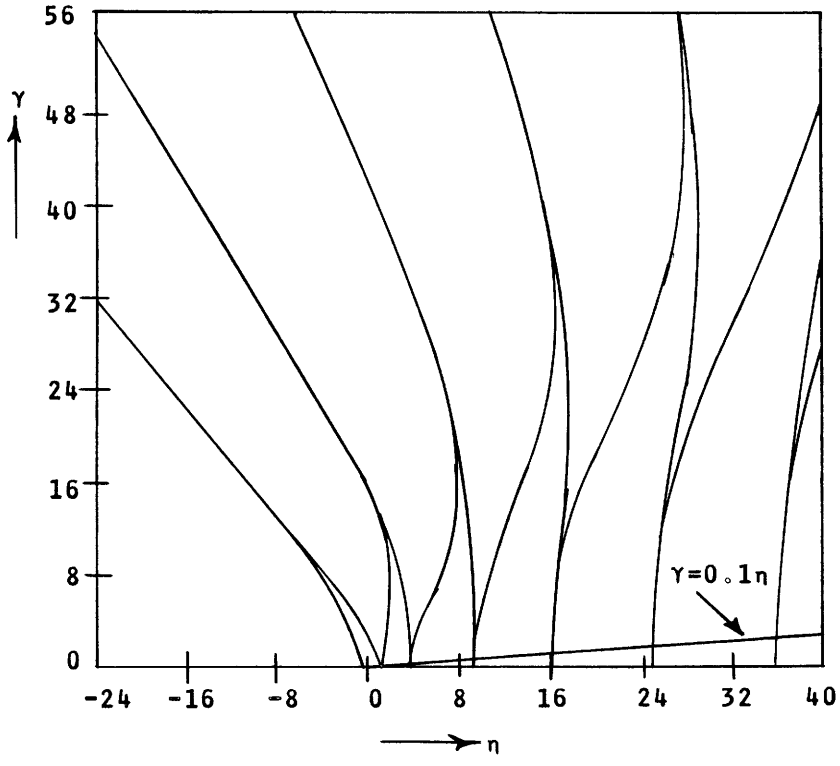

Fig. C-2. Regions of the solution of Mathieu's equation.

nonuniformity), they become infinitely narrow in the limit. For the longitudinal nonuniformity present in the experiment, stop bands exist but they are extremely narrow (in fact, not visible in Fig. C-2). The stop bands intersect the η-axis at

$$\eta = 1, 4, 9, \ldots, n^2, \tag{C.47}$$

where n is an integer. The frequencies of the stopping bands (ω_s) are then (with the use of C.46) given by

$$\omega_s = n \frac{0.6}{\pi} C_o. \tag{C.48}$$

The frequencies of the first few stopping bands are given in Table 4 for C_o = 30 m/sec.

Table 4. Typical stop-band frequencies.

n	$f_s = \frac{\omega_s}{2\pi}$ cps
1	0.91
2	1.83
3	2.74
4	3.65

These frequencies are all below the low-frequency diffusion cutoff in the hydromagnetic waveguide. As the index n of the stop band increases, the width of the band becomes narrower. Also, the effect of losses is to smooth over the stop band. The assumption of section C. 2 is then valid.

APPENDIX D

Hydromagnetic Columns

The starting point for this development is the linearized equations (6-9), but with $\vec{B}_o$ arbitrary in direction. The method of Rook[22] will be used. Let $\vec{\psi}$ and $\vec{A}$ be divergenceless vector potentials such that

$$\vec{v} = \nabla \times \vec{\psi} \quad ; \quad \nabla \cdot \vec{\psi} = 0 \tag{D. 1}$$

$$\vec{b} = \nabla \times \vec{A} \quad ; \quad \nabla \cdot \vec{A} = 0. \tag{D. 2}$$

Substituting in the linearized equations yields

$$\nabla^2 \vec{A} = -\sigma \mu_o [\vec{e} + (\nabla \times \vec{\psi}) \times \vec{B}_o] \tag{D. 3}$$

$$\mu_o \rho \frac{\partial}{\partial t} \nabla^2 \vec{\psi} = \nabla \times \left(\nabla^2 \vec{A} \times \vec{B}_o \right) \tag{D. 4}$$

$$\vec{e} = -\nabla \phi - \frac{\partial \vec{A}}{\partial t}, \tag{D. 5}$$

where ϕ is an arbitrary scalar potential. Further application of vector identities and manipulation yields

$$-\eta \nabla^2 \vec{A} = -\nabla \phi - \frac{\partial \vec{A}}{\partial t} + \left(\vec{B}_o \cdot \nabla \right) \vec{\psi} - \nabla \left(\vec{B}_o \cdot \vec{\psi} \right), \tag{D. 6}$$

where

$$\eta = \frac{1}{\mu_o \rho} = \text{magnetic diffusivity}, \tag{D. 7}$$

and

$$\mu_o \rho \frac{\partial}{\partial t} \nabla^2 \vec{\psi} = \left(\vec{B}_o \cdot \nabla \right) \nabla^2 \vec{A}. \tag{D. 8}$$

Since ϕ is arbitrary, let

$$\nabla \phi = -\nabla \left(\vec{B}_o \cdot \vec{\psi} \right). \tag{D. 9}$$

Equation D.6 now becomes

$$\eta \nabla^2 \vec{A} - \frac{\partial \vec{A}}{\partial t} = -\left(\vec{B}_o \cdot \nabla \right) \vec{\psi}. \tag{D. 10}$$

If, as assumed in Section II, $\vec{B}_o$ is aligned parallel to the z-axis, Eqs. D.6 and D.10 may be rewritten

$$\eta\nabla^2\vec{A} - \frac{\partial\vec{A}}{\partial t} = -B_o \frac{\partial\vec{\psi}}{\partial z} \tag{D.11}$$

$$\nabla^2 \frac{\partial\vec{\psi}}{\partial t} = \frac{C^2}{B_o} \frac{\partial^2\vec{A}}{\partial z^2}, \tag{D.12}$$

where

$$C^2 = \frac{B_o^2}{\mu_o \rho} \qquad \text{Alfvén speed} \tag{D.13}$$

Equations D. 11 and D. 12 may be combined to yield

$$\nabla^2 \left[\eta\nabla^2 \left(\frac{\partial\vec{A}}{\partial t}\right) - \frac{\partial^2\vec{A}}{\partial t^2} + C^2 \frac{\partial^2\vec{A}}{\partial z^2}\right] = 0 \tag{D.14}$$

and

$$\nabla^2 \left[\frac{\partial\vec{\psi}}{\partial t} - \frac{C^2}{B_o} \frac{\partial\vec{A}}{\partial z}\right] = 0. \tag{D.15}$$

Since (D.14) and (D.15) are linear, solutions will be of the form

$$\vec{A}(r, \theta, z, t) = \vec{a}(r)\, e^{i(n\theta+kz+\omega t)}. \tag{D.16}$$

Thus (D.14) and (D.15) become

$$\nabla^2[i\omega\eta\nabla^2\vec{a} + (\omega^2 - k^2C^2)\vec{a}\,] = 0 \tag{D.17}$$

$$\nabla^2 \left(\omega\vec{\psi} - \frac{kC^2}{B_o}\vec{a}\right) = 0. \tag{D.18}$$

There are four independent solutions to Eqs. D.17 and D.18. Two of them are given by $\nabla^2 = 0$ (potential flow), and one of these has zero curl resulting in identically zero fields. The two solutions corresponding to $\nabla^2 \neq 0$ give rise to the Alfvén TE and TM modes.

The results of section 2.1.1 may be obtained with this approach. If the problem is considered in rectangular coordinates, Eq. D.8 may be written

$$\nabla^2 \frac{\partial\vec{\psi}}{\partial t} = \frac{C^2}{B_o^2} \nabla^2[(\vec{B}_o \cdot \nabla)\vec{A}]. \tag{D.19}$$

Now (D.10) and (D.19) may be combined to give

$$\nabla^2\left[\nabla^2\frac{\partial\vec{A}}{\partial t}-\frac{\partial^2\vec{A}}{\partial t^2}+\frac{C^2}{B_o^2}(\vec{B}_o\cdot\nabla)^2\vec{A}\right]=0 \tag{D.20}$$

$$\nabla^2\left[\frac{\partial\vec{\psi}}{\partial t}-\frac{C^2}{B_o^2}(\vec{B}_o\cdot\nabla)\vec{A}\right]=0. \tag{D.21}$$

Again, there are two sets of solutions corresponding to $\nabla^2 = 0$ and $\nabla^2 \neq 0$. Only the $\nabla^2 \neq 0$, TM solution is of interest here.

Under the assumptions of section A.2.5, the x component of Eq. D.20 becomes

$$\left(C_{ox}^2+i\omega\eta\right)\frac{\partial^2 a_x}{\partial x^2}+2ikC_{ox}C_{oz}\frac{\partial a_x}{\partial x}+\left[\omega^2-k^2\left(C_{oz}^2+i\omega\eta\right)\right]a_{ox}=0 \tag{D.22}$$

which is seen to be the same as Eq. A.34 (Appendix A). Of the remaining components, $a_y = 0$ and a_z may be obtained through the divergence.

APPENDIX E

Alternative Derivation for Axisymmetric TM Modes in a Uniform Waveguide

The development is similar to that in Appendix B with the exception of Eqs. B.4, B.9, B.16, and B.17. Here the density and magnetic field are considered uniform, but the conductivity is taken to be a diagonal tensor.

$$\overleftrightarrow{\sigma} = \begin{bmatrix} \sigma_t & 0 & 0 \\ 0 & \sigma_t & 0 \\ 0 & 0 & \sigma_\ell \end{bmatrix} \tag{E.1}$$

Thus Eqs. B.16 and B.17 become

$$j_r = \sigma_t(e_r + v_\theta B_o) \tag{E.2}$$

$$j_z = \sigma_\ell e_z. \tag{E.3}$$

Defining a transverse and a longitudinal magnetic diffusivity η_t and η_ℓ,

$$\eta_{t,\ell} = \frac{1}{\mu_o \sigma_{t,\ell}} \tag{E.4}$$

and combining Eqs. B.12-B.25 and Eqs. E.2 and E.3 yields

$$\frac{\partial}{\partial r}\left[\frac{1}{r}\frac{\partial}{\partial r}(rb_\theta)\right] + \frac{1}{i\omega\eta_\ell}\left[\omega^2 - k^2\left(C^2 + i\omega\eta_t\right)\right] = 0 \tag{E.5}$$

for which the solutions that are finite at $r = 0$ are

$$b_\theta = B_\theta J_1(T_n r), \tag{E.6}$$

where

$$T_n^2 = \frac{\omega^2 - k^2\left(C^2 + i\omega\eta_t\right)}{i\omega\eta_\ell}. \tag{E.7}$$

With boundary condition of either a perfectly conducting or perfectly insulating wall fixing the value of T as a root of J_o or J_1, Eq. E.7 may be solved for k^2 to yield Eq. 48.

It may be noted from Fig. 3 that attenuation of the Alfvén wave is due primarily to currents flowing in the radial direction at high frequencies and by axial currents at low frequencies. This is also reflected in the dependence of the high-frequency limit on only the transverse conductivity, while the low-frequency limit depends on the longitudinal conductivity.

APPENDIX F

Resonator Design

The first problem that had to be solved in the resonator and pole-tip design (Appendix H) for nonuniform fields was the proportion of the available volume in the magnet gap which could be assigned to each one. Figure F-1 is a log-log plot of resonator

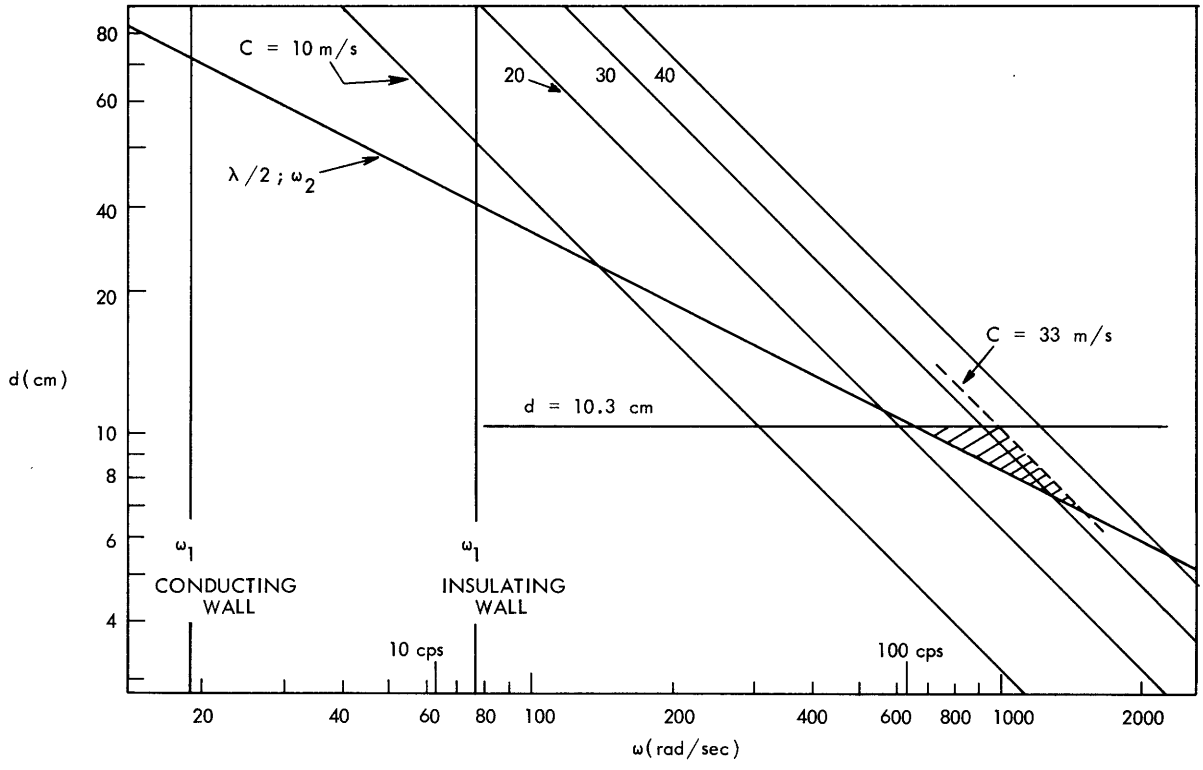

Fig. F-1. Design limitation chart for an NaK resonator.

length ℓ as a function of frequency for NaK and summarizes the important design criteria. The lines marked with various Alfvén speeds represent the length required to achieve a half-wave resonance. The line marked f_2 represents the upper critical frequency (Eq. 15) corresponding to the Alfvén speed on the intersecting lines. Clearly, if a resonance is to be observable, f_2 must be greater than the resonant frequency (see Fig. 2). The maximum Alfvén speed attainable is 33 m/sec shown by the dashed line (Fig. F-1). Therefore, a resonance will be observable only in the shaded region. Thus, in order to get the widest range of resonances, the length, ℓ, must be as large as possible.

A second consideration, independent of the foregoing, is the effect of f_1 (Eq. 14), which must be made as small as possible in order to reduce attenuation in the TM modes. The only way that this can be done is by making the radius, a, as large as possible.

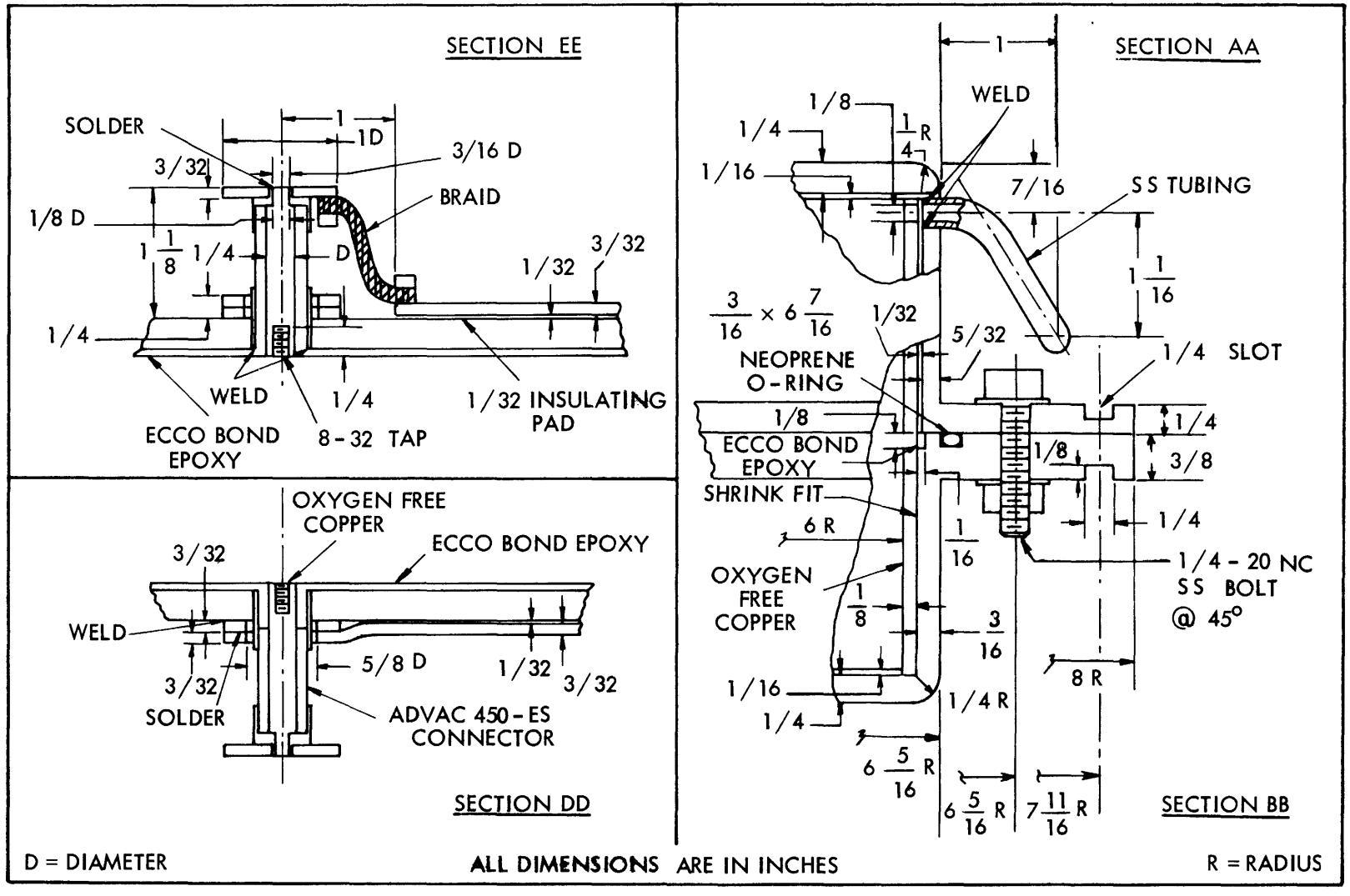

Fig. F-2. Construction and details of the resonator.
AA – Fill drain connection.
BB – Interior liners, sealing, and mounting.
DD and EE – Excitation terminals.

To the resonator length must be added 3/4" (1.9 cm) to allow for 1/32" clearances, the resonator shell, insulation, and excitation current leads (Fig. F-2). This plus the length ℓ must come from the availabe 7 1/2" (19.2 cm) available in the gap. The rest may be utilized for the pole tips. In order to get a reasonable variation of B_z in radius, the pole tips must extend as far as possible into the gap. The compromise arrived at was ℓ = 10.3 cm, which leaves 3.5 cm on each side for pole iron. The segment of the 10.3-cm line between the ω_2 and 33-m/sec lines is then the range of frequencies for the experiment (from 100 cps to 220 cps). Resonance was too weak to observe at the boundaries of the region.

Once the division of space had been made, the mechanical design of the resonator could proceed. The design objectives were the following.

1. Simplicity of construction to facilitate machining and cleaning.
2. Conformity to the theoretical model.
3. Compatibility with the nonuniform pole tips.
4. Ease of use.

APPENDIX G

Electronic Systems

The only major part of the electronic systems which was not available commercially was an amplifier that would reliably provide a sine-wave or square-wave signal of 100 amps peak-to-peak over a frequency range of 1-500 cps to an essentially short-circuit load. The amplifier diagramed in Fig. G-1 was constructed to meet these criteria.

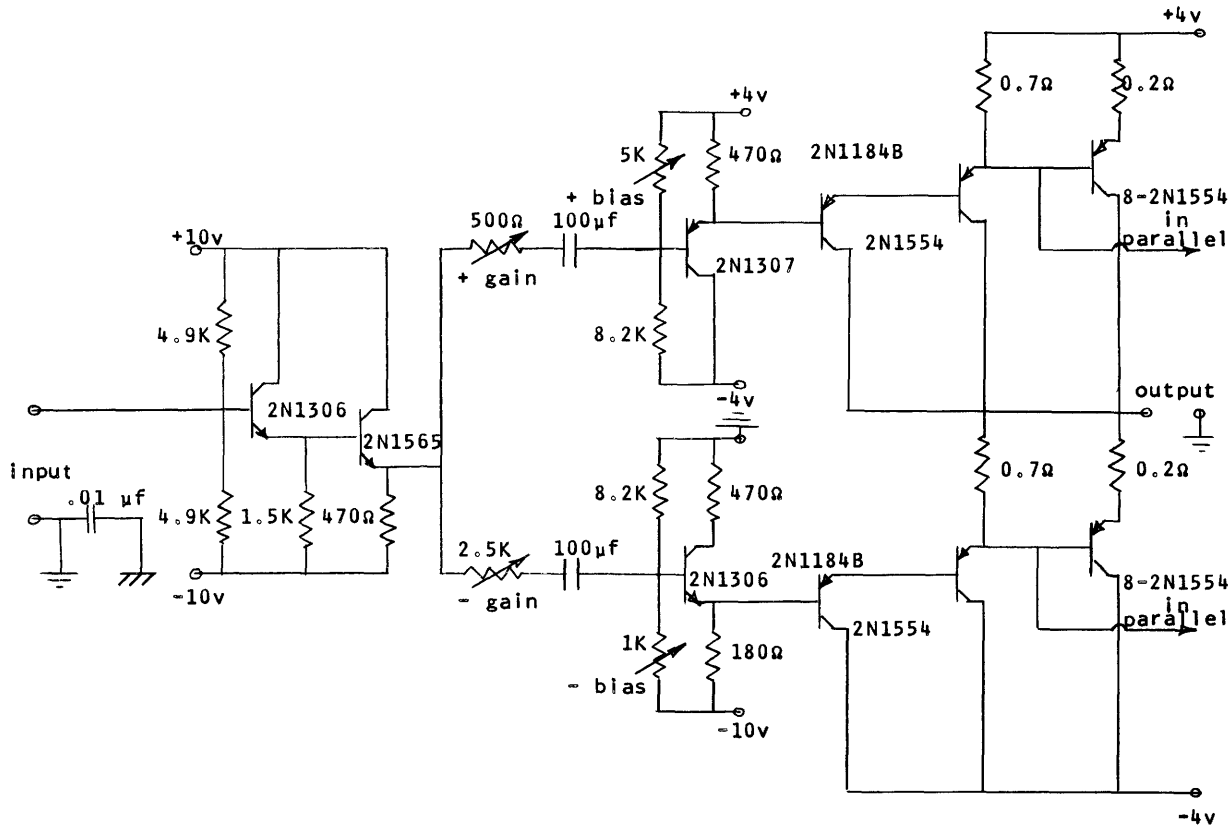

Fig. G-1. Amplifier schematic diagram.

APPENDIX H

Design of the Nonuniform Field

The pole trips were designed by an interaction of intuitive reasoning and checks with analog devices. The major proportions of the pole tips were arrived at by trying various shapes on the High Voltage Laboratory's cylindrical coordinate resistance network. Once the principal dimensions of the resonator and pole tips were set, details of the design were checked on Teledeltos paper.

Armco (pure) iron, heat-treated to give a saturation field of approximately 21,000 Gauss, was used. The pole tips were split in two in order to assemble the resonator and pole tips in the magnet gap.

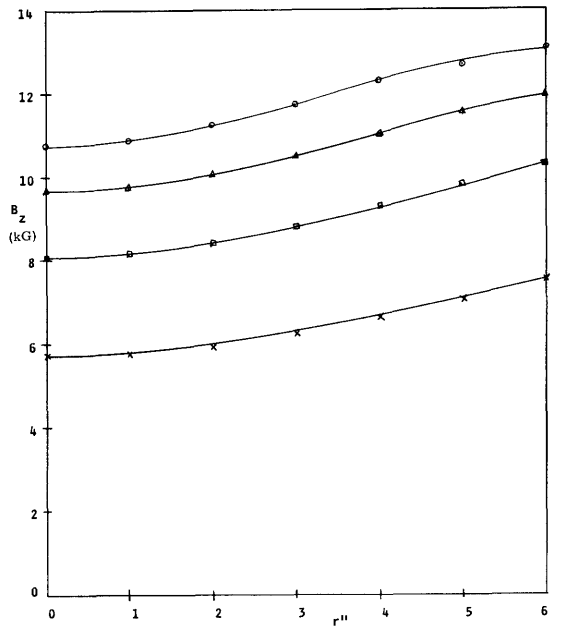

Fig. H-1. Nonuniform field B_z vs r; z = 1/4".

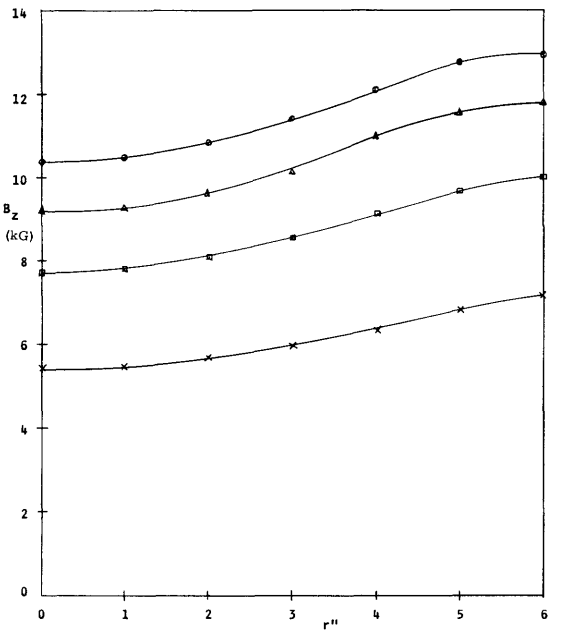

Fig. H-2. Nonuniform field B_z vs r; z = 3/4".

The results of the design are shown in the field maps of Figs. 15, 16, G-1, and H-1 through H-5. All of the fields were measured with a Rawson-Lush rotating coil gaussmeter.

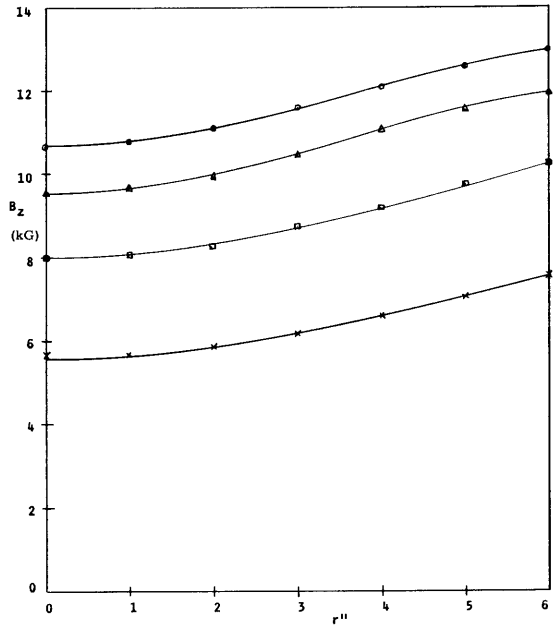

Fig. H-3. Nonuniform field B_z vs r; z = 1 1/4".

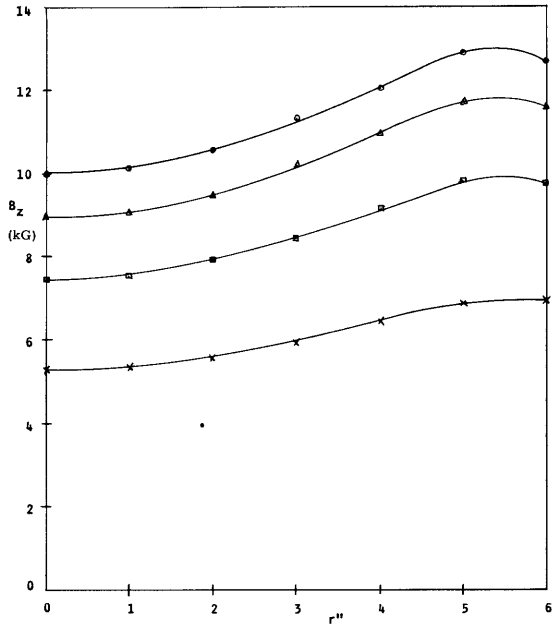

Fig. H-4. Nonuniform field B_z vs r; z = 1 3/4".

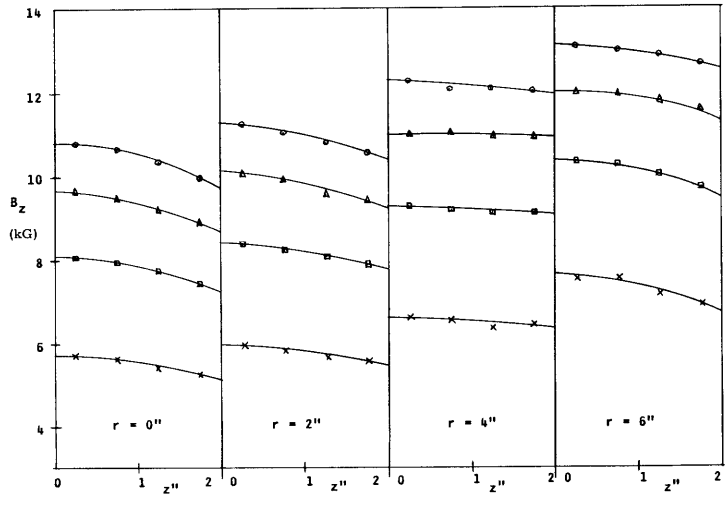

Fig. H-5. Nonuniform field B_z vs z for various r.

APPENDIX I

NaK Handling Techniques

In the use of liquid alkali metals for MHD experiments, two problems are always present. They are safety of personnel and structures and maintenance of purity. In this experiment, both problems were solved by building all NaK storage and handling apparatus in accordance with vacuum standards of cleanliness and leak proofing. NaK transfer was accomplished by pushing it from one place to another under dried argon pressure.

In practice, it has been found, at least in the experience of this experimenter, that handling NaK in this manner presents no great problems if much thought is given to the mechanical and chemical problems beforehand and if care is exercised in operation. The Liquid Metals Handbook (NaK Supplement)[31] is a good source of such information. Also, Eco-Body epoxy and Neoprene have been found to be compatible with NaK in these experiments at room temperature.

The philosophy in the design of this experiment was to use only proved materials and the simplest possible designs. It is well to keep in mind the fact that all parts must be cleaned of NaK after use; therefore, regions in which NaK can be trapped should be avoided. Similarly, since large parts should be cleaned with a fine spray of water (from a safe distance), materials that might be damaged by burning NaK should be avoided. Experience at the Massachusetts Institute of Technology has shown that if cleaning is done with suitable caution, after mechanically removing as much NaK as possible, even ordinary epoxies will survive in good condition.

APPENDIX J

Algebraic Details of the Perturbation Solution

In carrying out the perturbation solutions, certain particular integrals of the Bessel equations were required. These were found by construction. The solution to the equation

$$L(y) = r^n J_\ell(Tx) \tag{J.1}$$

is required, where ℓ may be either 0 or 1, and L(y) is given by

$$L(y) = \frac{d^2y}{dx^2} + \frac{1}{x}\frac{dy}{dx} + \left(T^2 - \frac{1}{x^2}\right) y. \tag{J.2}$$

For n odd and $\ell = 0$,

$$y = \sum_{k=1}^{n} C_k r^{n+2-k} J_m(Tr), \tag{J.3}$$

where

$$m = \begin{cases} 0 & k \text{ even} \\ 1 & k \text{ odd} \end{cases} \tag{J.4}$$

and ([A] is the integral part of A)

$$C_N = \frac{(-1)^{\left[\frac{N-1}{2}\right]}}{(2T)^N} \frac{(n+2-N)!}{(n+1)!} \prod_{k=0}^{\left[\frac{N}{2}\right]-1} (n+1-2k)(n-1-2k)$$

$$* \prod_{k=0}^{\left[\frac{N-1}{2}\right]-1} (n+1-2k)(n-1-2k) \qquad N \leq n;\ k \geq 0. \tag{J.5}$$

For n even and $\ell = 1$,

$$y = \sum_{k=1}^{n} C_k r^{n+2-k} J_m(Tr), \tag{J.6}$$

where

$$m = \begin{cases} 0 & k \text{ odd} \\ 1 & k \text{ even} \end{cases} \tag{J.7}$$

and

$$C_N = \frac{(-1)^{\left[\frac{N}{2}\right]+1}}{(2T)^N} \frac{(n+2-N)!}{(n+1)!} \prod_{k=0}^{\left[\frac{N-1}{2}\right]} (n+2-2k)(n-2k)$$

$$* \prod_{k=1}^{\left[\frac{N}{2}\right]-1} (n+2-2k)(n-2k) \qquad N \leq n;\ k \geq 0. \tag{J.8}$$

APPENDIX K

Hydromagnetic Capacitor

Consider a mass of fluid of density, ρ, to be excited by a current of the form

$$J_r = \frac{i_t}{(1-e^{\ell/L})\, 2\pi aL} \frac{e^{-z/L}}{r/a} \tag{K. 1}$$

in a hollow cylindrical structure as shown in Fig. 6. The cylinder is immersed in a non-uniform magnetic field, $B_z(r)$. The current is collected at the wall ($r = a$) and injected through a disk of radius g. If the fluid is assumed to rotate as a solid body, the equation of motion is

$$\frac{\pi\rho a^4 \ell}{2} \frac{d^2\theta}{dt^2} = \int_0^{\ell} \int_0^{2\pi} \int_g^a rJ_r B_z r \, dr d\theta dz. \tag{K. 2}$$

For the condition of this experiment, $B_z(r)$ is taken to be

$$B_z(r) = B_o \sqrt{1 + (r/b)^2}. \tag{K. 3}$$

Thus Eq. K. 2 becomes

$$\frac{d^2\theta}{dt^2} = \frac{2B_o b^2}{3\pi\rho a^4 \ell} i_t \left\{ \left[1 + \left(\frac{a}{b}\right)^2 \right]^{3/2} - \left[1 + \left(\frac{g}{b}\right)^2 \right]^{3/2} \right\}. \tag{K. 4}$$

Similarly, the terminal voltage, v_t, becomes

$$v_t = \int_g^a B_z r \frac{d\theta}{dt} \, dr. \tag{K. 5}$$

By utilizing (K. 3) and (K. 4), (K. 5) becomes

$$v_t = \frac{2B_o^2 b^4}{9\pi\rho a^4 \ell} \left\{ \left[1 + \left(\frac{a}{b}\right)^2 \right]^{3/2} - \left[1 + \left(\frac{g}{b}\right)^2 \right]^{3/2} \right\}^2 \int_{-\infty}^{t} i_t \, dt. \tag{K. 6}$$

Thus it is seen that as far as the electrical terminals are concerned, this is a capacitor

$$C_{HM} = \frac{\pi\rho a^4 \ell}{2B_{ave}^2}, \tag{K. 7}$$

where

$$v_t = \frac{1}{C_{HM}} \int_{-\infty}^{t} i_t \, dt. \tag{K. 8}$$

In the limit of uniform fields $b \to \infty$, and C_{HM} becomes

$$C_{HM} = \frac{2\pi a^4 \ell \rho}{B_o^2 (a^2 - g^2)^2} = \frac{2\pi a^4 \ell}{\mu_o C_o^2 (a^2 - g^2)^2} \tag{K. 9}$$

where

$$C_o^2 = \frac{B_o^2}{\mu_o \rho} \tag{K. 10}$$

is the Alfvén speed at $r = 0$ if the mass were liquid.

APPENDIX L

Hydromagnetic Resonators

Equations 21-24 may be put into a more convenient form for consideration of the hydromagnetic waveguide as an axisymmetric TM resonator. Thus

$$b_\theta = B_\theta^{\pm} J_1(Tr) \tag{L.1}$$

$$v_\theta = \mp \frac{kc^2}{\omega} \frac{b_\theta}{B_o} \tag{L.2}$$

$$e_z = \eta T B_\theta^{\pm} J_o(Tr) \tag{L.3}$$

$$j_z = \frac{T}{\mu_o} B_\theta^{\pm} J_o(Tr) \tag{L.4}$$

$$j_r = \pm \frac{ik}{\mu_o} B_\theta^{\pm} J_1(Tr) \tag{L.5}$$

$$e_r = \pm k \left(i\eta + \frac{c^2}{\omega}\right) b_\theta, \tag{L.6}$$

where $B_\theta^{\pm}$ is the coefficient for the waves travelling in the +z and -z directions, respectively, and all quantities vary as

$$e^{i(\omega t \mp kz)} \tag{L.7}$$

or typically

$$b_\theta(r,z,t) = J_1(Tr)\left[B_\theta^{+} e^{i(\omega t - kz)} + B_\theta^{-} e^{i(\omega t + kz)}\right]. \tag{L.8}$$

The cylindrical wall boundary conditions set T and in turn k. If the wall is a perfect conductor, $e_z(a) = 0$, and if a perfect insulator, $j_r(a) = 0$. The end walls specify the relation between B_θ^{+} and B_θ^{-}. In fact, for end walls of arbitrary electrical properties a general reflection coefficient

$$\Gamma = \frac{B_\theta^{-}(\ell)}{B_\theta^{+}(\ell)} \tag{L.9}$$

may be defined. Thus the situation is exactly analogous to an ordinary lossy waveguide, except that the propagation constant and field coefficients are quite different. If the end wall is a perfect conductor at z = 0,

$$e_r = 0 = k\left(i\eta - \frac{c^2}{\omega}\right) e^{i\omega t} J_1(Tr)\left[B_\theta^{+} - B_\theta^{-}\right], \tag{L.10}$$

and $\Gamma = +1$. If the end wall at z = 0 is a perfect insulator

$$j_z = 0 = \frac{T}{\mu_o} J_o(Tr)\, e^{i\omega t}\left[B_\theta^+ + B_\theta^-\right], \tag{L. 11}$$

and $\Gamma = -1$.

Consider a resonator constructed, as in Fig. 6, of a conducting cylinder of radius a and length ℓ insulated at both ends and driven at one end by a disk of radius g insulated except on the edges. The terminal voltage v_t is given by the line integral at z = 0,

$$v_t = \int_g^a e_r\, dr, \tag{L. 12}$$

and the terminal current i_t is given by the wall current at r = a which is in turn obtained by setting $\vec{n} \times \vec{b}(a) = \vec{k}$ or

$$i_t = 2\pi a b_\theta(a). \tag{L. 13}$$

Under these conditions Rink[24] has shown that (with an arbitrary termination) the input impedance is given for the lowest order mode by

$$Z_i = ik\left(\eta + \frac{c^2}{i\omega}\right)\frac{J_o^2(Tg)}{J_1^2(Ta)}\,\frac{\mu_o}{\pi a^2 T^2}\,\frac{1 - \Gamma e^{-2ik\ell}}{1 + \Gamma e^{-2ik\ell}}. \tag{L. 14}$$

(Note that slightly different results will be obtained by following the definitions (L. 12) and (L. 13) exactly. This formulation is, however, more realistic, as it is based on a consideration of all modes rather than just one.)

For the half-wave resonator with insulated end walls, $\Gamma = -1$ and Eq. L. 14 may be rewritten

$$Z_{i\frac{\lambda}{2}} = ik\eta\left(1 + \frac{2\omega_2}{i\omega}\right)\frac{J_o^2(Tg)}{J_1^2(Ta)}\,\frac{\mu_o}{\pi a^2 T^2}\cot k\ell, \tag{L. 15}$$

where the critical frequencies ω_1 and ω_2 are as defined in Appendix A.

If $\omega_1 \ll \omega \leq \omega_2$ or if $\sigma = \infty$ ($\eta = 0$ and $\omega_2 = \infty$), the equivalent parallel LC circuit may be found for the vicinity of an impedance maximum by expanding the input impedance Z_i of Eq. L. 15 about the resonance frequency and comparing this with a similar expansion for the input impedance of a parallel RLC circuit.

$$Z_{RLC} = \frac{i\omega L_e}{\left(1 - \omega^2 L_e C_e\right) + \frac{i\omega L}{R_e}}. \tag{L. 16}$$

This results in

$$C_e = \frac{\pi \ell a^2 T^2 J_1^2(Ta)}{2\mu_o C^2 J_o^2(Tg)} \qquad \text{(L. 17)}$$

$$L_e = \frac{2\ell\mu_o J_o^2(Tg)}{\pi^3 b^2 T^2 J_1^2(Ta)} \qquad \text{(L. 18)}$$

$$R_e = \frac{2\mu_o^2 \sigma C^2 J_o^2(Tg)}{\pi \ell g^2 T^4 J_1^2(Ta)}. \qquad \text{(L. 19)}$$

Acknowledgment

I wish to thank Professor William D. Jackson for his advice, encouragement and gentle prodding throughout the long course of this thesis. I also wish to thank Dr. John Penhune for his helpful advice and support and Professor Hermann A. Haus for his critical reviews which helped to keep this work on the right track.

I particularly want to thank my wife, Edith Moses Kliman, who contributed directly to this research with aid in computer programming and card punching, data taking in the laboratory, and general service as a laboratory technician.

Of the many people who have helped me directly and indirectly, I wish to single out a few who made major contributions: the student technicians, Richard Diephuis, who developed and built the power amplifier, and Richard Koralek, who aided me during the last trying year of this work; the machinists under the able direction of John Keefe of the Research Laboratory of Electronics machine shop, Fred Liljeholm, who made the nonuniform pole tips, and Ernie Schmid, who built the resonator; Paul Murray and Fred Broderick of the Electrical Engineering Department instrument rooms for their cooperation and patience; Professor Robert Cooper and Dr. Charles Rook for their stimulating discussions; and Dr. Sanborn Philp for the use of the High Voltage Laboratory cylindrical coordinate analog board.

Numerical calculations performed during this study were done in part at the Computation Center of the Massachusetts Institute of Technology. Use of the facilities of the Research Laboratory of Electronics, M. I. T., is gratefully acknowledged.

References

1. T. G. Cowling, Magnetohydrodynamics (Interscience Publishers, London, 1957).
2. H. Alfvén, Cosmical Electrodynamics (Oxford University Press, London, 1950), Chaps. 4 and 5.
3. B. Lehnert, "MHD Waves in Liquid Na," Phys. Rev. 94, 815-24 (1954).
4. S. Lundquist, "Experimental Investigation of MHD Waves," Phys. Rev. 76, 1805-9 (1949).
5. J. M. Wilcox, A. W. daSilva, W. S. Cooper III, and F. I. Boley, "Experiments on Alfvén Wave Propagation," Radiation and Waves in Plasma, M. Mitchner (ed.) (Stanford University Press, Stanford, Calif., 1961), p. 138.
6. D. F. Jephcott, P. M. Stocker, and L. C. Woods, "Alfvén Waves in a Real Plasma – Theory and Experiment," IAEA Report CN-10/62, 1962.
7. D. J. DeCourcy, Jr., and M. H. Bruce, Report AFCRL G2-550, 1962.
8. N. Gothard, "Excitation of Hydromagnetic Waves in a Highly Conducting Liquid," Phys. Fluids 7, 1784 (1964).
9. B. Wessler and W. D. Jackson (private communication, 1965).
10. N. Gothard, W. D. Jackson, and J. F. Carson, "Preliminary Experiments with a Liquid Metal MHD Waveguide," Bull. Am. Phys. Soc., Ser. 11, Vol. 9, p. 587, March 1964.
11. B. Wessler, W. D. Jackson, and G. B. Kliman, "Experiments with a Liquid-Metal Magnetohydrodynamic Waveguide," Quarterly Progress Report No. 77, Research Laboratory of Electronics, M.I.T., April 15, 1965, pp. 205-208.
12. P. Jameson, "A Demonstration of Alfvén Waves," J. Fluid Mech. 19, 513 (August 4, 1964).
13. J. D. Ramer, Bibliography on Plasma Physics and MHD and Their Relations to Controlled Thermonuclear Reactions (University of Maryland, Engineering and Physical Sciences Library, 1959).
14. F. H. Clauser (ed.), Symposium of Plasma Dynamics (Addison-Wesley Publishing Co., Inc., Reading, Mass., 1960).
15. A. Baños, "Fundamental Wave Functions in an Unbounded MHD Field," Phys. Rev. 97, 1435-53 (1955).
16. E. Blue, "Torsional MHD Waves in the Presence of Finite Viscosity," Report AD-115 096, 1957.
17. W. A. Newcomb, "The Hydromagnetic Wave Guide," in Magnetohydrodynamics, R. K. M. Landshoff (ed.) (Stanford University Press, Stanford, Calif., 1957), p. 109.
18. R. Gajewski, "MHD Waves in Wave-Guides," Phys. Fluids 2, 633 (1959).
19. J. Shmoys and E. Mishkin, "Hydromagnetic Waveguides with Finite Conductivity and Arbitrary Cross Section, Phys. Fluids 3, 473 (1960).
20. R. Gould, "Excitation of Alfvén Waves," STL Report TR-60-0000-09143, 1960.
21. L. C. Woods, "Hydromagnetic Waves in a Cylindrical Plasma," UKEA Research Group Report CLM-R5, 1961.
22. C. W. Rook, Jr., "Free Surface Waves on Electrically Conducting Fluids," Sc.D. Thesis, Department of Electrical Engineering, M.I.T., Cambridge, Mass., 1964.
23. R. Gajewski and O. K. Marwardi, "Hydromagnetic Resonators," Phys. Fluids 3, 820 (1960).
24. R. E. Rink, "Torsional Modes in Hydromagnetic Waveguides – Some Practical Considerations," S.B. Thesis, Department of Electrical Engineering, M. I. T., Cambridge, Mass., 1962.

25. G. W. Pneuman, "Hydromagnetic Waves in a Current Carrying Plasma Column With Non-uniform Mass Density," Phys. Fluids 8, 507 (1965).

26. A. D. Berk, "Cavities and Waveguides with Inhomogeneous and Anisotropic Media," Sc.D. Thesis, Department of Electrical Engineering, M.I.T., Cambridge, Mass., 1954.

27. R. Gajewski and F. Winterberg, "Alfvén Waves in Inhomogeneous Magnetic Fields," Report D1-82-0111, Boeing Scientific Research Laboratories, 1961.

28. R. Gajewski and F. Winterberg, "Hydromagnetic Waves in Certain Inhomogeneous Magnetic Fields, Report D1-82-0114, Boeing Scientific Research Laboratories, 1961.

29. V. Rojansky, Introductory Quantum Mechanics (Prentice Hall, Inc., Englewood Cliffs, N.J., 1938).

30. L. Brillouin, Wave Propagation in Periodic Structures (Dover Publications, Inc., New York, 1953).

31. Navexos, Liquid Metals Handbook: A Guide to the Use of Liquid Metals as Heat Transfer Media, R. V. Lyon (Ed.-in-Chief) (AEC, ONR, 1950); and NaK Supplement (1955).

32. S. Nagao and T. Sato, "Experimental Study on Plasma Alfvén Waves," Department of Electrical Engineering, Tohoku University, Sendai, Japan, 1961.

JOINT SERVICES ELECTRONICS PROGRAM
REPORTS DISTRIBUTION LIST

Department of Defense

Dr. Edward M. Reilley
Asst Director (Research)
Ofc of Defense Res & Eng
Department of Defense
Washington, D.C. 20301

Office of Deputy Director
(Research and Information Room 3D1037)
Department of Defense
The Pentagon
Washington, D.C. 20301

Director
Advanced Research Projects Agency
Department of Defense
Washington, D.C. 20301

Director for Materials Sciences
Advanced Research Projects Agency
Department of Defense
Washington, D.C. 20301

Headquarters
Defense Communications Agency (333)
The Pentagon
Washington, D.C. 20305

Defense Documentation Center
Attn: TISIA
Cameron Station, Bldg. 5
Alexandria, Virginia 22314

Director
National Security Agency
Attn: Librarian C-332
Fort George G. Meade, Maryland 20755

Weapons Systems Evaluation Group
Attn: Col. Daniel W. McElwee
Department of Defense
Washington, D.C. 20305

National Security Agency
Attn: R4-James Tippet
Office of Research
Fort George G. Meade, Maryland 20755

Central Intelligence Agency
Attn: OCR/DD Publications
Washington, D.C. 20505

Department of the Air Force

Colonel Kee
AFRSTE
Hqs. USAF
Room ID-429, The Pentagon
Washington, D.C. 20330

Colonel A. Swan
Aerospace Medical Division
Brooks Air Force Base, Texas 78235

AUL3T-9663
Maxwell AFB, Alabama 36112

AFFTC (FTBPP-2)
Technical Library
Edwards AFB, Calif. 93523

Space Systems Division
Air Force Systems Command
Los Angeles Air Force Station
Los Angeles, California 90045
Attn: SSSD

Major Charles Waespy
Technical Division
Deputy for Technology
Space Systems Division, AFSC
Los Angeles, California 90045

SSD(SSTRT/Lt. Starbuck)
AFUPO
Los Angeles, California 90045

Det #6, OAR (LOOAR)
Air Force Unit Post Office
Los Angeles, California 90045

Systems Engineering Group (RTD)
Technical Information Reference Branch
Attn: SEPIR
Directorate of Engineering Standards
and Technical Information
Wright-Patterson AFB, Ohio 45433

ARL (ARIY)
Wright-Patterson AFB, Ohio 45433

Dr. H. V. Noble
Air Force Avionics Laboratory
Wright-Patterson AFB, Ohio 45433

Mr. Peter Murray
Air Force Avionics Laboratory
Wright-Patterson AFB, Ohio 45433

AFAL (AVTE/R. D. Larson)
Wright-Patterson AFB, Ohio 45433

Commanding General
Attn: STEWS-WS-VT
White Sands Missile Range
New Mexico 88002

RADC (EMLAL-1)
Griffiss AFB, New York 13442
Attn: Documents Library

Academy Library (DFSLB)
U.S. Air Force Academy
Colorado Springs, Colorado 80912

Lt. Col. Bernard S. Morgan
Frank J. Seiler Research Laboratory
U.S. Air Force Academy
Colorado Springs, Colorado 80912

APGC (PGBPS-12)
Eglin AFB, Florida 32542

AFETR Technical Library
(ETV, MU-135)
Patrick AFB, Florida 32925

AFETR (ETLLG-1)
STINFO Officer (for Library)
Patrick AFB, Florida 32925

Dr. L. M. Hollingsworth
AFCRL (CRN)
L. G. Hanscom Field
Bedford, Massachusetts 01731

AFCRL (CRMXLR)
AFCRL Research Library, Stop 29
L. G. Hanscom Field
Bedford, Massachusetts 01731

Colonel Robert E. Fontana
Department of Electrical Engineering
Air Force Institute of Technology
Wright-Patterson AFB, Ohio 45433

Colonel A. D. Blue
RTD (RTTL)
Bolling Air Force Base, D.C. 20332

Dr. I. R. Mirman
AFSC (SCT)
Andrews Air Force Base, Maryland 20331

Colonel J. D. Warthman
AFSC (SCTR)
Andrews Air Force Base, Maryland 20331

Lt. Col. J. L. Reeves
AFSC (SCBB)
Andrews Air Force Base, Maryland 20331

ESD (ESTI)
L. G. Hanscom Field
Bedford, Massachusetts 01731

AEDC (ARO, INC)
Attn: Library/Documents
Arnold AFS, Tennessee 37389

European Office of Aerospace Research
Shell Building
47 Rue Cantersteen
Brussels, Belgium

Lt. Col. Robert B. Kalisch
Chief, Electronics Division
Directorate of Engineering Sciences
Air Force Office of Scientific Research
Arlington, Virginia 22209

Department of the Army

U.S. Army Research Office
Attn: Physical Sciences Division
3045 Columbia Pike
Arlington, Virginia 22204

Research Plans Office
U.S. Army Research Office
3045 Columbia Pike
Arlington, Virginia 22204

Commanding General
U.S. Army Materiel Command
Attn: AMCRD-RS-DE-E
Washington, D.C. 20315

Commanding General
U.S. Army Strategic Communications
Command
Washington, D.C. 20315

Commanding Officer
U.S. Army Materials Research Agency
Watertown Arsenal
Watertown, Massachusetts 02172

Commanding Officer
U.S. Army Ballistics Research Laboratory
Attn: V. W. Richards
Aberdeen Proving Ground
Aberdeen, Maryland 21005

Commandant
U.S. Army Air Defense School
Attn: Missile Sciences Division C&S Dept.
P.O. Box 9390
Fort Bliss, Texas 79916

Commanding General
U.S. Army Missile Command
Attn: Technical Library
Redstone Arsenal, Alabama 35809

Commanding General
Frankford Arsenal
Attn: L600-64-4 (Dr. Sidney Ross)
Philadelphia, Pennsylvania 19137

U.S. Army Munitions Command
Attn: Technical Information Branch
Picatinney Arsenal
Dover, New Jersey 07801

Commanding Officer
Harry Diamond Laboratories
Attn: Dr. Berthold Altman (AMXDO-TI)
Connecticut Avenue and Van Ness St. N. W.
Washington, D.C. 20438

Commanding Officer
U.S. Army Security Agency
Arlington Hall
Arlington, Virginia 22212

Commanding Officer
U.S. Army Limited War Laboratory
Attn: Technical Director
Aberdeen Proving Ground
Aberdeen, Maryland 21005

Commanding Officer
Human Engineering Laboratories
Aberdeen Proving Ground, Maryland 21005

Director
U.S. Army Engineer
Geodesy, Intelligence and Mapping
Research and Development Agency
Fort Belvoir, Virginia 22060

Commandant
U.S. Army Command and General
Staff College
Attn: Secretary
Fort Leavenworth, Kansas 66270

Dr. H. Robl, Deputy Chief Scientist
U.S. Army Research Office (Durham)
Box CM, Duke Station
Durham, North Carolina 27706

Commanding Officer
U.S. Army Research Office (Durham)
Attn: CRD-AA-IP (Richard O. Ulsh)
Box CM, Duke Station
Durham, North Carolina 27706

Librarian
U.S. Army Military Academy
West Point, New York 10996

The Walter Reed Institute of Research
Walter Reed Medical Center
Washington, D.C. 20012

Commanding Officer
U.S. Army Engineer R&D Laboratory
Attn: STINFO Branch
Fort Belvoir, Virginia 22060

Commanding Officer
U.S. Army Electronics R&D Activity
White Sands Missile Range,
New Mexico 88002

Dr. S. Benedict Levin, Director
Institute for Exploratory Research
U.S. Army Electronics Command
Fort Monmouth, New Jersey 07703

Director
Institute for Exploratory Research
U.S. Army Electronics Command
Attn: Mr. Robert O. Parker, Executive
Secretary, JSTAC (AMSEL-XL-D)
Fort Monmouth, New Jersey 07703

Commanding General
U.S. Army Electronics Command
Fort Monmouth, New Jersey 07703
Attn: AMSEL-SC
RD-D
RD-G
RD-GF
RD-MAT
XL-D
XL-E
XL-C
XL-S
HL-D
HL-CT-R
HL-CT-P
HL-CT-L
HL-CT-O
HL-CT-I
HL-CT-A
NL-D
NL-A
NL-P
NL-R
NL-S
KL-D
KL-E
KL-S
KL-TM
KL-TQ
KL-TS
VL-D
WL-D

Department of the Navy

Chief of Naval Research
Department of the Navy
Washington, D.C. 20360
Attn: Code 427

Naval Electronics Systems Command
ELEX 03
Falls Church, Virginia 22046

Naval Ship Systems Command
SHIP 031
Washington, D.C. 20360

Naval Ship Systems Command
SHIP 035
Washington, D.C. 20360

Naval Ordnance Systems Command
ORD 32
Washington, D.C. 20360

Naval Air Systems Command
AIR 03
Washington, D.C. 20360

Commanding Officer
Office of Naval Research Branch Office
Box 39, Navy No 100 F.P.O.
New York, New York 09510

Commanding Officer
Office of Naval Research Branch Office
219 South Dearborn Street
Chicago, Illinois 60604

Commanding Officer
Office of Naval Reasearch Branch Office
1030 East Green Street
Pasadena, California 91101

Commanding Officer
Office of Naval Research Branch Office
207 West 24th Street
New York, New York 10011

Commanding Officer
Office of Naval Research Branch Office
495 Summer Street
Boston, Massachusetts 02210

Director, Naval Research Laboratory
Technical Information Officer
Washington, D.C. 20360
Attn: Code 2000

Commander
Naval Air Development and Material Center
Johnsville, Pennsylvania 18974

Librarian
U.S. Naval Electronics Laboratory
San Diego, California 95152

Commanding Officer and Director
U.S. Naval Underwater Sound Laboratory
Fort Trumbull
New London, Connecticut 06840

Librarian
U.S. Navy Post Graduate School
Monterey, California 93940

Commander
U.S. Naval Air Missile Test Center
Point Magu, California 93041

Director
U.S. Naval Observatory
Washington, D.C. 20390

Chief of Naval Operations
OP-07
Washington, D.C. 20350

Director, U.S. Naval Security Group
Attn: G43
3801 Nebraska Avenue
Washington, D.C. 20390

Commanding Officer
Naval Ordnance Laboratory
White Oak, Maryland 21502

Commanding Officer
Naval Ordnance Laboratory
Corona, California 91720

Commanding Officer
Naval Ordnance Test Station
China Lake, California 93555

Commanding Officer
Naval Avionics Facility
Indianapolis, Indiana 46241

Commanding Officer
Naval Training Device Center
Orlando, Florida 32811

U.S. Naval Weapons Laboratory
Dahlgren, Virginia 22448

Weapons Systems Test Division
Naval Air Test Center
Patuxtent River, Maryland 20670
Attn: Library

Head, Technical Division
U.S. Naval Counter Intelligence
Support Center
Fairmont Building
4420 North Fairfax Drive
Arlington, Virginia 22203

Other Government Agencies

Mr. Charles F. Yost
Special Assistant to the Director
of Research
National Aeronautics and
Space Administration
Washington, D.C. 20546

Dr. H. Harrison, Code RRE
Chief, Electrophysics Branch
National Aeronautics and
Space Administration
Washington, D.C. 20546

Goddard Space Flight Center
National Aeronautics and
Space Administration
Attn: Library C3/TDL
Green Belt, Maryland 20771

NASA Lewis Research Center
Attn: Library
21000 Brookpark Road
Cleveland, Ohio 44135

National Science Foundation
Attn: Dr. John R. Lehmann
Division of Engineering
1800 G Street, N.W.
Washington, D.C. 20550

U.S. Atomic Energy Commission
Division of Technical Information Extension
P.O. Box 62
Oak Ridge, Tennessee 37831

Los Alamos Scientific Laboratory
Attn: Reports Library
P.O. Box 1663
Los Alamos, New Mexico 87544

NASA Scientific & Technical Information
Facility
Attn: Acquisitions Branch (S/AK/DL)
P.O. Box 33,
College Park, Maryland 20740

NASA, Langley Research Center
Langley Station
Hampton, Virginia 23365
Attn: Mr. R. V. Hess, Mail Stop 160

Non-Government Agencies

Director
Research Laboratory of Electronics
Massachusetts Institute of Technology
Cambridge, Massachusetts 02139

Polytechnic Institute of Brooklyn
55 Johnson Street
Brooklyn, New York 11201
Attn: Mr. Jerome Fox
Research Coordinator

Director
Columbia Radiation Laboratory
Columbia University
538 West 120th Street
New York, New York 10027

Director
Coordinated Science Laboratory
University of Illinois
Urbana, Illinois 61803

Director
Stanford Electronics Laboratories
Stanford University
Stanford, California 94305

Director
Electronics Research Laboratory
University of California
Berkeley, California 94720

Director
Electronic Sciences Laboratory
University of Southern California
Los Angeles, California 90007

Professor A. A. Dougal, Director
Laboratories for Electronics and
Related Sciences Research
University of Texas
Austin, Texas 78712

Gordon McKay Library A175
Technical Reports Collection
Harvard College
Cambridge, Massachusetts 02138

Aerospace Corporation
P.O. Box 95085
Los Angeles, California 90045
Attn: Library Acquisitions Group

Professor Nicholas George
California Institute of Technology
Pasadena, California 91109

Aeronautics Library
Graduate Aeronautical Laboratories
California Institute of Technology
1201 E. California Blvd.
Pasadena, California 91109

Director, USAF Project RAND
Via: Air Force Liaison Office
The RAND Corporation
1700 Main Street
Santa Monica, California 90406
Attn: Library

The Johns Hopkins University
Applied Physics Laboratory
8621 Georgia Avenue
Silver Spring, Maryland 20910
Attn: Boris W. Kuvshinoff
Document Librarian

Hunt Library
Carnegie Institute of Technology
Schenley Park
Pittsburgh, Pennsylvania 15213

Dr. Leo Young
Stanford Research Institute
Menlo Park, California 94025

Mr. Henry L. Bachmann
Assistant Chief Engineer
Wheeler Laboratories
122 Cuttermill Road
Great Neck, New York 11021

School of Engineering Sciences
Arizona State University
Tempe, Arizona 85281

Engineering and Mathematical
Sciences Library
University of California
405 Hilgrad Avenue
Los Angeles, California 90024

California Institute of Technology
Pasadena, California 91109
Attn: Documents Library

University of California
Santa Barbara, California 93106
Attn: Library

Carnegie Institute of Technology
Electrical Engineering Department
Pittsburgh, Pennsylvania 15213

University of Michigan
Electrical Engineering Department
Ann Arbor, Michigan 48104

New York University
College of Engineering
New York, New York 10019

Syracuse University
Dept. of Electrical Engineering
Syracuse, New York 13210

Yale University
Engineering Department
New Haven, Connecticut 06520

Airborne Instruments Laboratory
Deerpark, New York 11729

Bendix Pacific Division
11600 Sherman Way
North Hollywood, California 91605

General Electric Company
Research Laboratories
Schenectady, New York 12301

Lockheed Aircraft Corporation
P.O. Box 504
Sunnyvale, California 94088

Raytheon Company
Bedford, Massachusetts 01730
Attn: Librarian

Dr. G. J. Murphy
The Technological Institute
Northwestern University
Evanston, Illinois 60201

Dr. John C. Hancock, Director
Electronic Systems Research Laboratory
Purdue University
Lafayette, Indiana 47907

Director
Microwave Laboratory
Stanford University
Stanford, California 94305

Emil Schafer, Head
Electronics Properties Info Center
Hughes Aircraft Company
Culver City, California 90230

UNCLASSIFIED

Security Classification

DOCUMENT CONTROL DATA - R & D

(Security classification of title, body of abstract and indexing annotation must be entered when the overall report is classified)

1. ORIGINATING ACTIVITY *(Corporate author)*	2a. REPORT SECURITY CLASSIFICATION
Research Laboratory of Electronics Massachusetts Institute of Technology Cambridge, Massachusetts	Unclassified
	2b. GROUP None

3. REPORT TITLE

Axisymmetric Modes in Hydromagnetic Waveguide

4. DESCRIPTIVE NOTES *(Type of report and inclusive dates)*

Technical Report

5. AUTHOR(S) *(First name, middle initial, last name)*

Gerald B. Kliman

6. REPORT DATE	7a. TOTAL NO. OF PAGES	7b. NO. OF REFS
February 28, 1967	116	32

8a. CONTRACT OR GRANT NO.	9a. ORIGINATOR'S REPORT NUMBER(S)
DA 36-039-AMC-03200(E) b. PROJECT NO. 200-14501-B31F NSF Grant GK-524	Technical Report 449
	9b. OTHER REPORT NO(S) *(Any other numbers that may be assigned this report)*

10. DISTRIBUTION STATEMENT

Distribution of this report is unlimited.

11. SUPPLEMENTARY NOTES	12. SPONSORING MILITARY ACTIVITY
	Joint Services Electronics Program thru USAECOM, Fort Monmouth, N. J.

13. ABSTRACT

The axisymmetric, transverse magnetic field modes of a hydromagnetic or Alfvén waveguide are studied experimentally and theoretically. An experiment was performed to examine with precision measurements the steady-state half-wave resonances of a short section of hydromagnetic waveguide with a liquid metal (NaK) used as the fluid conductor. The response to a step of current was also examined. The theory of uniform hydromagnetic waveguides is reviewed and extended by reconsideration of the propagation constant and theories for the effects of transverse fields, viscosity, finite conductivity walls, and bulk motion. A theory predicting the effects of nonuniform density or magnetic field is developed and verified in the experiment.

14. KEY WORDS	LINK A		LINK B		LINK C	
	ROLE	WT	ROLE	WT	ROLE	WT
Hydromagnetic Waveguide Axisymmetric Modes Liquid Metal Fluid Conductor Transverse Field, effect of Viscosity, effect of Finite Conductivity Walls, effect of Bulk Motion, effect of						